THEORETICAL EVALUATION OF PYRAZOLYL-BASED IRON, COBALT, NICKEL AND PALLADIUM COMPLEXES AS ETHYLENE OLIGOMERIZATION CATALYSTS

SAMSON GUREMA KIDIGA

B. PHIL. ANALYTICAL CHEMISTRY (UON AT KPUC)

SPCX/05184P/2020

A Dissertation Submitted in Partial Fulfillment of the Requirements for the Award of the Degree of Master of Science in Computational Chemistry

in

The Department of Chemistry and Material Sciences

of

The Technical University of Kenya

(November 2025)

DECLARATION

I declare that this dissertation is my original work and as far as I am aware, it has not been presented for award of a degree in any university

Samson Gurema Kidiga

Reg. No. SPCX/05184P/2020

Signature _____ **Date** 12/09/2025

This dissertation has been submitted with our approval as supervisors for a degree of MSc in Computational Chemistry

Signature _____ **Date** 12/09/2025

Dr. Holliness Nose

Department of Chemistry and Materials Science

Technical University of Kenya

Signature _____ **Date** 12th September, 2025

Prof. Stephen Ojwach

School of Chemistry & Physics

University of Kwa Zulu-Natal, South Africa

Signature _____ **date** _____

Dr. Patrick Shem

Department of Chemistry and Materials Science

Technical University of Kenya

DEDICATION

I dedicate my research work and dissertation to my daughters Geraldine and Christine

ACKNOWLEDGMENT

I wish to thank my supervisors who were very generous with information, expertise and their very precious time in attending to me. I was listened to any time I made a call or went in person to consult with them.

Special thanks to Dr. Holliness Nose for her countless hours of reading through the dissertation. In addition, technical guidance she offered in modeling and simulations of the computational work. She mentored me and gave a word of encouragement throughout my research. Above all, her patience exercised in the entire journey. Thanks to Professor Stephen Ojwach for believing in me and accepting to be part of my supervisory team despite his busy schedules. Also, for providing me with technical advice on computational design of new oligomerization catalysts. My acknowledgements also extend to Dr. Patrick Shem for advising on style of writing, content build up and the overall organization of my dissertation.

Special thanks to all the lecturers who taught me in my Master's program: Prof. Amolo, Prof. Aluoch, Dr. Atambo, Dr. Obonyo, Dr. Otieno and Dr. Ndangili. Finally, I am thankful to all academic and technical staff of the Department of Chemistry and Materials Science at the Technical University of Kenya for morale support.

Lastly, my special gratitude goes to my mother for her prayers, my daughter Christine Muhonja who was eager to know every step I took towards completion of this research task and to my good friend Wills Wainaina for his tireless encouragement.

ABSTRACT

Transition metal complexes in catalysis have gained a lot of interest for a decade now. Because of the widespread importance and applications of transition metal complexes in catalytic reactions of industrial importance, it is desirable to theoretically design and evaluate their catalytic activities. This dissertation involves a series of modeling investigations that have been designed to probe the influence of the electronic structure of the metal cation, the nature of the ligand, as well as the effect of chelation and steric interactions on the activity of the catalysts for ethylene oligomerization reactions. A series of transition metal cations, Fe^{2+}, Co^{2+}, Ni^{2+}, and Pd^{2+} chelated by 2-(3, 5-dimethyl-pyrazol-1-yl)-ethanol and 1-(2-chloro-ethyl)-3, 5-dimethyl-1H-pyrazole ligands have been investigated as ethylene oligomerization catalysts. Six chelates in total were studied: Fe1, Co1, Ni1, Pd1, Co2, and Ni2. Electronic structure calculations were employed to determine stable low-energy structures, energetics, and chemical reactivity's of the transition metal complexes. Density Functional Theory (DFT) was employed to gain a conceptual understanding of the structures of the initial metal complexes in solution that are likely to be pre-catalysts in the ethylene oligomerization reaction. A further goal was to analyze the electronic factors and ligand effects that impact on the chemical reactivity order of the six metal complexes within the context of DFT simulations. Theoretical studies used B3LYP and B3PW91 DFT methods and LanL2DZ basis set for metal atoms and 6-311+G (2d, p) basis set for all the remaining atoms. Theoretical studies of the Ni1 and Ni2 metal complexes were compared to the previous experimental studies of analogous complexes. The ground-state structures of all the six metal complexes show that the ligands bind in a fashion consistent with the simple valence shell electron pair repulsion model, where minor distortions from the idealized geometries are correlated with the structure of the ligands and more significant distortions with the valence electron configuration of the metal cation. The nature of the metal cation and ligand moiety had a discernible impact on the global chemical reactivity's parameters of the six metal complexes. The chemical potential, the electrophilicity indices, the charge, and the electronegativity values suggest that Ni1 is the best catalyst in the series. Comparison between theory and experiment further confirm that Ni1 is indeed the best catalyst of the six catalysts studied for ethylene oligomerization reaction. Both electronic and steric factors correlate with the metal-ligand distances, and appear to be significant factors underpinning the reactivity of the six metal complexes. Thus, the results showcase the importance of using theoretical simulations to design catalysts rapidly and the ability to develop potentially active catalysts for ethylene oligomerization reaction through a thorough analysis of the global chemical reactivity parameters.

Keywords: Density Functional Theory, Chemical Potential, Electronic Structure Methods.

TABLE OF CONTENTS

LIST OF TABLES

LIST OF FIGURES

ABBREVIATIONS

1. B3LYP–Becke's three parameters exact exchange functional Lee, Yang, and Parr
2. B3PW91–Becke's three parameters exact exchange functional Perdew and Wang's 1991 gradient-corrected exchange
3. CCSDT–Coupled Cluster with Single Double and Triple
4. CI–Configuration Interaction
5. DFT–Density Functional Theory
6. DOs- Density of States
7. HDP– High-Density Polyethylene
8. HF–Hartree-Fock
9. HOMO–Highest Occupied Molecular Orbital
10. IEFPCM–Integral Equation Formalism Polarizable Continuum Model
11. LANL2DZ–Los Alamos National Laboratory 2 Double Zeta
12. LLDP–Linear Low-Density Polyethylene
13. LUMO–Lowest Unoccupied Molecular Orbital
14. MP–Moller-Plesset
15. NBO– Natural Bond Orbitals
16. PES – Potential Energy Surface
17. SCF – Self-consistency Field
18. SHOP – Shell Higher Olefin Oligomerization Process
19. TD-DFT– Time-Dependent Density Functional Theory
20. VSEPR –Valence Shell Electron Pair Repulsion

CHAPTER ONE

BACKGROUND INFORMATION

1.1 THEORETICAL CHEMISTRY AND COMPUTATIONAL MODELING

Computational modeling is a discipline of chemistry, which uses computer simulations to understand chemical reactions and processes. It uses efficient mathematical methods and programs, which originate from theoretical chemistry. Theoretical chemistry gives a mathematical description of chemistry by developing algorithms (Louis *et al.*, 2022). In addition, theoretical chemistry provides laws that govern chemical phenomena by applying physics and mathematical principles to account for atomic and molecular interactions (Choudhury, 2024).

Theoretical chemistry methods are automated for implementation by computer programs (Ma, 2022). A set of approximations such as Born-Oppenheimer approximation are used. These approximations are adequate to calculate observable properties of molecular systems with accuracy matching experimental results (Brambilla *et al.*, 2018) Chemical properties such as molecular structures, interaction energies, electron charge distribution, dipole moments, vibrational frequencies, and other spectroscopic quantities are simulated computationally. The knowledge acquired is used to solve chemical problems such as characterization of molecular species, prediction of properties, estimation of energy between states, evaluation of stability of chemical systems and determination of reaction pathways (Hayashi *et al*., 2023). This makes computational chemistry a perfect tool for the study of reactions such as catalytic processes. In catalysis, computational chemistry delivers practical strategies in rational design of catalysts, improvement those in use, study of catalytic pathways and processes, evaluation, and prediction of catalytic properties based on quantum chemical calculations (Vogiatzis *et al.*, 2019). The calculations present predictable results of

behaviour of atoms and molecules that are closer to experimental values (Durand & Fey, 2019).

1.1.1 Quantum Chemical Methods

The core function of quantum chemical methods is to find a solution to the Schrodinger equation. Fundamental Schrodinger wave function equation expresses changes in physical quantities such as energy over time. The equation describes electron position in space and time factoring its wave nature. The calculations give details of behavior of electrons revolving around a positively charged nucleus (Cetto *et al*., 2015). It accounts for the wave function in time dependent and time independent forms, which control electron motion. Time-dependent Schrodinger equation gives a description of energy of an electron against evolvement of time in a quantum system. Therefore, motion of an electron can be represented in terms of time-dependent Schrodinger equation, as in equation 1.1, where ħ is a half value of planks constant, t is time, $\hat{H}$ is Hamiltonian and ψ is wavefunction.

$$i\hbar\frac{\partial}{\partial t}|\psi(t)\rangle = \hat{H}(t)|\psi(t)\rangle \tag{1.1}$$

For a system where the Hamiltonian has no time dependence, it is in stationary state and its time dependance is given by equation 1.2.

$$y|\psi(t)\rangle = e^{-iEt/\hbar}|\psi_0\rangle \tag{1.2}$$

When the time-dependent Schrodinger equation, equation 1.2 is plugged in equation 1.1, the Schrodinger time-independent equation, equation 1.3 is obtained.

$$\hat{H}|\psi_0\rangle = E|\psi_0\rangle \tag{1.3}$$

Solving Schrodinger time-independent equation 1.3, yields molecular wavefunction, ψ, for stationary state, which depends on the coordinates of all electrons in relation to the nucleus. Molecular energy, E, is also obtained (Brambilla *et al*., 2018).

Solving for E and $|\psi_0\rangle$ values give the energy and wave function since it is an eigenvalue problem. The Schrodinger equation has led to development of quantum chemical methods, which calculate energy of an electron as a result of interactions with nuclei and other electrons. The calculations reveal behavior of atoms and electrons during chemical reactions. The information acquired is used to elucidate chemical reactions (Sumiya *et al*., 2022). There are four categories of quantum chemical methods namely: Ab initio which computes energy and other properties as functions of the position of the nuclei from first principles without experimental input, Semi-empirical, Density Functional Theory, and electron correlation methods (Guo *et al*., 2021). Their merits and demerits are as shown in Table 1.1.

Table 1. 1 Applications, merits and demerits of theoretical methods

Theoretical Methods	**Applications**	**Merits**	**Demerits**
Semi-empirical	For large molecules	Low cost, parametrized	Less accuracy compared to DFT
Density Functional Theory	Material science study	Good accuracy at a modest cost, takes care of electrons interactions, dispersion effects and long-range interactions effects	A specific DFT method has to be selected for a specific calculation
Molecular Mechanics	Based classical mechanics. Applied to very large molecules	Fast and affordable	Low accuracy compared to DFT
Ab initio	Material science study	High accuracy	High cost

Source: Foresman (2015).

In general, electronic structure methods solve the fundamental time-independent Schrodinger Equation. The solution to the equation gives information about the system including probability and distribution of electrons, energy and configuration (Scerri, 2025). The time-independent Schrodinger is made simpler by use of Born-Oppenheimer approximation which makes an assumption that, nuclei of atoms are thousands of times slower than electrons. This makes it possible to separation calculations of electrons and nuclei energy.

For many nuclei arrangements, the time-independent Schrodinger permits construction of potential energy surface (PES). In practice, the PES at a ground sate is of interest for quantum chemical calculations (Lewars, 2016).

The first Ab initio method being the Hartree-Fock (HF) method produces reasonably good results comparable to experimental values for many properties. However, it fails in describing chemical reactions with electron correlation accurately. The Hartree-Fock method completely ignores interactions of electrons (Sanjeeva Kumar *et al.*, 2024). Density Functional Theory (DFT) is a post Hartree-Fock electronic structural method that is used for deeper understanding of reactivity trends for reactions such as catalysis, electrochemical processes and mechanisms. Modeling of transition metal complexes is done using DFT. All these help in accelerating discovery of new catalyst design and evaluation (Winther *et al*., 2019). The relative energies for individual catalysts involved are determined from their PES. In addition, the relevant features such as transition states and barriers on PES give useful information on molecular structures and their energy relationships. The target of computational catalysis research is to gain understanding of at molecular level for better catalyst rational design (Funes-Ardoiz & Schoenebeck, 2020).

The two aspects of theoretical studies include determination of a starting point of experimental synthetic reaction and assisting in understanding of experimental data. Secondly, prediction of unknown molecular properties and reaction mechanism before experimental studies. Chemical complexity determines theoretical methods to be used which vary with number of electrons, cost and accuracy (Ma, 2022). The post Hartree-Fock methods such as Moller-Plesset (MP) perturbation theory, coupled cluster (CC), coupled cluster with single double and triple perturbation excitations (CCSDT) and DFT address the limitations of Hartree-Fock methods. The post Hartree-Fock methods capture the electron interactions and correlations missing in the original HF method (Tolasa, 2025).

The methods work in two ways. They either correct the single determinant approximation or introduce correlated energy through perturbation theory to improve results. The Configuration Interaction (CI) methods retrieve statistical correlations. The Moller–Plesset (MP) perturbation theoretical methods deal with dynamical correlations. In MP methods, the Hamiltonian is expressed as a form of perturbation. The perturbation is a difference between the real electron-electron repulsion and an average one. The zeroth order and the first perturbation correction energy are equal to HF energy. The second order correction (MP2) is the first contribution to electron correction and captures correlations due to dynamics with no significant computational cost (Tolasa, 2025).

In CI methods, many electron systems, wavefunction is written in form of linear combination of different electron configurations. This is done by use of HF wavefunctions for each configuration. In case of complete expansion, the best wavefunction is constructed for a given set of orbitals. In self-consistent Field (SCF) procedures, optimization of orbitals in expansion coefficients take place which includes all possible dynamical and nondyamical correlations (Tolasa, 2025).

The DFT captures electron-electron interactions originally missing in HF formulation. Unlike other post Hartree-Fock methods, DFT does not use wavefunction to calculate energy. It works on the principle that, in a system, electron energy is a function of electron density. This phenomenon is applied to model and simulate quantum chemical systems in order to understand chemical reactions at molecular level (Weijing *et al.*, 2018). The DFT quantum chemical calculations give a higher accuracy in the prediction of PES. DFT is used to study and elucidate electronic and steric effects, reaction mechanisms and rates of catalytic systems. It provides information on geometries, stabilities and reactivities of catalytic species. Therefore, it helps to understand a corrected picture of chemical phenomena at the lowest energy electronic level. The DFT method models electron-electron interactions in chemical

systems at the lowest energy level (Dong & Deng, 2019). In addition, DFT provides key characteristics that control catalytic activities (descriptors) for evaluation of catalysts at computational design stage of a catalyst (Nzuzo *et al*., 2024).

1.1.2 Schrodinger Equation

Quantum chemical methods are efficient, user friendly and developed to make inquiries into organic and organometallic catalysis processes and mechanisms, among others. The methods have ability to predict the path of reaction from the initial mixture of reactants, additives, to products with associated energy changes (Durand & Fey, 2021). This achieved through solving of the Schrodinger equation by providing an understanding of mechanisms and reaction pathway that are essential in rational design and evaluation of new catalysts.

In establishing reaction mechanisms, quantum chemical calculations are performed on a series of molecular configurations at various points along the reaction path. The motion of atoms along the path are projected and assessed for energetic feasibility through solving of electronic Schrodinger equation (Sumiya *et al*., 2022). Through comparison of kinetic and thermodynamic energies of various paths, identification of actual path of motion of atoms can be made. This gives the probable path the reaction takes (Grambow *et al*., 2018).

To understand a quantum chemical system, the relevant molecular intermediates and reactions on PES and their evolution should be known. The in-depth understanding of a chemical system, aid in catalysis research to improve on efficiency (Simm *et al.*, 2019). Thus, computational chemistry can be applied to predict viability and outcomes of chemical reactions before they occur and give an explanation to experimental results obtained.

In rational design of new catalysts, quantum chemical calculations gives insights that assist in understanding and predicting geometrical properties of molecular structures, selectivity, activity of a catalyst, energy of reactants, transition states, and final product in a chemical system (Lee, 2021). Also, quantum chemical calculations generate electronic excited states,

spectroscopic data and thermodynamic properties of catalytic models and processes. This makes computational chemistry a reliable tool in providing insights in new catalysts design, evaluation, and prediction of properties.

In industrial catalytic production set up, computational chemistry models are used in probing progress of reactions. This is useful in making adjustments in experimental processes to get improved results and yields. Computational chemistry achieves its needs through use of modeling tools. Models are restricted representations of reality (Sauer & Freund, 2015). They are miniature replica of what is the true scenario with integrated environment. Essential aspects of chemical systems are emphasized through modeling and corrections made to bring the results closer to experimental reality (Sauer & Freund, 2015).

In computational chemistry modeling techniques are tools for prediction and or explanation of chemical phenomenon. Modeling techniques have been widely embraced in chemical research. Researchers model chemical reactions for predictions and resolution of unexplained chemical behavior. In addition, modeling techniques are used to study materials that cannot be handled physically such as radioactive, toxic, flammable etc. (Ahn *et al*., 2019). In addition, computational chemistry models are used to elucidate unclear or ambiguous experimental data, which is not easily observed directly or carried out experimentally. This includes the study of short-lived radioisotopes, unstable intermediates, or transition states. Although molecules have infinite sizes with forces acting between them, models are created by neglecting and approximating certain features. Quantum chemical calculations employ models to enable calculation of energy of smaller systems with accuracy.

Applications of computational chemistry include finding stationary points position on PES. This is achieved by varying position of a nuclei, storage of a database, identifying correlation between chemical structures and properties. The information attained is used in solving biological science, material science, and engineering problems among others. Many

industries are using molecular modeling and simulations to drive innovations in area such as drug design and development, chemoinformatics, drug target validation, and surface chemistry, among others.

The DFT functionals are used in the study and improvement of solid active pharmaceutical ingredients (APIs) (Mazurek *et* a*l*., 2020). It is used for validation of experimentally synthesized pharmaceutical drug crystal structures and prediction of chemical properties. In drug design, DFT studies gives insights into crystallization and solvation processes as well as definition of morphology and improvement of formulation techniques (Mazurek *et* a*l*., 2020). In rational design of ethylene oligomerization catalysts, DFT and microkinetic calculations are crucial. The calculations are used to obtain properties on surface reactions. Micro-kinetic modeling of the surfaces give a link to quantum chemical to macroscopic behaviour of catalytic activity and process (Mao *et al*., 2017). The ability of DFT, therefore is best suited in the design, evaluation and study of catalysis for ethylene oligomerization process.

1.2 TRANSITION METAL COMPLEXES IN CATALYSIS

Coordination chemistry of complexes determines their properties and applications such as catalytic properties (Kocharekar, 2021) magnetic properties (Moments & Molecules, 2018), and electrical conductivity (Talari *et al*., 2025) among others. Transition metal complexes undergo a variety of useful catalytic reaction cycles of industrial importance. Transition metal complexes are unique in their reactions due to tunability of metals' electronic properties by appropriate choice of ligand. The ability to fine-tune electronic and steric properties a metal complex gives unique reaction chemistry. The metals involved exhibit variable oxidation numbers making the transition metal complexes, especially of the late transition metals to be electrophilic due to empty orbitals resulting in electron-deficiency (Pfennig, 2015). Most of the early transition metal complexes exhibit nucleophile behavior due to their electron-rich

orbital filled, especially with low oxidation states and with donor ligands. The size of the transition metal, its electrophilicity, the electron counts in their d-orbital, and the steric bulkiness of ligand control associative reaction and dissociative reactions. In the transition metal complexes, ligands dissociate with ease determined by the bond strength of Metal-Ligand bond. The bond strength depends on the interplay of electronic and steric properties.

Bulky ligands crowd around the metal. Crowding around the transition metal cation reduces Metal-Ligand orbital overlap (Echanisms, 2014). It also, causes Metal-Ligand bond to elongate leading to rapid dissociation relieving steric effects on transition metal center. It is difficult to predict ligand bulkiness and electronic effects, which influence the dissociation rate of Metal-Ligand bond. Therefore, ligand bulkiness and electronic effects on the Metal-Ligand bond are considered on a case-by-case basis (Miessler *et al.,* 2014).

Many of the industrial catalytic reactions involve changes in metal coordination numbers by gaining or losing electrons or ligands. The reactions are classified based on the oxidation states on the central metal cation using donor pair method. The electron count factors ligand charges and oxidation states of metals (Comas-Vilà & Salvador, 2024). On retaining oxidation state of the transition metal, the reaction is addition or dissociation. When oxidation state is changed the reaction is oxidative addition or reductive elimination as illustrated in the Table 1.2

Ligands of a given transition metal complex are also important during a reaction as illustrated in equation 1.4 where L represents a spectator ligand, M is the metal, X is the leaving ligand group and Y is the entrant ligand. The n after L is the number of ligands.

$$LnM - X + Y \rightarrow LnM - Y + X \qquad (1.4)$$

Table 1.2. Type of reaction change of coordination number and oxidation states

No	Type of Reaction[a]	Change of Coordination Number	Charge in Formal Oxidation
1.	Addition	Increase	None
2.	Dissociation	Decrease	None
3.	Oxidative addition	Increase	Increase
4.	Reductive elimination	Decrease	Decrease

[a]Classification of catalytic reactions based on determination of oxidation states.
Source: Miessler *et al* (2014).

Transition metal complexes reactions occur through associative, dissociative or interchange pathways. The aspect of associative-dissociative, defines the mechanisms of transition metal complexes reactions. Associative reactions involve addition of a ligand to the metal cation and dissociative a ligand is lost (Pfennig, 2015). Transition metal size, electrophilicity, degree of saturation, Metal-Leaving group bond strength, the basicity of Y, size of ligand and nature of other ligands bound to the metal, determine precise mechanism of a reaction. Second-row transition metals are more reactive than the first and third row metals due to their ability to balance between larger steric size and effective nuclear charge.

The reactivity of transition metals plays a great role in design of new catalysts. Catalysts control the rate and direction of a reaction. Comparison between early and late transition metal complexes catalysis of oligomerization reactions show that early transition metal complexes are hard to improve on properties or expand on applications due to their limitations. They are hindered by the tendency of being poisoned by polar groups (Mahmood & Sun, 2018) unlike the late transition metal complexes which are functional tolerant.

Early transition metal complexes are naturally oxophilic. They have a tendency to form oxides by hydrolysis or abstraction of oxygen from other molecules. This leads to ease of being poisoned. The oxophilicity property of early transition metal catalysts makes their use where polar groups are involved a challenge (Guo *et al.*, 2016). Late transition metal

catalysts are a key to development of desired catalytic systems for oligomerization where polar functional groups are involved due to their tolerance. The late transition metal complexes used for ethylene oligomerization, can lead to attaining oligomers of desired molecular weights. Also, in production of functionalized polymers and oligomers (Bogdos *et al*., 2022).

1.2.1 Hemilabile Metal Based Catalysts

Properties of a transition metal complexes are as a result of interactions between metal centers with the surrounding ligands. Ligands stabilize metal cation in catalysts and provide the required sterically hindered space for substrate to bind (Reek *et al*., 2022). The number of ligands forming complexes with a central metal cation can range from one (mono), two (bis), three (tris), or many (poly). The ligands can contain different types of chemical groups. Each donor atom confers different and unique reactivity to the metal complex (Adams & Weller, 2018).

Hemilabile ligands modify and control properties of catalysts. They provide a convenient approach to fine tune selectivity, yield, and rates of reactions. Hemilabile ligands have a weakly bound ligand in equilibrium with an open metal site or competing type or an easily displaceable ligand (Enders, 2020) illustrated in Figure 1.1.

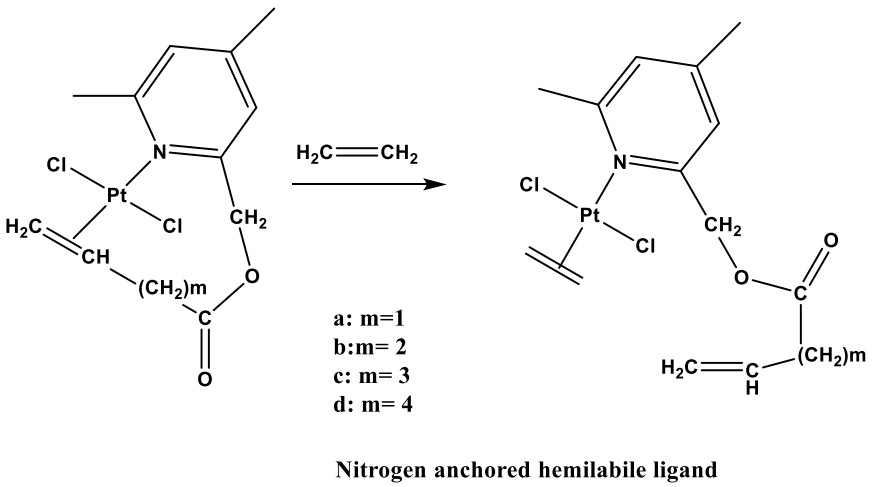

Figure 1.1: Scheme for the working of a hemilabile based catalyst
Source: Enders M (2020). doi.org/10.1002/9783527809080.cataz07876

Hemilabile ligands have two or more potential donor groups attached to the metal center. The donor groups have ability to dissociate to give an open coordination site for reactivity by the transition metal complex and stabilization (Adams & Weller, 2018). Catalysts designs based on late transition metals complexed with hemilabile ligands are used in transformative organic reactions including ethylene oligomerization and polymerization (Nyamato *et al.*, 2015).

In new catalyst designs, hemilabile ligands are attractive to use due to ease of their synthesis, stabilization ability of central transition metal cation with varied oxidation states, and ease to fine-tune both steric and electronic properties (Wang & Chen, 2019). Hemilabile ligands complexed with transition metal are used to design ethylene oligomerization and polymerization catalysts (Ahmad & Bühl, 2019).

Architectural design and performance of a metal catalyst, fine-tuning its selectivity, efficiency and separation of catalyst from final product schemes highly depends on its ligand. For example, research done by Brookhart and coworkers in 1995 on late transition metal catalysts showed that a hemilabile α-diimine palladium (Pd^{2+}) and nickel (Ni^{2+}) complex catalysts produced superior ethylene oligomers. In addition, molecular structures of the oligomers depend on electronic and steric properties of ligands in the catalyst (Wang & Chen, 2019). For example, the bidentate donor ligands can stabilize the late transition metal centre through chelation and at the same time allowing substrate monomer to coordinate to the transition metal centre. Therefore, the hemilabile ligands determine physical and chemical properties of catalyst formed. In the regulation of transition metal complex catalytic activity, modification of the ligand can be done. Also, the transition metal cation at the centre of complex (Goonesinghe *et* a*l.*, 2020).

Properties of the hemilabile ligands on late transition metals are difficult to predict because different transition metals at the centre of a catalytic complex behave differently towards

different ligands. Similarly, different ligands completely modify chemical properties of metals they are coordinated differently (Adams & Weller, 2018). Examples of hemilabile ligands include: Phosphorous-Oxygen-Phosphorus (P^O^P), Phosphorous-Oxygen (P^O), Phosphorous-Nitrogen (P^N), Nitrogen-Nitrogen (N^N), Nitrogen-Oxygen (N^O), Phosphorous-Sulphur (P^S) among others (Adams & Weller, 2018). Many of the ligands containing hemilabile groups have been incorporated in metallic complexes for catalytic transformations and found to be more advantageous over nonfunctional ligands in catalysis. For example amino phosphines make metal centers electron rich by direct Metal-Phosphorus bond or Metal-Nitrogen bond interactions (Gogoi *et al*., 2019). This enables oxidative addition and reductive elimination reactions to occur. The binding of ligands to metal atoms can be in different ways depending on ligand structure and metal oxidation state.

The P-donor group stabilizes low oxidation state metals and the N-donor group creates a coordinating site for binding of substrate (Gogoi *et al*., 2019). The P^N donor hemilabile ligands are widely used in coordination chemistry work due to their ability to bind and form both monodentate through either P or N or as bidentate through both P and N or as bridging ligands depending with metal hardness and ligand steric (Kandel, 2018). For example, the P-N hemilabile ligands metal complexes react with small molecules to undergo fluxional ligand exchange processes.

Nitrogen moieties such as amines, pyridines, imines and nitriles are weakly binding and exhibit hemi-lability. In these complexes, a late transition metal forms a monodentate ligand through complexing with either P or N and a bidentate by complexing with both P and N depending on the ligand steric effect (Kandel, 2018). Activity of metal cation can be manipulated and controlled by hemilabile ligands. The phosphorous is considered to be a soft donor and inert while nitrogen is considered to be hard donor and labile. Phosphorus

stabilizes metal ions of low oxidation states due to its π-electron accepting behavior (soft P site) while nitrogen uses σ-donating ability of the hard N site (Kandel, 2018).

1.2.2 Pyrazolyl Metal Complexes in Catalysis

Pyrazolyl ligands are a type of hemilabile ligand. They are based on the pyrazole ring, a five (5)-membered ring heterocyclic compounds with three carbon atoms and two nitrogen atoms. Pyrazoles and their derivatives are highly attractive due to their versatility in synthesis of a series of analogues with various moieties. Pyrazolyl ligands are used to prepare metal complexes as nitrogen donor ligands. The complexes formed from the nitrogen donor ligands have structural diversity with potential applications as catalysts. Pyrazolyl ligands are not extensively used as imines and pyridines in catalysis. Pyrazolyl ligands been used as nitrogen-donor groups in carbon-carbon coupling reactions such as olefin oligomerization and polymerization. In addition, in heck and Suzuki coupling and ring opening reactions (Ojwach & Darkwa, 2010). Pyrazolyl-based ligands have been used for different purposes such as motifs pharmacophores for medicinal compounds used as anticancer, antimicrobial and anti-inflammatory and complexes for catalysts.

Pyrazole-Metal based complexes have various coordination geometry (Mukherjee, 2000). The pyrazole-based ligands are preferred for use because they are weak electron donors compared to other nitrogen donor groups such as imines and pyridines. This renders the complex central metal to be more electrophilic. Also, the pyrazolyl based ligands can be easily modified by use of substituent attachments to fine tune steric and electronic properties. Some pyrazolyl-based metal complexes used for oligomerization and polymerization reactions are shown below Figure 1.2

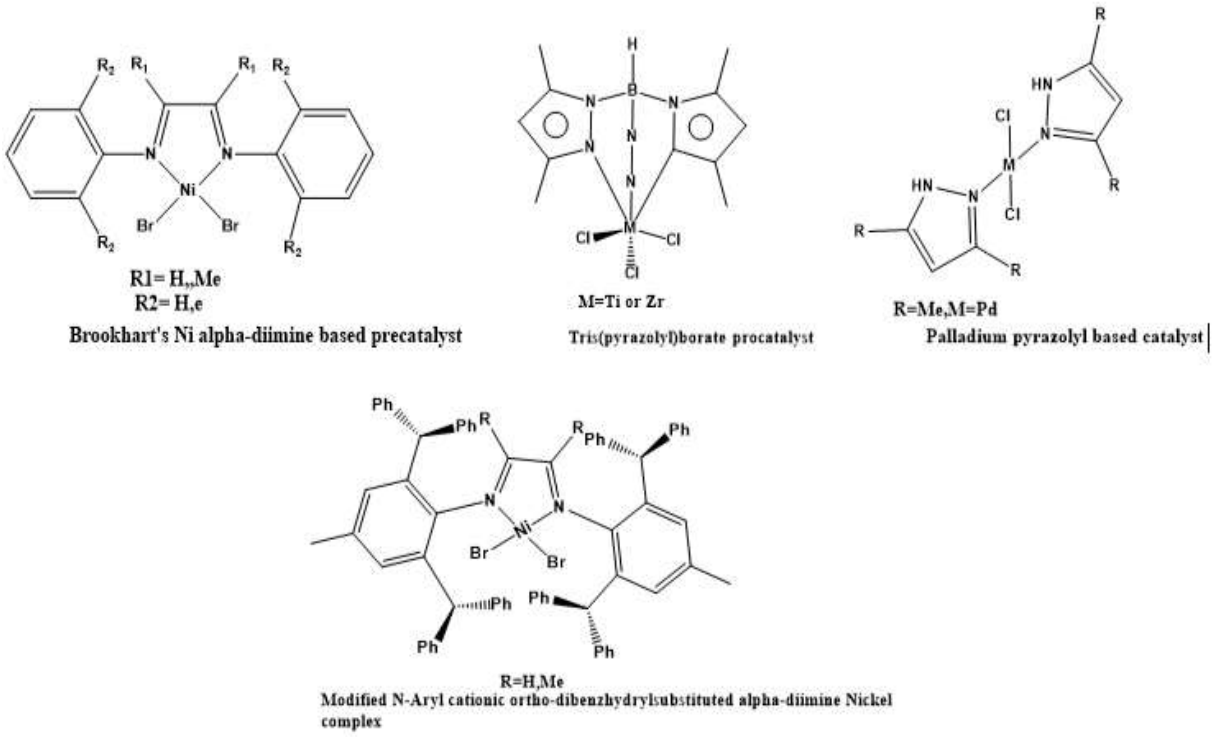

Figure 1.2. Representatives of hemilabile pyrazolyl-based complexes used in polymerization and oligomerization catalysis.

Source: Mukherjee R(2000).

According to Mukherjee, pyrazolyl ligands coordination chemistry is influenced by other donor atoms such as oxygen, nitrogen and sulphur (Mukherjee, 2000). Pons *et al* (2010) reported on characteristics of coordination chemistry in alkylpyrazolyl with a second atom as nitrogen or other hetero atoms such as oxygen and sulphur with the first row or second row transition elements. They pointed out that when oxygen is the second atom bonded to second row metals, it does not coordinate (Aragay *et* a*l*., 2010). After development of symmetric diimine catalyst by Brookhart and coworkers for ethylene oligomerization, later a number of imine based late transition metal pre-catalysts were developed both with and without bulky substituents (Wang *et al*., 2017).

There exist a variety of nickel bearing imine nickel (II) complexes with five and six membered chelate rings analogues of Brookhart type catalysts (Bekmukhamedov *et al.*, 2020). Designing of transition metal catalysts require ligands with specific functionality of tailor made electronic and steric properties (Raugei *et al*., 2015). Advantage of

pyrazolyl-based metal complex catalysts is ability to fine tune ligand to get tailored catalytic properties and performance. Ligand's structural composition helps in prediction of electronic structural changes and steric characteristics of the ligand such as electron withdrawing and donating abilities (Rauge*i et al.*, 2015). The yield, rate of reaction and selectivity of a catalyst can be linked to steric and electronic descriptors of a ligand. Therefore, models derived from the descriptors can be used in discovery, optimization design, and evaluation of new catalysts (Durand & Fey, 2019).

1.3 COMPUTATIONAL INVESTIGATION OF A CATALYST

Molecular structural design of a catalyst has to be made based on the choice of method and technique to use on investigation of their reaction nature. Key decisions have to be made on the problem definition, theoretical model progression, presentation of chemical progression, calculation series progressions, and environmental modeling progression. Geometry optimization is the first step of most computational studies. It factors environmental modeling progression where solvent chemical environment is considered (Foresman J.B., 2015). Selection of the model chemistry capable of handling the problem being addressed accurately has to be made. For example, when addressing a problem related to excited states, the model chemistry selected should be able to run excited states. Also, the geometry of the model has to be right. It is an essential factor contributing to availability of a catalytic site. Catalytic sites help in comprehending performance of a given catalyst (Liu, 2024). In modeling parameters, optimization is critical for it is done to match experimental data (Chacko *et al*., 2023). Planning a series of calculations necessary to predict the desired properties of a catalyst is also critical. Making decisions in each area inherently involves trade-offs between ideal computational accuracy, exigencies of real-world time requirements and computing resource availability to achieve the accuracy required (Foresman J.B., 2015).

Catalysts play a critical role in determining performance and results of oligomerization process. Catalysts accelerate chemical transformations of ethylene monomers into oligomers. A selected catalyst design system determines the product selectivity and type of oligomerization mechanism which the reaction can follow. The path can be linear or metallacyclic mechanism. In addition, the catalyst design controls the microstructure properties of an oligomer such as formation of linear or branched oligomers (Sydora, 2019).

In modern chemical industries, catalysis is used in many processes such as energy conversions, chemical transformations, and pollutant remediation among others. Catalysis reduces input costs and improves production yields (Mou *et al*., 2023).

Research in catalysis is focused on identification of optimal reaction conditions, designing of efficient catalysts and study of reaction mechanisms (Chen *et al*., 2024). These can be done by trial-and-error methods or computationally. Trial and error experimental methods of catalyst design are irrational. It is costly and difficult to optimize catalytic processes, predict outcome, and improve or develop new and better performing catalysts. Computational chemistry offers an accelerated approach to catalysis research due to its predictive abilities. This is possible with use of appropriate global descriptors to play a role of improving accuracy in studying and evaluating activity and selectivity of catalysts.

1.4 STATEMENT OF THE PROBLEM

Catalytic industrial processes need urgent sustainable industrial solutions to production challenges such as non-selectivity and high cost of research. Industrialist are continuously seeking new catalysts with ability to decreases production costs, possess high efficiency, resist poisoning, minimize environmental contamination and reusable (Gupta *et al*., 2023). Most ethylene oligomerization catalysts are non-selective leading to uncontrolled reactions which produce a range of C4 to C30 oligomers (Sydora, 2019). To achieve desired oligomer, further chemical processing of the mixture has to be done. During further processing, higher

molecular weight oligomers hinder the flow of the mixture of oligomers making the process time consuming and less efficient (Soleimani *et al.*, 2012). In addition, due to changes in environmental and economic needs by industrialists, there is a demand for new more efficient easy to work with catalysts.

The persistent industrial challenges in catalytic oligomerization of ethylene processes coupled with trial-and-error methods hinder design of new catalyst as fast as possible, lead to high costs involved in research production and tedious evaluation processes, inaccurate prediction of properties, and lack of control of microstructure of oligomers produced. This slows down or stops the progress of achieving faster solutions to oligomerization problems such as lack of selectivity, activity and stability. Ultimately, new catalysts should be active, selective, stable, and able to control microstructures and molecular weight of oligomers. In addition, they should be cost effective with no residues of catalyst trapped as impurities in the final product, should operate at lower temperatures and pressure to save energy with non-toxic effects to the environment. Lack of fundamental insights in catalyst design, predictability, and evaluation of properties, is a hindrance in timely optimization of performance of oligomerization process and scaling up of production of oligomers.

1.5 JUSTIFICATION

Due to industrial and scientific importance of catalysis, researchers are increasingly seeking new strategies to make catalysts discovery fast and more predictable (Pelletier & Basset, 2016). The major concern in oligomerization industry is to provide faster, reliable designs, better and comprehensive understanding of chemical mechanisms governing oligomerization of ethylene catalysis, also predictive and evaluation of performance of various designs. The outdated trial-and-error methods of catalysts design and their evaluation is inefficient, expensive and non-predictive. These methods require a lot of time, substantial investment of finances and are labor intensive with repeated sequential steps.

The remedy to the prevailing persistent industrial challenges affecting new catalysts design, high speed evaluation, prediction of properties and control of oligomerization process, lie in research and development work rooted in computational chemistry. Catalyst discovery and optimization need understanding of mode of action at molecular level theoretically.

Computational chemistry is an innovative way that is cost effective, precise, predictive and a critical better alternative to the traditional trial and error experimentation methods of design, development and evaluation of new oligomerization catalysts. It applies mathematical modeling techniques and simulations to explore, understand mechanism of a reaction, predict intricate properties of catalyst electronic and steric characteristics and evaluation of oligomerization catalysts. Computational methods empower a guided approach towards catalytic design and predictive capabilities. The methods are based on global descriptors that rely on the understanding of oligomerization reaction process (Chen *et al*., 2021).

The coordination geometry and energy of transition metal catalysts can be studied theoretically using DFT. DFT calculations enable determination of possible microscopic properties of a catalytic system through computational simulations (Mao *et al.*, 2017). In this study, computational modeling is used as a vital tool in designing transition metal catalysts. It demonstrates its capability of alleviating the lengths of time burden associated with design, study of activity, prediction of properties and evaluation of new designs of catalyst based on geometry, energy, and catalytic global descriptors. Thus, computational chemistry provides an accelerated approach to new catalyst development, optimization, evaluation and prediction of catalytic properties and abilities.

1.6 OBJECTIVES

1.6.1 Main Objective

To probe the influence of the electronic structure of the metal cation, the nature of the ligand, as well as the effect of chelation and steric interactions on the activity of the catalysts in ethylene oligomerization reactions.

1.6.2 Specific Objectives

1. To determine stable low-energy structures, geometries around the metal center and geometrical parameters of the Fe^{2+}, Co^{2+}, Ni^{2+} and Pd^{2+} metal complexes.
2. To determine the global descriptors of the Fe^{2+} Co^{2+} Ni^{2+} and Pd^{2+} metal complexes.
3. To examine the electronic-, chelate-, and steric effects of the metal complexes by: -
    a. changing the electron configuration of the metal complexes from Fe^{2+} to Co^{2+} to Ni^{2+} to Pd^{2+}
    b. comparing the two ligands, L1 and L2
        - L1 - [2-(3,5-dimethyl-pyrazol-1-yl)-ethanol] and
        - L2 - [1-(2-chloro-ethyl)-3,5-dimethyl-1H-pyrazole]
4. To compare theoretical results of the Fe^{2+}, Co^{2+}, Ni^{2+} and Pd^{2+} complexes to experimental results of the analogous complexes.

CHAPTER TWO

LITERATURE REVIEW

2.1 INTRODUCTION

2.1.1 Development of Computational Chemistry

Earlier days, chemists carried out chemical transformations without computational modeling and simulations. When Fischer-Tropsch reaction for liquefaction of coal was achieved in 1925 (Sarkar*i et al*., 2012) and the development of Ziegler-Natta catalysts by Karl Ziegler and Gulio Natta in the 1950s (Zhang *et al*., 2012), computational chemistry did not play any role**.** The historical application of computational chemistry started when Neil Bohr introduced quantum description of an atom. In the early years of the twentieth century, Neil Bohr and Sommerfeld came up with the laws that govern the microscopic world in the quantum mechanical and wave description of electronic orbitals (Bhattacharjee, 2022). The discoveries differentiated classical and quantum domains. In an independent effort, Schrodinger laid the foundation of quantum mechanics by coming up with a generalized mathematical model that validated Bohr's correspondence principle.

In 1925, Schrodinger expressed atomic system using mathematical functions of coordinates of electronic positions called a wavefunction. A wavefunction holds a system's information which can be extracted by treatment of a mathematical operator corresponding to a physical observable parameter of interest known as an eigenvalue (Bhattacharjee, 2022). A significant advancement in computational chemistry came with derivation of Hartree-Fock (HF) equations. The equations approximated wavefunction as a single slater determinant and optimized it according to variational principles (Recchia *et al*., 2024). This solved many electron system solutions for wave function calculation for Schrodinger equation. In general, the HF equations are one of the methods for solving Schrodinger equation(Jensen *et al*., 2023). The limitations were inability to precisely solve atoms with more than one electron

with a variety of many forces involved. The forces include electrons-nucleus attraction, electro-electron repulsion and weaker magnetic forces arising from spin and electrons orbital motion (Sandhu, 2018).

2.1.2 Trends in Computational Design of New Catalysts

Discovery of new effective and efficient catalysts is key in chemical industries. It is a driving force in achieving global goals towards sustainability, decreases in energy use and development of environmentally friendly processes (Soyemi & Szilvási, 2021). However, new catalyst design consumes a lot of time and resources. Therefore, it is necessary to increase reliance on properties and performance predictive tools.

Computational chemistry methods are powerful tools compared to traditional experimental methods in designing new catalysts**.** These methods offer useful predictions of properties and performance and decreases time used on screening of new catalysts (Soyemi & Szilvási, 2021). Current computational methods used in computational design of new catalysts are based on three approaches, that is, reaction mechanism based, descriptor based and data driven approach (machine learning) (Soyemi & Szilvási, 2021).

2.1.3 The Future of Computational Design of New Catalysts

A long standing goal in catalysis research, is development of methods for determining catalytic activity, selectivity, and prediction of chemical properties in the shortest time possible (Bell, 2004). Quantum chemical methods and codes have made great contribution and advancements with impressive achievements in terms of speed in the field of research. The quantum chemical methods define what is possible to be done (Bell, 2004). Furthermore, the use of computers has revolutionalised theoretical design and development of new catalysts. Computational chemistry methods are used to design, screen and evaluate novel pre-catalysts. They have become acceptable strategies in catalyst discovery (Medford *et al.*, 2015). Coupling computational chemistry with experimental methods result reveals puzzling

observations and enhances better understanding of catalytic processes (Medford *et al*., 2015). Additionally, computational chemistry theoretical simulations and calculations can capture critical aspects of a catalytic system. The challenge in catalyst design is when the molecule is a complex and needs big computer memory and speed making computational cost high.

Catalysts are evaluated based on energy on potential energy surface (PES), mechanism of action, charges, free energies etc. Theoretical simulations provide geometric and electronic information for catalytic descriptor development (Mou *et al*., 2023). Global descriptors easily show computed catalytic activity in prediction of intrinsic atomic properties. Modeling of a reactivity trend of a singled-out parameter to describe activity or selectivity are perquisites for a specific catalytic descriptor.

Computational calculations provide descriptor based inherent atomic properties such as electronegativity, HOMO-LUMO energy gap, polarizability, charge distribution etc. Spectral descriptors predict interactions between the catalyst ligand and central metal. Also, interaction between catalyst and monomer. An ideal descriptor should be a function of electronic behavior of ligand and metal cation and or monomer. The descriptor should also contain information on electron distribution spatially and produce quantitative values that are comparable experimentally and computationally (Hu *et al*., 2019). In addition, molecular dipoles have strong association with Raman, Ultraviolet-Visible (UV-Vis), Nuclear Magnetic Resonance (NMR), and Infra-red (IR) vibrational spectra. The spectra for a catalyst can be theoretically simulated and experimentally determined (Hu *et al*., 2019).

Surface adsorption interactions including charge transfers and energy absorption can be measured quantitatively by utilizing vibrational spectral signals from Raman and IR spectra (Wang & Jiang, 2023). Accuracy and efficiency of electronic structure methods in new catalyst design is prediction of properties. Accuracy of prediction depend on physical description parameters such as spectra which are highly valued in achieving research goals

(Marzari *et al*., 2021). This is driven by modeling and simulations for accelerated identification, characterization and optimization.

2.2 THE QUANTUM CHEMICAL THEORY AND CATALYSIS

2.2.1 Electronic Structure Theory

Computational chemistry entails the use of computers to solve chemical problems. It includes computational techniques applicable in chemistry that originate from quantum physics, statistical mechanics, informatics among other scientific disciplines (Lewars, E. G. 2016). The key role of electronic structure theory with respect to catalysis is to elucidate the energetics and mechanisms of catalytic reactions. The accuracy of the results depend on electronic structure methods derived from quantum chemistry and model chemistry used for calculation (Vogiatzis *et* a*l*., 2019). Quantum chemistry has a set of methods derived partly or wholly from laws of quantum mechanics (Lewars, 2016). The laws have a direct bearing to time-independent version of Schrodinger equation, equation 2.1., which underlies electronic structure theory methods (Lewars, 2016).

$$H\Psi(r, R) = E\Psi(r, R) \tag{2.1}$$

In the equation, Ψ is wavefunction of a molecule with respect to positions of electrons and nuclei, r and R, respectively. As stated by the equation, applying the Hamiltonian Operator, H, to the wavefunction, Ψ, yields energy, E, of the molecule multiplied with wavefunction, Ψ. Mathematically, an equation where an operator, H, is applied to a function, Ψ, to yield the same function, (Hamiltonian) multiplied by a constant is an eigenvalue equation. The Ψ is an eigenfunction of the operator H (Foresman J.B., 2015). The time-independent, non-relativistic Schrodinger equation, H, is given as in equation 2.2.

$$\hat{H} = -\sum_{i}^{\text{Electrons}} \frac{\hbar^2}{2m_e}\nabla_i^2 - \sum_{A}^{\text{Nuclei}} \frac{\hbar^2}{2m_A}\nabla_A^2 - \sum_{i}^{\text{Electrons}}\sum_{A}^{\text{Nuclei}} \frac{Z_A e^2}{r_{iA}} + \sum_{i>j}^{\text{Electrons}} \frac{e^2}{r_{ij}} + \sum_{A>B}^{\text{Nuclei}} \frac{Z_A Z_B e^2}{r_{AB}} \tag{2.2}$$

Where r represents the distance between ί and n, j is the subscript for electron and nucleon and A is subscript for nuclei. M_e and M_A are masses of electron and nucleon, respectively. The ħ is planks constant divided by two (2). In Equation 2.2, first and second terms represent kinetic energy of electrons and nuclei respectively. The third term represent potential energy due to nuclei-electron attraction, the fourth is electron-electron repulsion and finally the fifth term represent nuclear-nuclear repulsion energies.

The energy and wavefunction of quantum system depends on electrons coordinates. To get total energy of a system, term one, three and four which remain eigenvalue problems can be added to term two which is calculated if the charge of the nucleus is known. All information about the chemical system and its available states is contained in the wavefunction. Every quantum mechanical system has an associated operator and measurements on the system or collapse of wavefunction into one of its states yields an eigenstate operator.

2.2.2 Applications of Electronic Structure Theory

Conceptionally, quantum chemistry approach treats the nuclei of a molecule as stationary particles with electrons moving around it. This approach are known as electronic structure methods (Götz, 2016). There are other approaches that model the behavior of a system over time and are known as chemical dynamics methods (Pratihar *et* a*l*., 2017). These methods use quantum dynamics, molecular dynamics, or semi classical dynamics. Molecular Mechanics (MM) methods, use force fields, they are based on classical mechanics and are inexpensive. The MM methods are applied on large molecules (Nochebuena *et al*., 2021). The molecular dynamics methods are beyond the scope of discussion in this dissertation.

Some electronic structure methods base their calculations on quantum mechanics and fundamental physical constants like speed of light, masses and charges of electrons and nuclei (Pratihar *et* a*l*., 2017). Other methods combine versions of the first cases with experimental parameters and others are hybrid. A good example of the latter is the

semi-empirical methods. As a result, they are inexpensive and provide a fairly accurate prediction of structures and energy compared to DFT methods (Lewars, 2016).

The most widely accepted descriptive technique of computational modeling is DFT, a quantum-mechanical atomistic first principle simulation technique for computation of molecular properties (Bhattacharjee, 2022). Density Functional Theory computes total electron of a molecular system. It does not require calculation of wavefunction (Baseden & Tye, 2014). It uses pseudo wavefunction for computation of part of energy of a system and the rest calculated by electron density.

2.2.3 The Density Functional Theory (DFT)

The DFT is a theory of electronic structure. It is based on electron density distribution instead of many electrons wavefunction. In DFT framework, total electron density (ρ) is related to normalized wavefunction (ψ) as shown in equation 2.3 below, where n is the total number of electrons.

$$\rho = \frac{|\varphi|}{N} \tag{2.3}$$

It is useful in understanding and calculating of ground state density and energy of any system having electrons and nuclei such as molecules, clusters and solids. The calculation is performed with or without application of static perturbations (Kohn *et* a*l*., 1996).

DFT calculations are high quality predictions with broad range of application at a reasonable cost. The foundation of DFT are two theorems by Hohenberg and Kohn. The first theorem states that, the ground-state energy is uniquely determined by electron density and can be obtained variationally (Vogiatzis *et al*., 2019). The second theorem states that if the exact expression of density of electron was known then an energy greater or equal to the true energy can be computed. The current Kohn-Sham DFT equation is derived from Hartree-Fock equation via Self-Consistency-Field (SCF). DFT is the most practical

Kohn-Sham DFT method that considers electron-electron interactions (Vogiatzis *et al*., 2019).

2.2.4 Application of DFT in Development of Oligomerization Catalysts

Computational chemistry calculations are useful in providing interpretation of energetics and mechanisms of catalytic reactions. DFT in particular, has refined the understanding of chemical catalytic reactions such as ethylene oligomerization using organometallic systems (Vogiatzis *et al.*, 2019). Oligomerization is an advanced industrial process which applies organometallic chemistry in the formulation of catalysts (Sydora, 2019). Such catalysts are either a single or bimetallic active site metal complexes consisting of transition metals such as cobalt, nickel, palladium, and chromium in a divalent state (LiBrett*o et al*., 2021). In some cases, the catalytic systems are made of an alkyl group or a halogen derivative of a transition metal with an organoaluminium compound (Belov, 2008). A good example of such a system is $Ti(OC_4H_9)_4$-$Al(C_3H_5)$, a Ziegler-Natta type of catalyst with high oligomerization activity (Belov & Matkovsky, 2010). High catalytic activity in oligomerization of ethylene is influenced by electron deficiency in transition metal complexes. Presence of coordination sites at active metal centers bordering a growing oligomer or polymer chain consist of a positive charge for enhancing electrophilicity of the metal cation. Additionally, the positive charge aids in inhibiting and deactivating occurrence of dimerization and stabilizing the active catalytic sites of the metal cation (Mecking, 2001).

The use of DFT in modeling catalytic reactions is becoming a routine. It allows deeper understanding of molecular systems in situations where application of experimental techniques are unfeasible (Bhattacharjee, 2022). DFT functional is preferred in calculating a variety of molecular properties such as thermochemistry and reaction kinetics for organometallic compounds (Bursch *et al*., 2022). The functionals are grouped into two major categories, pure and hybrid. The DFT pure functionals describe two different terms of energy

expression, that is, exchange and correlation. The third category is hybrid functionals for DFT calculations which include some Hartree–Fock exchange in their formulation (Tognetti & Joubert, 2024). The DFT advances in the recent past also include dispersion effects and long range interactions of electrons in excitations state in transition to higher orbitals (Tsuneda & Hirao, 2014).

In the study of organometallic systems, there is a compromise between desire for highest possible accuracy and the need to complete the calculation within a reasonable time limit and cost. Although coupled cluster methods CCSD (T) is considered to be a gold standard, DFT is a method of choice for catalysis studies. It has a good compromise between speed and accuracy (Smith *et al.*, 2019). Also, DFT computations can be done on a broad range of systems on any element in any chemical environment and produce high quality predictions. A variety of DFT methods commonly used are shown in Table 2.1

Table 2.1: Commonly used DFT methods

GGA	Meta GGA	Hybrid -Meta-GGA	Hybrid-GGA	Range Separated
BP86	M06L	M06	B3LYP	ωB97X-D
B97D	TPSS	M062X	B3PW91	DFT -D3
			PBEO	
			APFD	

Source: Sancho-García & Adamo (2013*)*

Hybrid functionals have enhanced accuracy and precision and DFT is synonymous with them (Qi *et al*., 2016). The first generation DFT methods are the Becke's three parameters exact exchange functional (B3LYP) in combination with gradient corrected correctional functionals of Lee, Yang, and Parr (LYP) and the Beck's three parameters incorporating Perdew and Wang's 1991gradient-corrected exchange and correlation functions and include 20% Hartree-Fock exchange method (B3PW91) (Avcl *et al.*, 2015). Others include the Amplitude Probability Frequency Distribution (APFD) method. The APFD functional is used to avoid the unjustified long range attractive or repulsive interactions in DFT (Austin *et al*., 2012).

It provides a basis for addition of dispersions correction terms coming out of spherical atom model. Also, it has nine adjustable parameters which include ionization potentials and effective atomic polarizability for elements. The APFD method, describes accurately potential energy surface (PES) of noble gases, various diatomic molecules, dimers of hydrocarbons. The APFD method is also accurate in producing conformational energies of organic molecules comparable to coupled cluster method CCSD (T)/aug-ccpVTZ methods (Austin *et al.*, 2012). The three DFT methods i.e. B3LYP, B3PW91, and APFD combined with a basis sets linearly create molecular orbitals used in computing energies of a given system (Hill, 2013).

2.2.5 The Model Chemistry

The choice of the correct a model chemistry and sufficient description of route section instructions, modeling will not give susceptible or ambiguous results. Wrong results could lead to poor correlation of computational predictions against experimental results. The end results would be incomplete understanding of the chemical system being investigated. (Bhattacharjee, 2022). To achieve knowledge of system, model chemistry has to be right.

Theoretical functional method and a basis set make up a model chemistry or level of theory. Basis sets are used to define the space in which molecular orbitals are built (Donchev *et al.*, 2021). The selection of a right basis set results in reliable geometry and energies of the predicted molecule. For example, DFT functionals with selected basis sets were used to model organometallic complexes involving metal–metal bonds.

Metal-Metal and Metal-Carbon distances of organometallic complexes are computed using double-ξ and triple-ξ (theta) plus polarization basis sets (Narendrapurapu *et al.*, 2013). According to Zhao and Truhlar who examined 57 functionals with double and triple-ξ basis sets, suggested that G96LYP, MPWLYP1M, XLYP, MOHLYP and MPWLYP are the best choices of DFT functionals for the systems (Fernandes *et al.*, 2007). The study showed that

triple-ξ basis sets are preferred to double-ξ because they are more accurate. In addition, increase in basis set size increases convergence (Spackman *et al*., 2016).

In another study conducted by Cundari, Wilson and co-workers suggested that calculations of enthalpy accuracy increases with increase in basis set size (Tekarli *et al*., 2009). Therefore, increase of basis set has a direct effect on the geometry the bond parameters and energies in modeling.

2.2.6 Modelling of Ethylene Oligomerization Catalysts

Ethylene Oligomerization catalysis is a kinetic phenomenon characterized by transformation of ethylene at a low energy by a catalyst. The catalyst lowers activation energy of the system without it being part of the finished product (Sydora, 2019). Transition metal catalyzed oligomerization reactions are metal centered and the reactions are thermodynamically accelerated by taking a reaction path of lower energy. The reactions consist of substitution, oxidative addition, reductive elimination and migratory insertion reactions. These fundamental transformations can be elucidated and predicted computationally using quantum chemical methods (Funes-Ardoiz & Maseras, 2018). The methods involved in calculating geometry and energy of reactants, intermediates, transition states, and final products. Accuracy of calculations of obtained geometry parameters and energy depend on electronic structure method and the model chemistry or level of theory used (Bogojeski et al., 2020) .

If the ingredients of a catalyst are known, to unravel how catalysts work, requires a systematic approach to mimic interactions and observations of a working catalyst (Sauer & Freund, 2015). Electronic structure methods have emerged to be reliable in understanding catalytic functions and aid in the discovery of new catalysts. Thus, adopting computational approach, quantum chemical calculations can integrate complex systems to unravel successfully desired properties (Stamatakis, 2015). Modeling catalysts according to quantum mechanics postulates that a particle in a quantum mechanical system has a wavefunction

associated with it. The wavefunction contains all knowable information related to a quantum chemical system. A wavefunction of a molecule is a superposition of all available states and depends on coordinates and time of electrons and nuclei. Consequently, coordinates of atoms and nuclei and time determines the wavefunction of a quantum chemical system (Foresman J.B, 2015). In order to obtain reliable information such as energy of a catalytic system, the molecular geometry of the chemical system must be right. Proper selection of the metal and ligand set, a single-site catalyst can be designed to target a given chemical transformation. The coordination chemistry and lifetime of oligomerization of catalyst for ethylene can be defined. In addition, the understanding of structure-activity relationship, selectivity of transition metal catalyst can be achieved (Pelletier & Basset, 2016).

2.3 APPLICATION OF THEORETICAL METHODS MECHANISM STUDY

Theoretical methods make a significant contribution to mechanistic studies of transition metal catalysis. The use of quantum mechanical calculations has led to improved understanding of oligomerization process (Forget *et al.*, 2017). Oligomerization of ethylene occurs in sequential steps whereby an activator converts a pro-catalyst into a cationic oligomerization initiator. Ethylene coordinates to the cationic oligomerization initiator (activated catalyst) to form unstable intermediates. These intermediates rearrange to stable forms intermediate through migratory insertion of ethylene monomer into a metal alkyl bond. A second ethylene monomer binds and undergoes migratory insertion leading to chain elongation. The growth can be linear or branched through ß-hydride elimination and reinsertion of ethylene monomeric units (Sydora, 2019). Termination occurs though chain transfer (ß-hydride elimination and olefin dissociation) shown Figure 2.1

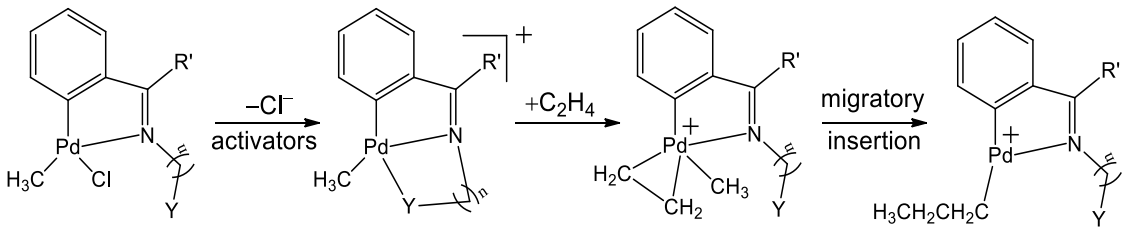

Figure 2.1: Scheme for catalyst activation for oligomerization process
Source: Researcher (2024)

The formation of unstable intermediates between reacting molecules and catalyst intermediate decomposes into oligomers. The intermediate formation and decomposition determine product selectivity and rate of chemical reaction. Also, this processes are accompanied by changes in Gibbs free energy of the system (Freema*n et al*., 2020). Analysis of both primary and secondary oligomerization products is used to postulate mechanistic pathway for ethylene oligomerization (Forget *et al.*, 2017).

2.4 ROLE OF TRANSITION METALS IN ETHYLENE OLIGOMERIZATION CATALYSIS

The need for maximum catalytic activity and selectivity of specific α-olefin production is driven by industrial needs. Oligomer manufacturers need to cut production cost and address changing customer and market requirements (Herron *et al*., 2016). The technology of designing catalysts is now shifting away from producing mixed chain length oligomers to single chain lengths. The cost of further chemical processing of mixed α-olefins to isolate the desired one is high and time consuming (Sydora, 2018).

The late transition metals research application in oligomerization catalysis attracts intense interest due to their properties. In particular, valence, electronic configuration, ionization potential, ionic radii and greater tolerance towards polar functional groups. Polar functional groups are used in polyolefins to improve on surface properties such as rheology and ease to mix the polyolefins in the end use applications. The polar properties potentially adding value to applicability of polyolefin in the end use product. Early transition metal elements such as

titanium, zirconium, vanadium and chromium and hafnium are mainly used to make homogeneous catalysts (Chen *et al*., 2020).

Homogenous catalysts are less preferred in industrial applications because they are fragile with short lifespan, unstable and not easily separated from reaction mixture after oligomerization (Pelletier & Basset, 2016). Ethylene oligomerization reactions using early transition metal catalysts are hard to improve on properties and expand on applications due to their limitation. They have a low tendency to form oxides and they are easily poisoned unlike late transition metal catalysts making their direct polymerization using polar groups a challenge (Guo *et al*., 2016). A desire to develop catalytic systems with polar functional groups tolerance is a key in addressing the limitations.

When early transition elements are complexed with bidentate and tridentate ligands they can selectively oligomerize ethylene with high efficiency (Kinoshita *et al.*, 2011). A chromium complexed with monoanionic tridentate phenoxy–imine (O,N,N) ligand is more active catalyst(de Oliveira *et al*., 2021). Mitsui chemical company developed phenoxy-imine (O, N) ligand for making metal complexes for control of polymerization and oligomerization of ethylene (Kinoshita *et al.*, 2011). The catalyst when activated increased efficiency of polymerization. The working of the catalysts, showed remarkable electronic flexibility of phenoxy-imine ligands in insertion process of ethylene oligomerization using a catalytic early transition metal complex (Matsugi & Fujita, 2008). This lead to upsurge in early transition metals with phenoxy-imine complexes and related ligands application in oligomerization reactions of ethylene (Kinoshita *et al*., 2011).

Apart from heterogeneous nature, late transition metal can be used as catalysts for binuclear catalytic systems (Cao et al., 2023), dienes polymerizing systems, cyclic olefins (Lu *et al*., 2014), allenes (Bai *et al*., 2009), norbornene (Lee *et al*., 2009) and styrenes (Camacho & Guan, 2010). Late transition metal catalysts are advantageous due to ease of preparation,

good stability and high catalytic activity (Gansukh *et al*., 2020). Besides the advantages, the catalyzed products of late transition metal complexes can be linear or branched (Qiu *et al*., 2024). The properties create a desire to develop catalytic systems based on late–transition metals.

CHAPTER THREE

COMPUTATIONAL METHODOLOGY

3.1 STUDY DESIGN

In this work, the late transition metals Pd^{2+}, Co^{2+}, Ni^{2+} and Fe^{2+} were varied in metal complexes. The ligands under investigation were hemilabile N^N-donor type of Ll-[2-(3,5-dimethyl-pyrazol-1-yl)-ethanol] and $[(L_2)_2CoCl_2]$ and L2=[1-(2-chloro-ethyl) -3,5-dimethyl-1H-pyrazole] alkylpyrazolyl ligands. After modeling and conformer search using Gaussian Suite of programs (www.https://gaussian.com/gaussian16) and PC Model version 10.0700 **(**WWW.serenasoft.com.**,** 2020) respectively, quantum chemical calculations were done on low and high spins states models as per guidelines of GaussView 6.1 program (Foresman J.B, 2015). A series of Gaussian optimizations and frequency calculations were done on selected PCM 10 model located conformers.

3.2 GEOMETRY OPTIMIZATIONS AND FREQUENCY CALCULATION

The DFT functionals B3LYP and B3PW91 with 6-311G (d, p) (a relatively low-cost basis set) and LANL2DZ basis sets for nonmetals and for metals respectively were used for first optimization with frequency calculations. Further optimization and frequency calculations were done using a bigger basis set of 6-311+G (2d, p) for nonmetals and LANL2DZ for metals in dichloromethane (DCM) solution phase. This was to allow the second calculation to start from a reasonable accurate value. For the two model chemistries, the route section # opt= (calcfc, tight) freq B3LYP or B3PW91/gen pseudo=read scrf= (SMD, solvent=dichloromethane) nosymm scf=xqc int=ultrafinegrid iop (9/40=3) Basis sets: 6-311+G (2d, p) for non-metals and LanL2DZ for metals was used.

The optimized structures were examined for their corresponding energies and compared within and across the model chemistries. Structures with lowest energy were isolated for further calculations. In all cases, the default methods were used. For closed-shell systems, a

spin restricted model was employed, whereas for open-shell systems a spin-unrestricted model was employed. All geometries and energies for second optimization, were calculated in dichloromethane solution using the SMD implicit solvation model for solvation effects. Optimized geometries were confirmed to be minima with zero imaginary frequencies. Computed vibrational frequencies were calculated using B3LYP level of theory and scaled using 0.9804 factor (Foresman J.B, 2015). Other subsequent calculations were carried out after second optimization.

3.3 DETERMINATION OF LOW ENERGY CONFORMERS

Using output file (.log file) the structures were examined for normal termination and convergence. Corresponding energy of the equilibrium structures were documented. The route section for the single point energy was, b3lyp/6-311+G (2d, p) SCRF (SMD, solvent=Dichloromethane) SCF=Tight.

3.4 BOND PARAMETERS AND CORDINATION GEOMETRY

Bond lengths, and bond angle for Lowest energy conformers (LECs) per pyrazolyl based metal complex were determined using GaussView 6.1 program. Definition of coordination geometry was done depending on dimension of angle, visual analysis and VSEPR criteria of judgement.

3.5 DETERMINATION OF ELECTROSTATIC POTENTIAL MAPS.

The optimization frequency calculation output check file was converted to formatted check file, then another optimization frequency calculation using a key word population = full (Pop= Full) was used to display electrostatic potential maps. Higher and lower values of electrostatic potential and Mulliken charges on the metal atom were documented.

3.6 DETERMINATION OF POLARIZABILITY

Polarizability was computed after optimization frequency calculation. Redundant internal coordinates were taken and resubmitted to high performance computing calculations using with a key word polar=gamma in the route section. Isotropic polarizability values extracted from .log file were document.

3.7 DETERMINATION OF DIPOLE MOMENTS

Dipole moment, mean polarizability and first order hyper-polarizability (nonlinear optical) (NLO) properties of complexes, were computed using DFT functional B3LYP and B3PW91 using LanL2DZ basis set for metal cation and 6-311+G (2d, p) basis set for all the remaining atom. Dipole moments were extracted from .log file output of the single point energy calculation for pyrazolyl–metal complexes. Using GaussView results, selection of summary was done and the magnitude of dipole moments in Debye were extracted for documentation.

3.8 FRONTIER MOLECULAR ORBITALS AND CATALYTIC DESCRIPTORS ANALYSIS

Frontier molecular orbitals which are mathematical functions describing behavior of electron(s) within a molecule were generated on the surface of the molecular structures. Highest Occupied Molecular Orbital (HOMO) and Lowest Unoccupied Molecular Orbital (LUMO) energies were determined by TD-DFT method. The HOMO-LUMO energy gap calculations were done to evaluate the energy behavior of metal complexes. To visualize the HOMOs and LUMOs of the transition metal complexes, GaussView 6.0 program was used.

The singlet excitation calculation was done through route section # td= (Singlets, nstates=400, root=1) b3lyp/6-311+G (2d, p) SCRF (SMD, solvent=dichloromethane) Pop=NPA Density=Current int=ultrafinegrid iop (9/40=3). Check files from singlet excitation were formatted by opening them in GaussView 6.1 program and clicked on molecular orbital (MO) editor icon for a new MO window to pop up. The method changed to load MOs from

excited Fchk file. The Fchk files were loaded and HOMO-LUMO visualized by clicking type of orbitals and waited for them to form. Ionization potential, electron affinity, chemical potential, chemical hardness, chemical softness, electronegativity and electrophilicity index properties were calculated from HOMO and LUMO energies.

3.8.1 Calculation of HOMO-LUMO Gap (EG)

HOMO-LUMO energy gap was calculated as a difference between HOMO energy (E_{HOMO}) and LUMO energy (E_{LUMO})

$$(EG) = E_{HOMO} - E_{LUMO}$$

3.8.2 Calculation of Ionization Potential (IP)

Ionization potential which is energy required to remove an electron from atom or molecule helps in determining reactivity of a material. It was calculated as

$$IP = -E_{HOMO}$$

3.8.3 Calculation of Electron Affinity (EA)

Electron affinity which is the energy released when an electron is added to a compound to form a negative species from a neural one in gas phase. It was calculated as

$$\text{Electron affinity is} = -E_{LUMO}$$

3.8.4 Calculation of Electronegativity (χ)

Electronegativity which is the energy of ions compared to neutral atom. In a molecule with two atoms, an atom with net negative charge was compared with other more electronegative. The electronegativity values were determined as

$$\text{Electronegativity } (\chi) = (IP + EA)/ 2$$

3.8.5 Calculation of Chemical Potential (μ)

Chemical potential which is partial molar free energy is energy that can be absorbed or released during a chemical reaction. It was calculated as

$$\text{Chemical Potential } (\mu) = -(IP + EA)/2$$

3.8.6 Calculation of Chemical Hardness (η)

To assign values to chemical hardness, the calculation was done as below

$$\text{Chemical Hardness } (\eta) = (IP - EA)/2$$

3.8.7 Calculation of Global Electrophilicity Index (ω)

Electrophilicity measures stabilization in energy when a molecule acquires an additional electronic charge from the environment. It was calculated as

$$\text{Global Electrophilicity index } (\omega) = \mu 2/ 2\eta$$

3.9 DETERMINATION OF NBOs

Natural bond orbital (NBO) analysis were performed with the Gaussian 16 integrated NBO program (Reed *et al*., 1985). The route section used was, **NBO CALCS**: opt= (calcfc, tight) freq b3lyp/6-311+G (d, p) SCRF (SMD, solvent=Dichloromethane (DCM) Pop= (NBO, SAVENBO) int=ultrafinegrid iop (9/40=3).

3.10 DETERMINATION OF DENSITY OF STATES (DOs)

The singlet excited states output files (.log file) were opened in GaussSum. The frequencies icon was clicked followed by the image. To get DOs spectra the Dos icon was highlighted then orbitals were chosen.

3.11 DETERMINATION OF ZERO-POINT ENERGY CORRECTIONS

Zero-point energy (ZPE) corrections calculations in solution using the SMD model were studied using the B3LYP and B3PW91 DFT functional using LanL2DZ basis set for metal atom and 6-311+G (2d, p) basis set for all the remaining atom. Cartesian coordinates for the optimized geometries are provided in Appendix A1.

3.12 DETERMINATION OF BASIS SET SUPERPOSITION ERROR

Basis set superposition error (BSSE) is a limitation due to usage of incomplete basis set. This results into the description of an atom or molecular fragment under study improved by basis function of other atoms or fragments having a complete basis set. Estimation of BSSE in a counterpoise correction interaction energy between fragments A and B, in the molecule, the energy of molecule AB was computed as in equation 3.1, where A and B are described in their own basis sets.

$$\Delta E = E_{AB} - E_A - E_B \tag{3.1}$$

Due to incompleteness of basis set A, energy of A was improved by the basis set of AB in the molecule. This gives a better interaction of energy, equation 3.2.

$$\Delta E = E_{AB} - E_{A(AB)} - E_{B(AB)} \tag{3.2}$$

From equation 3.2., it was concluded that the three calculations; molecule AB, fragment A and fragment B were performed with the full basis set for AB. Since the finite basis set EA(AB) < EA and EB(AB) < EB, AE from equation 3.2 was less than values of 3.1.

CHAPTER FOUR

RESULTS AND DISCUSSION

4.1 THEORETICAL CALCULATIONS

Theoretical structures of the Fe1, Co1, Ni1, Pd1, Co2, and Ni2 metal complexes were studied using Gaussian 16 suite of programs described in details in chapter three (Foresman J.B., 2015). ChemDraw structures of the complexes are shown in Figure 4.1.

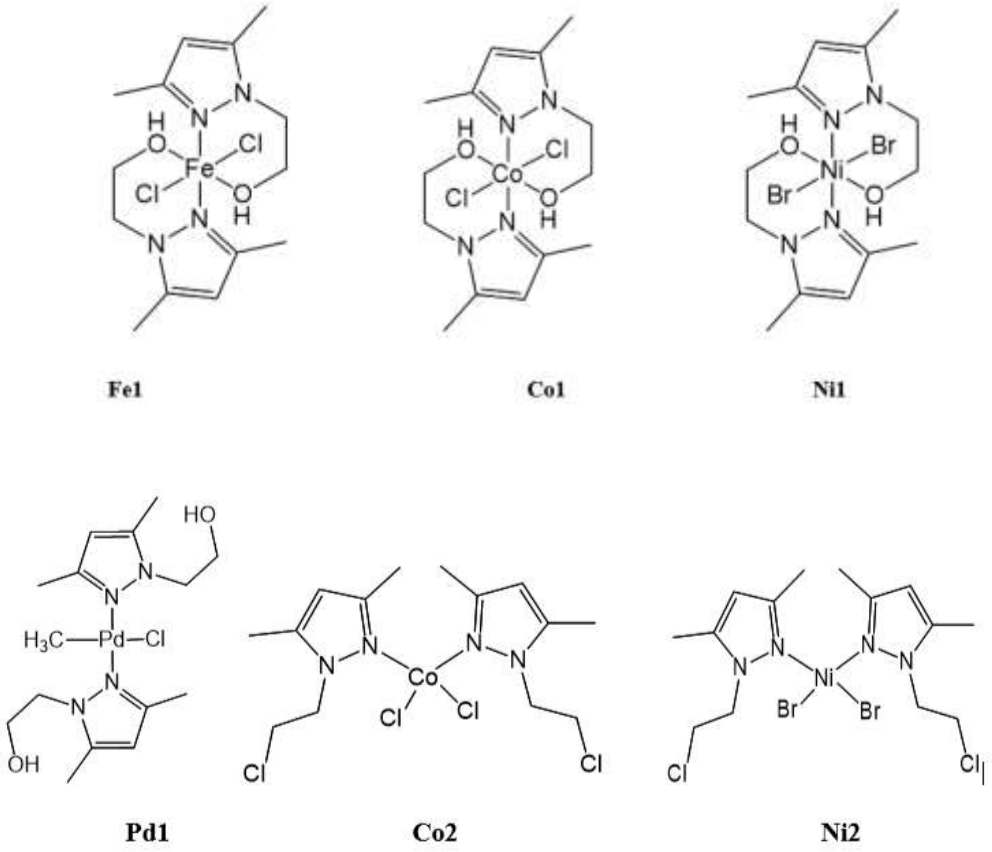

Figure 4.1: ChemDraw structures of pyrazolyl-based metal complexes.
Source: Researcher (2024)

Structures of two ligands, 2-(3, 5-dimethyl-pyrazol-1-yl)-ethanol (L1) and 1-(2-chloro-ethyl)-3,5-dimethyl-1H-pyrazole (L2) that coordinate to the Fe^{2+}, Co^{2+}, Ni^{2+}, and Pd^{2+} metal cations to form Fe1, Co1, Ni1, Pd1, Co2, and Ni2 transition metal complexes shown in Figure 4.2.

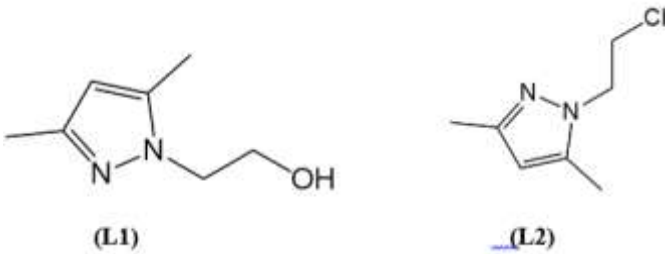

Figure 4.2: The structures of 2-(3,5-dimethyl-pyrazol-1yl)-ethanol (L1) and 1-(2-chloro-ethyl)-3,5-dimethyl-1H-pyrazole (L2) ligands.
Source: Researcher (2024)

The ground electronic spin states of metal complexes based on Fe^{2+}, Co^{2+}, Ni^{2+}, and Pd^{2+} ions were found to be the same as those of bare metal cation, quintet, quartet, triplet, and singlet, respectively. Relative energies of Fe1, Co1, Ni1, Pd1, Co2, and Ni2 metal complexes computed for various possible spin states of Fe^{2+}, Co^{2+}, Ni^{2+}, and $Pd1^{2+}$ are summarized in Table 4.1. In all cases, spin contamination of the metal complexes was eliminated in the geometry and wavefunction optimization procedures.

Table 4.1: Relative energies of the various spin states of transition metal complexes in their ground-state conformations at STP in Hartrees.

Metal Complex	Multiplicity	Ground-state Structures	Gibbs Free Energy (Hartrees)[a]	ΔG^{STP} (milliHartrees)[a]
Fe1 High spin	5		– 1961.7701	0.0
Fe1 Low spin	1		– 1961.6945	– 75.6
Co1 High spin	4		– 1983.3686	0.0
Co1 Low spin	2		– 1983.3505	– 18.1

Source: Researcher (2024)

Table 4.1. (continued) Relative energies of the various spin states of transition metal complexes in their ground-state conformations at STP in Hartrees.

Metal Complex	Multiplicity	Ground-state Structures	Gibbs Free Energy (Hartrees)[a]	ΔG^{STP} (milliHartrees)[a]
Ni1 High spin	3		– 6235.4256	0.0
Ni1 Low spin	1		– 6235.3895	– 36.1
Co2 High spin	4		– 2752.1354	0.0
Co2 Low spin	2	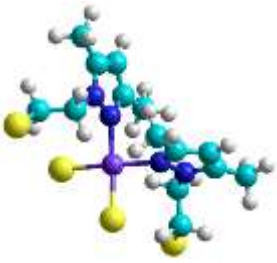	– 2752.1040	– 31.4

Table 4.1. (continued) Relative energies of the various spin states of transition metal complexes in their ground-state conformations at STP in Hartrees.

Complex	Multiplicity	Ground-state Structures	Gibbs Free Energy (Hartrees)[a]	ΔG^{STP} (milliHartrees)[a]
Pd1 High spin	1		– 1544.6731	0.0
Ni2 High spin	3	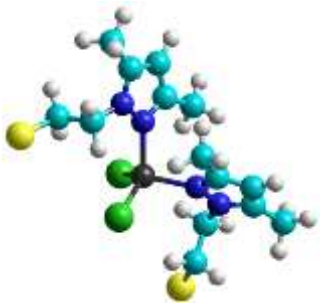	– 7004.1810	0.0
Ni2 Low spin			– 7004.1738	– 7.2

[a]Structures and energies are calculated at the B3LYP level of theory using LanL2DZ basis set for metal atoms and 6-311+G (2d, p) basis set for non-metal atoms. (Color codes: Carbon-cyan, Hydrogen – white, Nitrogen – blue, Oxygen – red, Chlorine – yellow, Bromine – dark green, Iron – light blue, Cobalt – purple, Nickel – black, Palladium – brown).

Source: Researcher (2024)

The B3LYP ground-state structures of the Fe1, Co1, Ni1, Pd1, Co2, and Ni2 metal complexes are shown in Figure 4.3.

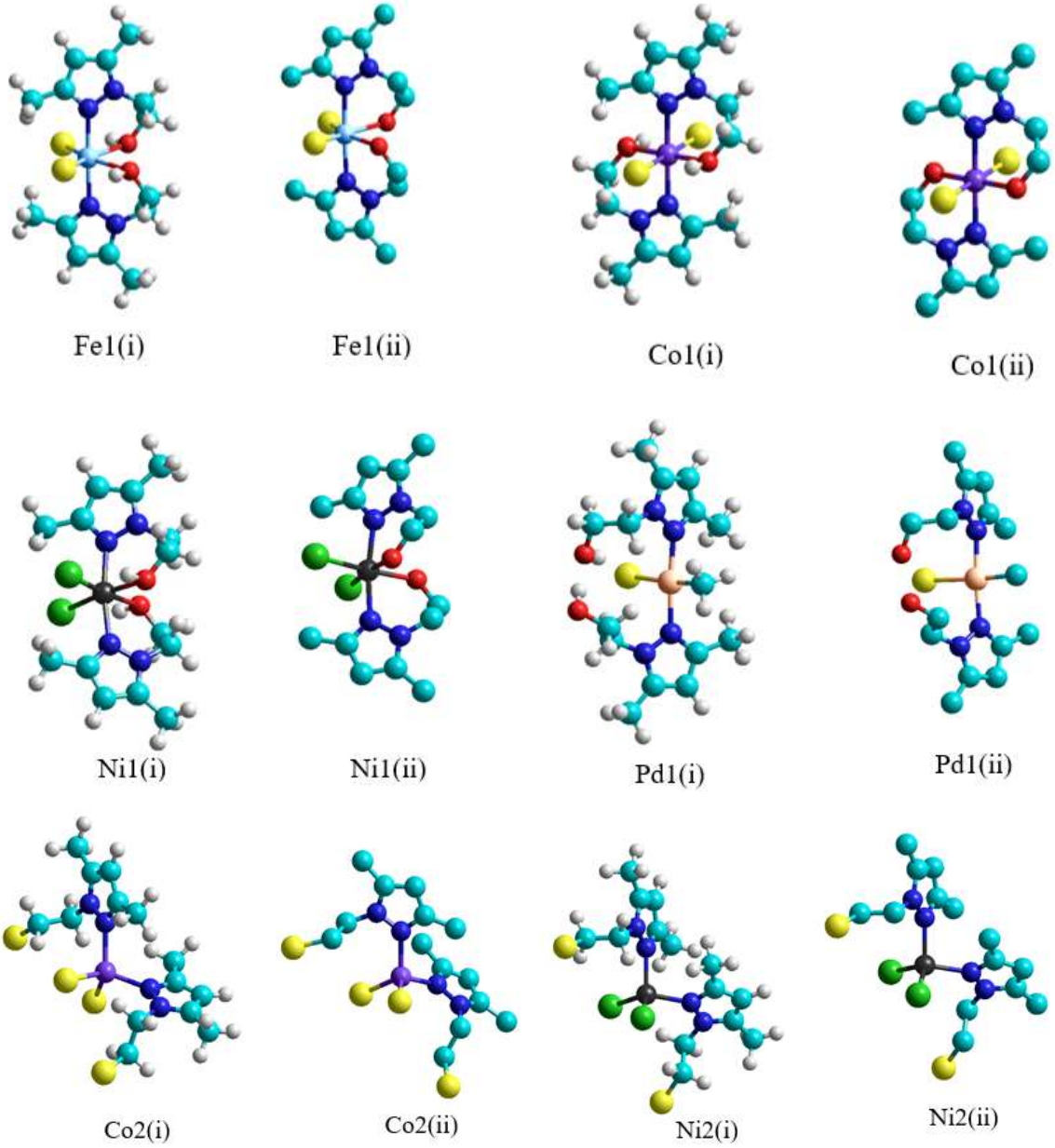

Figure 4.3: B3LYP optimized geometries of the Fe1, Co1, Ni1, Pd1, Co2, and Ni2 complexes (i) B3LYP optimized geometries of the Fe1, Co1, Ni1, Pd1, Co2, and Ni2 complexes using B3LYP functional and LanL2DZ basis set for metal atom and 6-311+G (2d, p) basis set for all the remaining atoms.(Color codes: Carbon (C) – cyan, Hydrogen (H) – white, Nitrogen (N) – blue, Oxygen (O) – red, Chlorine (Cl) – yellow, Bromine (Br) – dark green, Iron (Fe) – light blue, Cobalt (Co) – purple, Nickel (Ni) – black, Palladium (Pd1) – brown). (ii) All hydrogen atoms omitted for clarity.

Source: Researcher (2024)

Ground-state structures of the Fe1, Co1, Ni1, Pd1, Co2, and Ni2 metal complexes at the B3PW91 level of theory are highly parallel to those found using B3LYP theory. Figure 4.4. shows the trends in the average bond distances calculated using B3LYP and B3PW91 levels of theory.

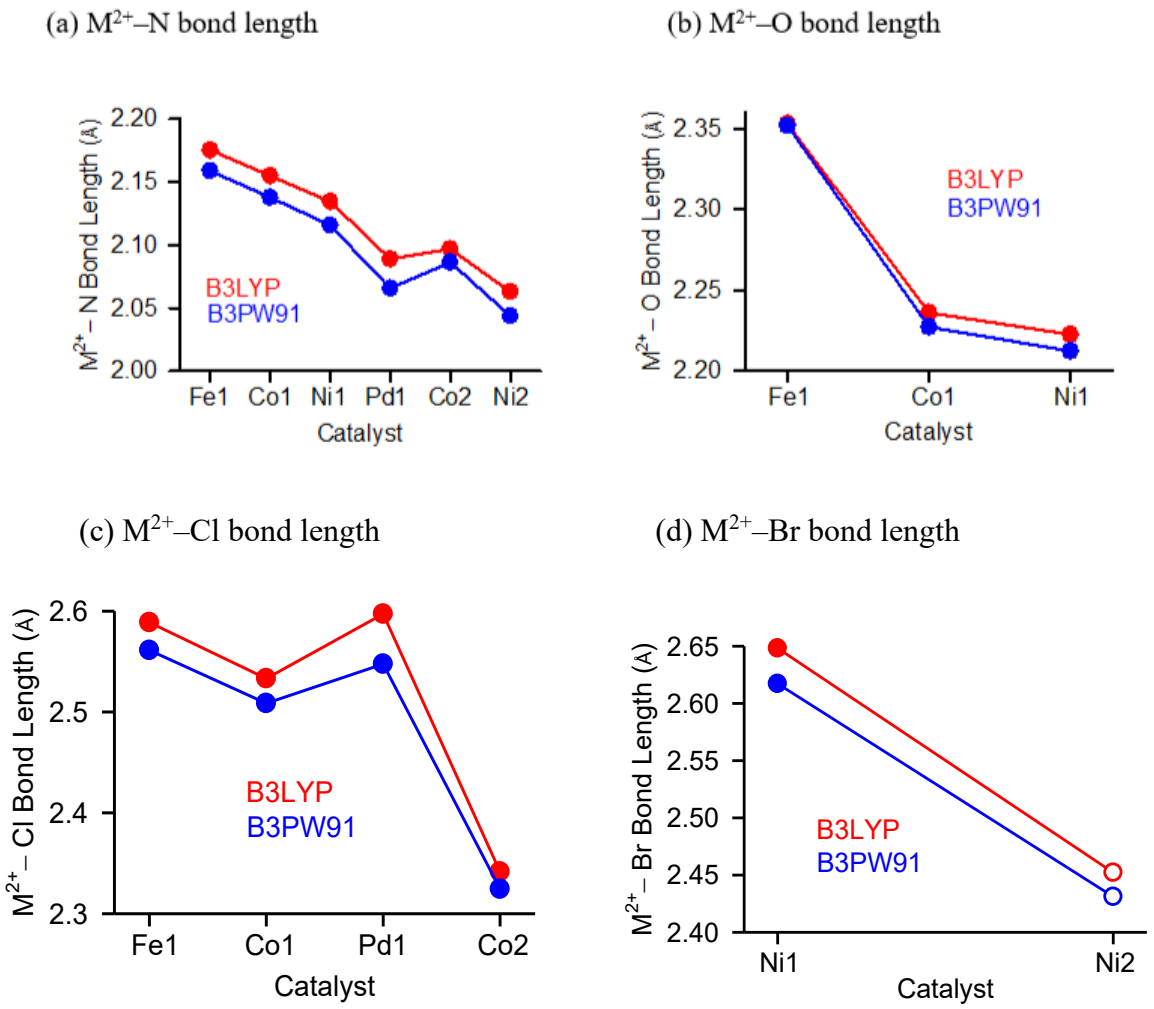

Figure 4.4. Variations in the average bond lengths in Fe1, Co1, Ni1, Pd1, Co2, and Ni2 metal complexes calculated using B3LYP and B3PW91 levels of theory.
Source: Researcher (2024)

Relevant structural details of the B3LYP and B3PW91 geometry optimized structures for the Fe1, Co1, Ni1, Pd1, Co2, and Ni2 metal complexes are listed in Table 4.2 and Table 4.3, respectively.

Table 4.2: Select geometrical parameters of the B3LYP ground-state structures of the Fe1, Co1, Ni1, Pd1, Co2 and Ni2 metal complexes[a]

Complex	Bond Lengths (Å)	Bond Angles (∠) in degrees
Fe1	Fe–N = 2.1753 (2)	∠NFeO = 82.5 (2), 95.9 (2), ∠NFeCl = 87.7, 91.3 (3)
	Fe–O = 2.3528 (2)	∠NFeN = 177.1, ∠OFeCl = 74.0 (2), 154.6 (2)
	Fe–Cl = 2.5888 (2)	∠OFeO = 82.1, ∠ClFeCl = 130.8
Co1	Co–N = 2.1548 (2)	∠NCoO = 84.3 (2), 95.7 (2), ∠NCoCl = 90.0 (4)
	Co–O = 2.2359 (2)	∠NCoN = 180.0, ∠OCoCl = 77.8 (2), 102.2 (2)
	Co–Cl = 2.5332 (2)	∠OCoO = 180.0, ∠ClCoCl = 180.0
Ni1	Ni–N = 2.1345 (2)	∠NNiO = 87.0 (4), ∠NNiBr = 89.8 (2), 95.3 (2)
	Ni–O = 2.2224 (2)	∠NNiN = 171.1, ∠ONiBr = 78.0, 109.9, 172.0 (2)
	Ni–Br = 2.6482 (2)	∠ONiO = 94.1, ∠BrNiBr = 109.9
Pd1	Pd –N = 2.0889 (2)	∠NPdCl = 91.2 (2), ∠NPdN = 175.8
	Pd –Cl = 2.5972	∠NPdC = 88.8 (2), ∠ClPdC = 176.4
	Pd –C = 2.0433	
Co2	Co–N = 2.0969 (2)	∠NCoCl = 100.3 (2), 119.2 (2)
	Co–Cl = 2.3415 (2)	∠NCoN = 110.5, ∠ClCoCl = 108.4
Ni2	Ni–N = 2.0629 (2)	∠NNiBr = 99.0 (2), 118.5 (2)
	Ni–Br = 2.4522 (2)	∠NNiN = 99.5, ∠BrNiBr = 121.3

[a]Theoretically determined geometrical parameters using B3LYP functional and LanL2DZ basis set for metal atom and 6-311+G (2d, p) basis set for all the remaining atoms. Average values are given for similar bond distances or angles; degeneracies are listed in parentheses for values that differ significantly such that more than one value is needed to describe the bond angle or bond distance. Bond angles (∠) are given in degrees (^{O}) and bond lengths in angstroms (Å).

Source: Researcher (2024)

Table 4.3: Select geometrical parameters of the B3PW91 ground-state structures of the Fe1, Co1, Ni1, Pd1, Co2 and Ni2 metal complexes[a]

Complex	Bond Lengths (Å)	Bond Angles (∠)
Fe1	Fe–N = 2.1588 (2)	∠NFeO = 82.5 (2), 96.1 (2), ∠NFeCl = 88.3, 91.1 (3)
	Fe–O = 2.3517 (2)	∠NFeN = 177.8, ∠OFeCl = 73.6 (2), 154.4 (2)
	Fe–Cl = 2.5612 (2)	∠OFeO = 82.3, ∠ClFeCl = 131.4
Co1	Co–N = 2.1377 (2)	∠NCoO = 84.5 (2), 95.5 (2), ∠NCoCl = 90.0 (4)
	Co–O = 2.2271 (2)	∠NCoN = 180.0, ∠OCoCl = 77.4 (2), 102.6 (2)
	Co–Cl = 2.5086 (2)	∠OCoO = 180.0, ∠ClCoCl = 180.0
Ni1	Ni–N = 2.1156 (2)	∠NNiO = 87.0 (4), ∠NNiBr = 89.7 (2), 95.3 (2)
	Ni–O = 2.2122 (2)	∠NNiN = 171.2, ∠ONiBr = 77.8 (2), 172.3 (2)
	Ni–Br = 2.6172 (2)	∠ONiO = 94.7, ∠BrNiBr = 109.7
Pd1	Pd –N = 2.0657 (2)	∠NPdCl = 91.4 (2), ∠NPdN = 175.5
	Pd –Cl = 2.5476	∠NPdC = 88.7 (2), ∠ClPdC = 176.7
	Pd –C = 2.0286	
Co2	Co–N = 2.0864 (2)	∠NCoCl = 100.4 (2), 119.4 (2)
	Co–Cl = 2.3245 (2)	∠NCoN = 110.2, ∠ClCoCl = 108.2
Ni2	Ni–N = 2.0437 (2)	∠NNiBr = 98.4 (2), 118.4 (2)
	Ni–Br = 2.4311 (2)	∠NNiN = 100.0, ∠BrNiBr = 122.2

[a]Theoretically determined geometrical parameters using B3PW91 functional and LanL2DZ basis set for metal atom and 6-311+G(2d,p) basis set for all the remaining atoms. Average values are given for similar bond distances or angles; degeneracies are listed in parentheses for values that differ significantly such that more than one value is needed to describe the bond angle or bond distance. Bond angles (∠) are given in degrees (^{O}) and bond lengths in angstroms (Å).

Source: Researcher (2024)

Cartesian coordinates of the B3LYP and B3PW91 optimized geometries of the ground-state structures of the Fe1, Co1, Ni1, Pd1, Co2, and Ni2 metal complexes are shown in Appendix A.1. The B3LYP scaled vibrational frequencies, IR activities and Raman activities for the ground-state structures of the Fe1, Co1, Ni1, Pd1, Co2, and Ni2 metal complexes are also listed in Appendix A.2.

4.2 RELATIVE ENERGIES OF THE SPIN STATES

The relative energies of all possible spin states of the Fe1, Co1, Ni1, Pd1, Co2, and Ni2 transition metal complexes were carefully evaluated to determine the spin states of the ground-state species. In this work, the following spin states were examined: quintet and singlet for Fe1, quartet and doublet for Co1 and Co2, triplet and singlet for Ni1 and Ni2, and singlet for Pd1. Relative energies of the Fe1, Co1, Ni1, Pd1, Co2, and Ni2 metal complexes computed for the various possible spin states of the Fe^{2+}, Co^{2+}, Ni^{2+}, and Pd^{2+} are summarized in Table 4.1.

Ground-state structures of the both the high spin and low spin states of the metal complexes are also shown in Table 4.1. In all the five complexes with different spin states shown in Table 4.1, the high spin structures were predicted to be lower in energy by about -75.6, -18.1, – 36.1, – 31.4, – 7.2 millihartres, for Fe1, Co1, Ni1, Co2, and Ni2 complexes, respectively. The Pd1 complex had only one spin state, singlet state at ground state. Energy differences of the sizes shown in Table 4.1 indicates that, given the experimental conditions and equilibrium between the two spin states, only the high spin states will lead to the synthesis of products, a result in agreement with related experimental results where Fe1, Co1, Ni1, Co2, and Ni2 complexes were found to be paramagnetic in nature (Ainooson *et al*., 2011).

4.3 DFT–SIMULATED STRUCTURES

Structures and structural details of metal complexes calculated at the B3LYP level of theory using LanL2DZ basis set for metal atoms and 6-311+G (2d, p) basis set for non-metals are shown in Figure 4.3 and Table 4.2, respectively. As shown in Figure 4.3, in all the metal complexes, the M^{2+} cation, where M = Fe, Co, Ni, and Pd, binds to the nitrogen, oxygen, chlorine, and/or bromine lone pair(s) regardless of the identity of the metal cation. The Fe1, Co1, Ni1, Pd1, Co2, and Ni2 metal complexes adopt coordination geometries that closely approach the ideal geometries predicted by the valence shell electron pair repulsion (VSEPR)

model (Hargittai & Chamberland, 1986). The B3PW91 optimized geometries of the Fe1, Co1, Ni1, Pd1, Co2, and Ni2 complexes using B3PW91 functional are as shown in Figure 4.5. below. Relevant geometrical parameters are shown in Table 4.3. As can be seen from Figure 4.3 and Figure 4.5, B3LYP and B3PW91 levels of theory show similar results. Both theoretical levels of theory have been found to perform best for Fe, Co, Ni, and Pd transition metals (Ngcobo *et al*., 2022). Therefore, the discussion that follows focuses on the B3LYP results with comparisons to B3PW91 theory.

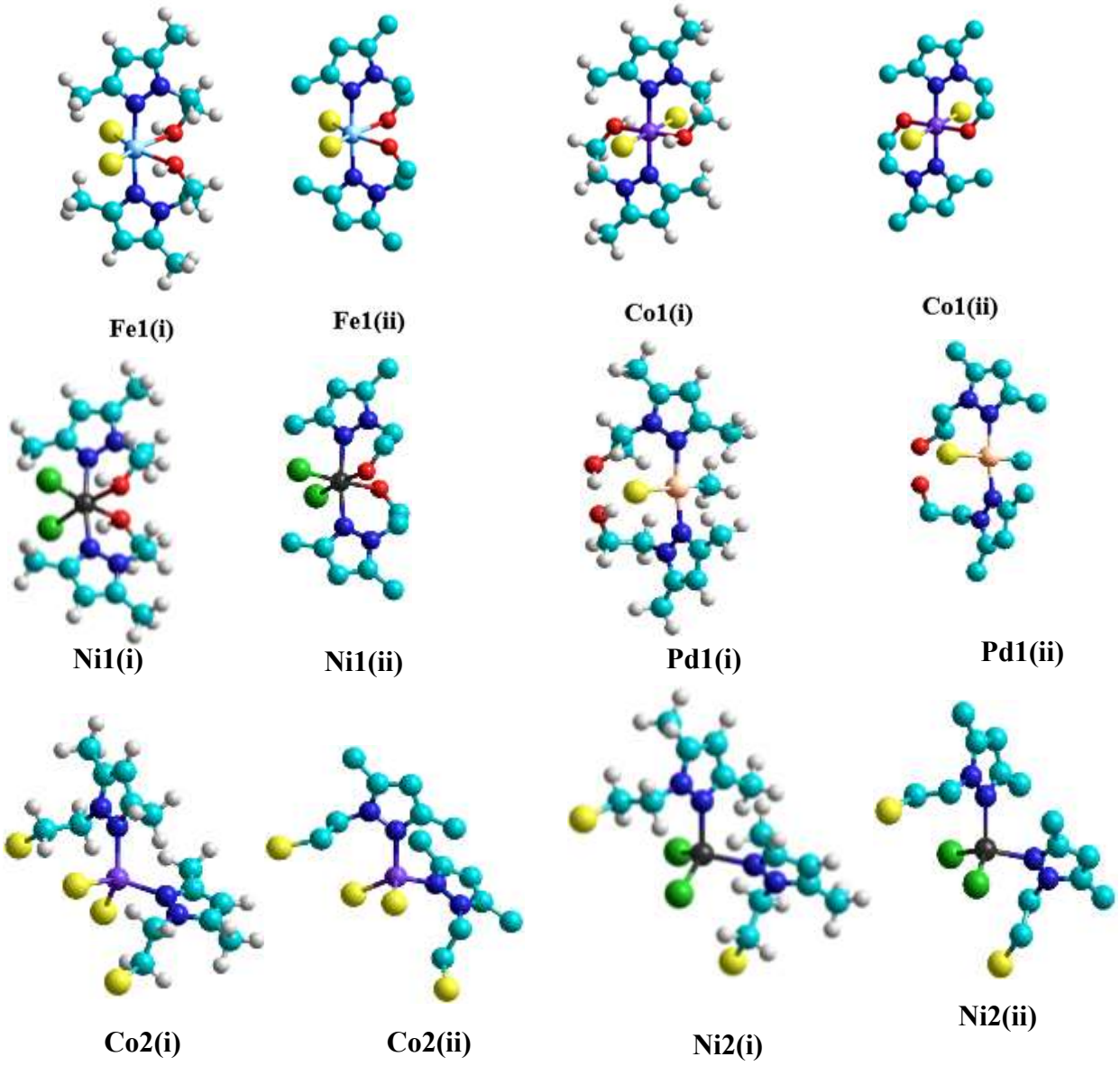

Figure 4.5. B3PW91 optimized geometries of the Fe1, Co1, Ni1, Pd1, Co2, and Ni2 complexes (i) B3PW91 optimized geometries of the Fe1, Co1, Ni1, Pd1, Co2, and Ni2 complexes using B3PW91 functional and LanL2DZ basis set for Pd1 metal atom and 6-311+G (2d, p) basis set for all the remaining atoms. (Color codes: Carbon (C) – cyan, Hydrogen (H) – white, Nitrogen (N) – blue, Oxygen (O) – red, Chlorine (Cl) – yellow, Bromine (Br) – dark green, Iron (Fe) – light blue, Cobalt (Co) – purple, Nickel (Ni) – black, Palladium (Pd1) – brown). (ii) All hydrogen atoms omitted for clarity.

Source: Researcher (2024)

It's important to mention that X-ray structures of the metal complexes were obtained only for Ni1, Pd1, Co2, and Ni2 metal complexes and hence these are the only structures that will be discussed in this section. In general, the B3LYP geometry optimized structures of the Ni1, Pd1, Co2, and Ni2 metal complexes are similar to the experimentally determined structures obtained by X-ray crystallography (Ainooson *et al*., 2011). The mean absolute deviation

(MAD) between theory and X-ray data for metal-nitrogen bond lengths in Pd1, Ni1, Co2, and Ni2 is 0.06±0.01 Å and 0.04±0.002 Å for B3LYP and B3PW91, respectively. For the metal-chlorine bond distances in Pd1 and Co2, the MAD between theory and experiment is 0.12±0.01 Å and 0.09±0.003 Å for B3LYP and B3PW91, respectively. The MAD values suggest a good agreement between the experimentally and theoretically determined bond lengths for the metal complexes. The MAD between theory and experiment for all the bond angles in Pd1 complex is 1.4±0.9^{O} and 1.5±0.9^{O} for B3LYP and B3PW91, respectively. In Ni1complex, the MAD between theory and experiment for all the bond angles is 2.8±3.0^{O} and 3.1±3.3^{O} for B3LYP and B3PW91, respectively. For Co2 metal complex, the MAD between theory and experiment for all the bond angles is 10.8±3.7^{O} and10.8±3.7^{O} for B3LYP and B3PW91, respectively whereas in Ni2 metal complex, the MAD between theory and experiment for all the bond angles is 2.9±1.7^{O} and 3.3±1.8^{O} for B3LYP and B3PW91, respectively. The MAD values further suggest that theoretically determined structures are in good agreement with the experimentally determined X-ray structures.

4.3.1 Structures of the Fe1, Co1, and Ni1 Metal Complexes

The B3LYP ground-state structures of the Fe1, Co1, and Ni1 metal complexes are shown in Figure 4.3. Relevant structural details of the B3LYP geometry optimized structures for the Fe1, Co1, and Ni1 metal complexes are listed in Table 4.2. The Fe1, Co1, and Ni1 metal complexes adopt distorted octahedral coordination geometries. The equatorial plane is formed by two oxygen atoms from the two bidentate ligands and two chlorine atoms for Fe1 and Co1 (two bromine atoms for Ni1). The apical positions are occupied by two nitrogen atoms of the two bidentate ligands with the N–M^{2+}–N angle spanning 177.1^{O}, 180.0 ^{O}, and 171.1 ^{O} for Fe1, Co1, and Ni1, respectively, where M = Fe, Co, and Ni. The nitrogen atoms of the bidentate ligands are cis to each other, and the oxygen atoms of the bidentate are also cis with respect to each other for Fe1 and Ni1 complexes whereas for the Co1 metal complex,

both the nitrogen atoms and oxygen atoms of the bidentate ligands are trans to each other. The six-membered metallacycle, M^{2+}–N1–N3–C1–C3–O1 has a distorted envelope conformation whereas the heterocyle, M^{2+}–N2–N4–C2–C4–O2 most closely approaches a boat conformation. In all the three metal complexes, the M^{2+}–N bond lengths predicted by B3LYP theory decrease from Fe^{2+} (2.1753 Å) to Co^{2+} (2.1548) to Ni^{2+} (2.1345) as shown in Figure 4.6a. Again, the M^{2+}–O bond lengths predicted by B3LYP theory decrease from Fe^{2+} (2.3528 Å) to Co^{2+} (2.2359 Å) to Ni^{2+} (2.2224 Å) as shown in Figure 4.6b. Parallel behavior is found for the B3PW91 structures of the analogous metal complexes (see Table 4.3). Trends across the two levels of theory in terms of the bond lengths are very similar with B3PW91 bond lengths generally being the shortest and the B3LYP the longest (see Tables 4.2 and 4.3).

(a) M^{2+}–N bond length

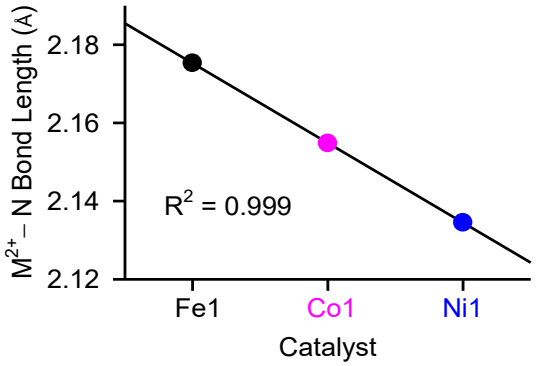

(b) M^{2+}–O bond length

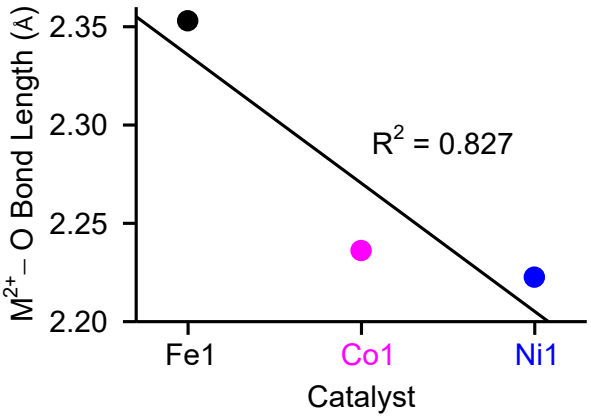

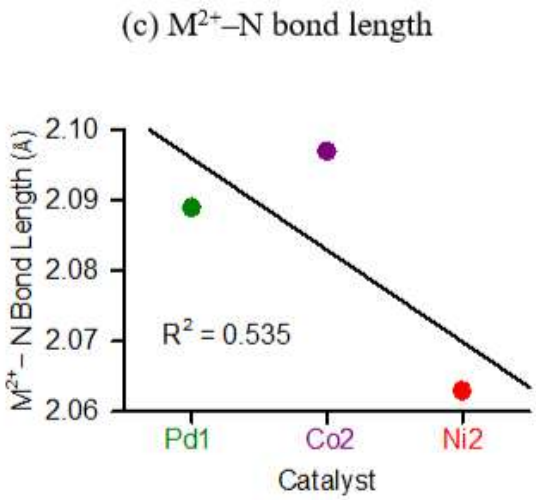

Figure 4.6. Trends in the average M^{2+}–N and M^{2+}–O bond distances in B3LYP optimized geometries of the Fe1, Co1, Ni1, Pd1, Co2, and Ni2 metal complexes.
Source: Researcher (2024)

4.3.2 Structure of the Pd1 Metal Complex

The geometry around the palladium atom in Pd1 is a distorted square planar as shown in Table 4.2. The ∠NPdCl, ∠NPdC, ∠NPdN, and ∠ClPdC bond angles are 91.2°, 88.8°, 175.8°, and 176.4°, respectively, deviate from the expected 90° and 180° for a perfect square planar and thus demonstrate a distorted square planar. Two pyrazole ligands bind to the palladium cation through the nitrogen atom in a monodentate fashion. One chlorine atom and one methyl group complete the coordination sphere around the metal center with the -CH_2CH_2OH pendant arm of the pyrazole hanging uncoordinated. The two pyrazole ligands bound to the palladium cation are cis to each other. The Pd–N, Pd–Cl, and Pd–C bond lengths in Pd1 determined at B3LYP level of theory are 2.0889 Å, 2.5972 Å and 2.0433 Å, respectively, being typical for this kind of compounds (Ainooson *et al*., 2011). Nearly parallel behavior is found for Pd1 structure determined at B3PW91 theory as shown in Figure 4.5. Trends across the two levels of theory are generally systematic such that the B3PW91 bond lengths are shortest and B3LYP the longest as observed for Fe1, Co1, and Ni1.

4.3.3 Structures of the Co2 and Ni2 Metal Complexes

As shown in Figure 4.3, the Co2 adopts an almost perfect tetrahedral coordination geometry whereas the Ni2 complex adopts a distorted tetrahedral geometry. In both cases, the bond angles deviate from 109.5^{O} for a perfect tetrahedral (see Tables 4.2). Two pyrazole ligands bind to the metal center through the nitrogen atom in a monodentate fashion with the-CH_2CH_2Cl pendant arm being uncoordinated. Two chloro ligands complete the coordination in Co2 whereas two bromo ligands complete the coordination in Ni2 compound. The M^{2+}–N bond length determined using B3LYP theory again decreases from Co^{2+} (2.0969 Å) to Ni^{2+} (2.0629 Å) as shown in Figure 4.6c. Analogous behavior is found for B3PW91 structures of Co2 and Ni2 as shown in Table 4.3. Again, B3PW91 predicts the shortest bond lengths whereas B3LYP predicts the longest for Co2 and Ni2 complexes as already observed for the remaining metal complexes.

4.4 SIMULATED CHEMICAL REACTIVITY PARAMETERS

4.4.1 E_{HOMO} and E_{LUMO}

The determination of energies of the HOMO and LUMO are important parameters in quantum chemical calculations. The HOMO is the highest occupied molecular orbital in a given system while the LUMO is the lowest unoccupied molecular orbital. The HOMO and LUMO are called the frontier molecular orbitals (FMOs). The HOMO acts as an electron donor while the LUMO largely acts as the electron acceptor (El-Gammal *et al*., 2014). According to the concept of HSAB, hard acids prefer to coordinate to hard bases and soft acids to soft bases. Soft molecules guarantee properties that the HOMO is relatively high in energy and the LUMO is relatively low, whereas hard molecules have the opposite properties. Chemical reactivity's of the transition metal complexes can be deduced from the HOMO and LUMO values and are shown in Table 4.4. The HOMO-LUMO maps of the corresponding metal complexes are shown in Appendices A.3 and A.4.

Table 4.4: Global reactivity descriptors using B3LYP of the Fe1, Co1, Ni1, Pd1, Co2, and Ni2 metal complexes[a]

	Fe1	Co1	Ni1	Pd1	Co2	Ni2
E_{HOMO}	– 6.55	– 6.65	– 6.25	– 6.02	– 6.98	– 6.69
Ionization Energy	6.55	6.65	6.25	6.02	6.98	6.69
E_{LUMO}	– 0.18	– 0.20	– 0.16	– 1.13	– 0.51	– 0.55
Electron affinity	0.18	0.20	0.16	1.13	0.51	0.55
Energy gap	6.37	6.45	6.09	4.89	6.47	6.14
Electronegativity	3.365	3.425	3.205	3.575	3.745	3.620
Chemical potential	– 3.365	– 3.425	– 3.205	– 3.575	– 3.745	– 3.620
Chemical hardness	3.185	3.225	3.045	2.445	3.235	3.070
Global softness (Ev^{-1})	0.157	0.155	0.164	0.204	0.155	0.163
Global electrophilicity index	1.778	1.819	1.687	2.614	2.168	2.134
NBO charge on M^{2+} metal cation	2.3291	1.7797	1.1685	0.3361	1.7686	1.1575

[a]Theoretically determined global reactivity descriptors using B3LYP functional and LanL2DZ basis set for the metal atoms and 6-311+G (2d, p) basis set for all the remaining atoms. All values are given in electron volts (eV) except for the global softness and are as indicated in parenthesis.

Source: Researcher (2024)

As seen in Table 4.4, the E_{HOMO} and E_{LUMO} are all negative which indicates that the compounds are stable (Yousef, T. A., 2012). The E_{HOMO} of the six metal complexes are – 6.98 eV, – 6.69 eV, – 6.65 eV, – 6.55 eV, – 6.25 eV, and – 6.02 eV for Co2, Ni2, Co1, Fe1, Ni1, and Pd1, respectively. Comparison between the six complexes shows that the energy of the HOMO increases in the order, Co2 < Ni2 < Co1 < Fe1 < Ni1 < Pd1, indicating that the HOMO for Pd1 is relatively higher in energy compared to that of the rest of the complexes, implying that Pd1 is a good electron donor. The lower HOMO energy value for Co2 shows that the compound donating ability is the weakest. The E_{LUMO} of the six metal complexes is – 1.13 eV, – 0.55 eV, – 0.51 eV, – 0.20 eV, – 0.18, and – 0.16 eV for Pd1, Ni2, Co2, Co1, Fe1, and Ni1, respectively. The LUMO values indicate that the complexes have the ability to receive electron(s). In terms of the energy, the energy of the LUMO in these complexes is

increasing in this order, Pd1 < Ni2 < Co2 < Co1 < Fe1 < Ni1 in general. Those with Ligand L1 the trend is Pd1 > Fe1 > Co1 > Ni1 while for the L2 based, the trend is Ni2 > Co2. In general, the trend indicates that the LUMO for Pd1 is relatively low in energy compared to that of the remaining compounds. According to this trend, Pd1 has the highest ability to receive electrons.

4.4.2 Energy Gap (*Egap*)

The energy gap is the energy difference between the ionization potential (I) and the electron affinity (A), *Equation* 4.1. (El-Gammal *et al*., 2012).

$$Energy\ gap, E_{gap} = I - A \qquad Equation\ 4.1$$

As shown in Table 4.4 and Figure 4.7, the energy gap of the six metal complexes is 4.89 eV, 6.09 eV, 6.14 eV, 6.37 eV, 6.45 eV, and 6.47 eV for Pd1, Ni1, Ni2, Fe1, Co1, and Co2, respectively. The E_{gap} is increasing in the order, Pd1 < Ni1 < Ni2 < Fe1 < Co1 < Co2. This trend shows that Pd1 has the smallest E_{gap} in this series followed by Ni1. A small gap means high polarizability and such compounds will be easily polarized, meaning that their electron density will be changed more easily and a reaction can occur more readily. A large HOMO–LUMO gap increases stability, meaning that Co2 is the most stable compound in this series. In this set of complexes, Pd1 is considered to be a soft compound since it has a small energy gap whereas Co2 is considered to be a hard compound since it has a large energy gap. This implies that Pd1 complex is the most reactive catalyst, followed by Ni1, compared to the remaining complexes and that a small amount of excitation energy is needed for a reaction to take place for these complexes. This is also supported by the fact that the HOMO for Pd1 is relatively high in energy and its LUMO is relatively low in energy compared to the remaining compounds, making Pd1 a soft compound. Variation in the E_{gap} of the Fe1, Co1, Ni1, Pd1, Co2, and Ni2 metal complexes.

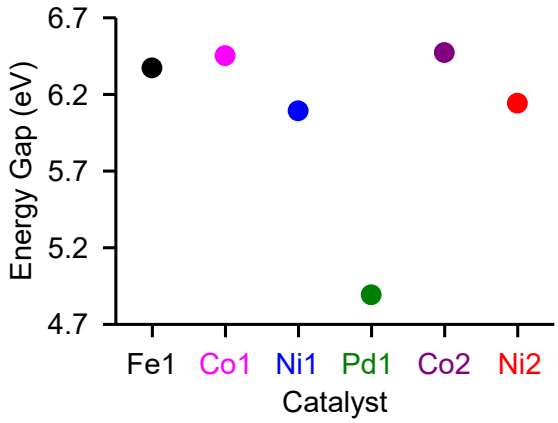

Figure 4.7: Variations in the *Egap* of the Fe1, Co1, Ni1, Pd1, Co2, and Ni2 metal complexes. Values determined at B3LYP level of theory
Source: Researcher (2024)

4.4.3 Ionization Potential (IP)

The ionization potential of a molecule is the orbital energy of the HOMO with changes in sign, *Equation* 4.2 (Fukui, K. 1982).

$$Ionization\ Potential\ (I) = -E_{HOMO} \qquad Equation\ 4.2$$

The ionization potential of the six metal complexes is 6.02 eV, 6.25 eV, 6.55 eV, 6.65 eV, 6.69 eV, and 6.98 eV for Pd1, Ni1, Fe1, Co1, Ni2, and Co2, respectively, as shown in Figure 4.8. This trend shows that a small amount of energy is required to remove an electron in gaseous state from the Pd1 compound where Co2 will require the largest.

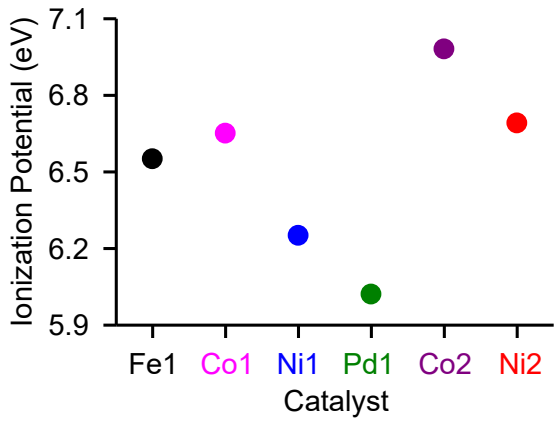

Figure 4.8: Variation in the ionization potential of the Fe1, Co1, Ni1, Pd1, Co2, and Ni2 metal complexes. Values determined at B3LYP level of theory.
Source: Researcher (2024)

4.4.4 Chemical Hardness

The concept of chemical hardness is useful in understanding the behavior of chemical systems. Chemical hardness in a collection of nuclei and electrons, is a measure of resistance to change distribution. The gap between the HOMO and the LUMO (E_{gap}) is equal to twice the value of the chemical hardness, which implies that the chemical hardness is half the value of the E_{gap}, *Equation* 4.3 (Yousef *et al*., 2012).

$$\eta = \frac{1}{2} E_{gap} \qquad \textit{Equation } 4.3$$

Hard molecules are less reactive than soft molecules and do not have an easily changed electron distribution whereas a soft molecule do not resist changes in its electronic charge cloud. As shown in Figure 4.9, the values for the chemical hardness of the six metal complexes are 2.445 eV, 3.045 eV, 3.070 eV, 3.185 eV, 3.225 eV, and 3.235 eV for Pd1, Ni1, Ni2, Fe1, Co1, and Co2, respectively. A small value for the chemical hardness implies that the compound can readily transfer electrons. For these complexes, the chemical hardness decreases in the order, Co2 > Co1 > Fe1 > Ni2 > Ni1 > Pd1. This means that Pd1 is the most reactive complex, followed by Ni1 in this series and Co2 is the least reactive. Chemical hardness and E_{gap} are intertwined. A hard compound has a large E_{gap} between the HOMO and LUMO, and a soft compound has a small E_{gap} (El-Gammal *et al*., 2012). The chemical hardness values agree well with the E_{gap} values for these complexes as they all indicate that Pd1, Ni1, and Ni2 are soft compounds relative to the remaining compounds

Chemical Hardness trend 2.335(Pd1) <3.045(Ni1) < 3.070 (Ni2) < 3.185 (Fe1) < 3.225 (Co1) < (3.235 (Co2)

E_{gap} trend = 4.89 (Pd1) < 6.09 (Ni1) < 6.14 (Ni2) < Fe1(6.37) < 6.45 (Co1) < 6.47(Co2)

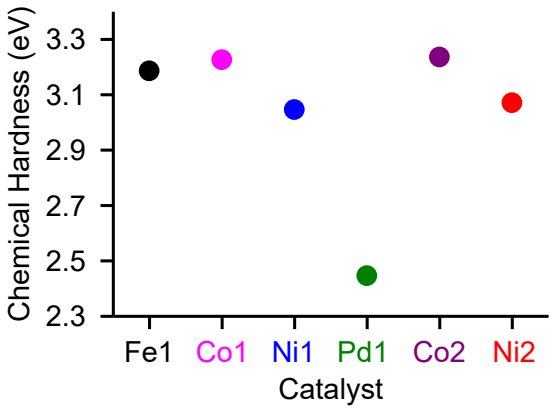

Figure 4.9. Variation in the chemical hardness of the Fe1, Co1, Ni1, Pd1, Co2, and Ni2 metal complexes. Values determined at B3LYP level of theory.
Source: Researcher (2024)

4.4.5 Global Softness

The global softness, S, is expressed as shown in *Equation* 4.4, where η is the chemical hardness.

$$S = \frac{1}{2\eta} \qquad \textit{Equation 4.4}$$

The values for the global softness of the six metal complexes are 0.204 Ev^{-1}, 0.164 Ev^{-1}, 0.163 Ev^{-1}, 0.157 Ev^{-1}, 0.155 Ev^{-1}, and 0.155 Ev^{-1} for Pd1, Ni1, Ni2, Fe1, Co1, and Co2, respectively. In this series of compounds, Pd1 has the largest value of the global softness and Co1 and Co2 have the least. A small value of the global softness indicates that the compound is a stable molecule and therefore very hard to react (Kaya & Kaya, 2015). Both Co1 and Co2 have seemingly small global softness values. On the contrary, a large global softness value means that a compound is unstable and can react easily. This shows that Pd1, Ni1, and Ni2 are quite reactive with Pd1 being the most reactive. This may partly offer an explanation as to why Fe1, Co1, and Co2 were found to be inactive for ethylene oligomerization reaction. This trend in global softness agrees well with the E_{gap} and chemical hardness values of similar compounds. Variation in the global softness of the Fe1, Co1, Ni1, Pd1, Co2, and Ni2 metal complexes as shown in Figure 4.10.

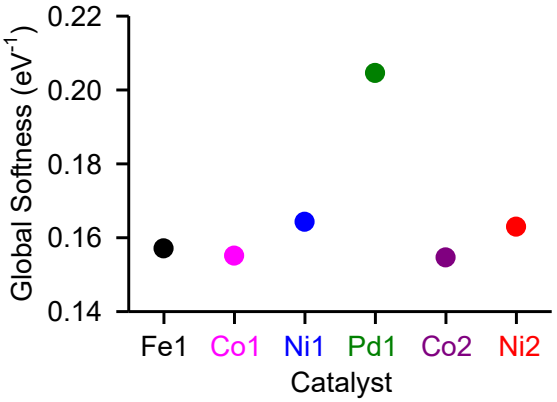

Figure 4.10: Variations in the global softness of the Fe1, Co1, Ni1, Pd1, Co2 and Ni2 complexes. Values determined at B3LYP level of theory.
Source: Researcher (2024)

4.4.5 Chemical Potential

Chemical potential (μ) measures the tendency of electrons to escape in the species (Abu El-Reash *et al*., 2014). Chemical potential is given by equation 4.5, where I is the ionization potential and A is the electron affinity. A more positive value indicates a good electron acceptor (Abu El-Reash *et al*., 2014). Variation in the chemical potential and the electron affinity of the Fe1, Co1, Ni1, Pd1, Co2, and Ni2 metal complexes as shown in Figure 4.11a.

$$\mu = -\left(\frac{I + A}{2}\right) \qquad \textit{Equation 4.5}$$

As shown in Figure 4.11a, the chemical potential values for the six metal complexes are -3.745 eV, – 3.620 eV, – 3.575 eV, – 3.425 eV, – 3.365 eV, and – 3.205 eV for Co2, Ni2, Pd1, Co1, Fe1, and Ni1, respectively. The trend shows that Ni1 is a good electron acceptor compared to the remaining compound. In addition, the trend shows that the octahedral complexes, Fe1, Co1, and Ni1 are good electron acceptors compared to both the square planar, Pd1 complex and the tetrahedral, Co2 and Ni2 complexes. The results also suggest that Ni1 will make a good catalyst for ethylene oligomerization reaction.

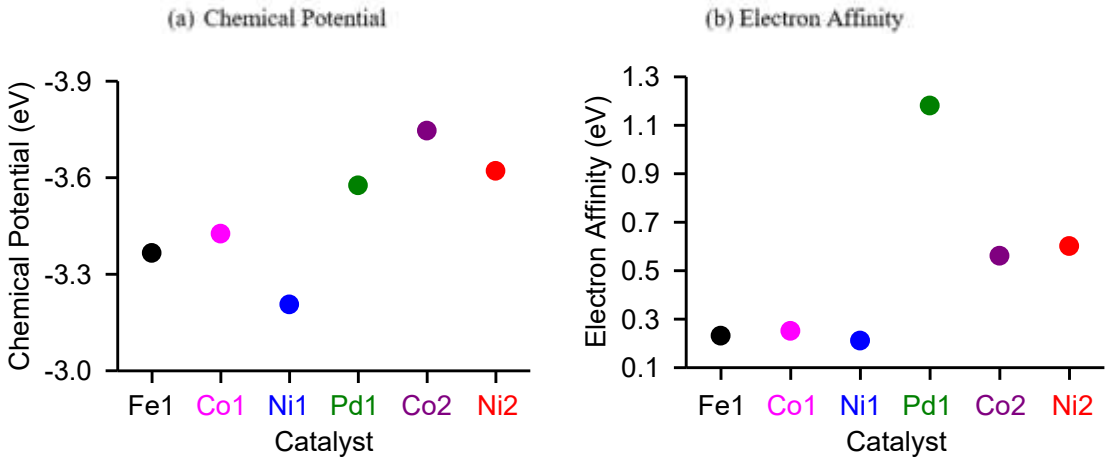

Figure 4.11: Variations in the chemical potential and the electron affinity of the Fe1, Co1, Ni1, Pd1, Co2, and Ni2 metal complexes. Values determined at B3LYP level of theory. Source: Researcher (2024)

4.4.6 Electron Affinity

The electron affinity (A) of a molecule is the orbital energy of the LUMO with changes in sign, *Equation* 4.6 (Parr & Pearson, 1983).

$$Electron\ Affinity = -E_{LUMO} \qquad Equation\ 4.6$$

As shown in Figure 4.11b above, the electron affinity of the six metal complexes is 0.16 eV, 0.18 eV, 0.20 eV, 0.51 eV, 0.55 eV, and 1.13 eV for Ni1, Fe1, Co1, Co2, Ni2, and Pd1, respectively. This trend shows that Ni1 has the highest capability to attract precisely one electron from a donor compared to the rest of the metal complexes.

4.4.7 Electronegativity

Electronegativity (χ) is the average energy of the ionization potential (I) and electron affinity (A). It is a measure of the ability of a molecule to attract electrons to itself, equation 4.7 (Kaya & Kaya, 2015).

$$Electronegativity = {}^{(I+A)}/_{2} \qquad Equation\ 4.7$$

Variation in the electronegativity of the Fe1, Co1, Ni1, Pd1, Co2, and Ni2 metal complexes is as shown in Figure 4.12. As shown in Figure 4.12, the electronegativity values of the six metal complexes are 3.745 eV, 3.620 eV, 3.575 eV, 3.425 eV, 3.365 eV, and 3.205 eV for

Co2, Ni2, Pd1, Co1, Fe1, and Ni1, respectively. The result shows that Ni1 complex has the highest ability to attract electrons to its self and this makes Ni1 a good electrophile compared to the remaining complexes.

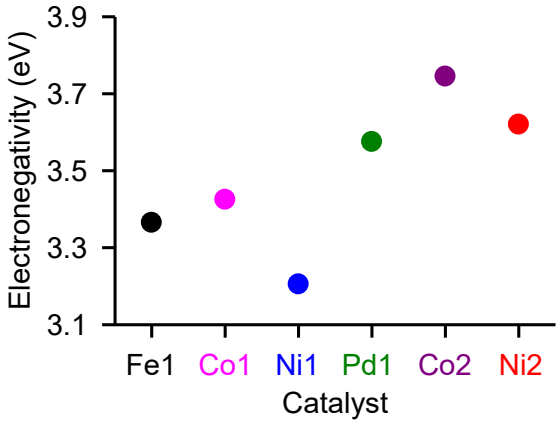

Figure 4.12: Variations in the electronegativity of the Fe1, Co1, Ni1, Pd1, Co2, and Ni2 metal complexes. Values determined at B3LYP level of theory.
Source: Researcher (2024)

4.4.8 Global Electrophilicity Index

Electrophilicity index (ω) is a measure of the electrophilicity of a compound whereas electron affinity reflects the capability of a compound to accept one electron from the environment (Pal & Chattaraj, 2023). The electrophilicity index, *Equation* 4.8, measures the energy lowering of a compound due to maximal electron flow between donor and acceptor (Comp Theo & Karakaş, 2017). Electronegativity squared divided by the chemical hardness measures the electrophilic power of a compound, that is its propensity to soak up electrons.

$$\omega = \frac{\mu^2}{2\eta} \qquad \textit{Equation 4.8}$$

$$\textit{where } \mu = \textit{chemical potential } (-\textit{ve of electronegativity and } \eta = \textit{chemical hardness}$$

Variation in the electrophilicity index of the Fe1, Co1, Ni1, Pd1, Co2, and Ni2 metal complexes as shown in Figure 4.13. As indicated in Figure 4.13, the electrophilicity indices for the six metal complexes are 2.614 eV, 2.168 eV, 2.134 eV, 1.819 eV, 1.778 eV, and 1.687 eV for Pd1, Co2, Ni2, Co1, Fe1, and Ni1, respectively. A small value indicates a good

electron acceptor. The trend shows that Ni1 has the highest electrophilic power compared to the remaining compounds. This also means that Ni1 has the highest capability to accept electrons and can make a good electrophile for ethylene oligomerization reaction. The trend also shows that the octahedral complexes, Fe1, Co1, and Ni1 make better electrophiles compared to the tetrahedral complexes (Co2 and Ni2) and square planar complex (Pd1). The results also agree quite well with both trends observed for electron affinities and electronegativity.

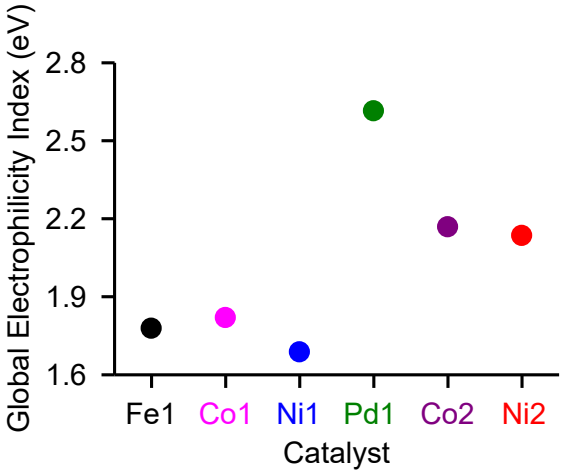

Figure 4.13: Variations in the electrophilicity index of the Fe1, Co1, Ni1, Pd1, Co2, and Ni2 metal complexes. Values determined at B3LYP level of theory.
Source: Researcher (2024)

4.4.9 NBO Charge

The NBO charge of the Fe1, Co1, Ni1, Pd1, Co2, and Ni2 metal complexes was obtained by NBO analysis with B3LYP and B3PW91 functionals using LanL2DZ basis set for metal atoms and 6-311+G (2d, p) for all the remaining atoms. The calculation of effective NBO charges plays an important role in the application of quantum chemical calculations to molecular systems. For the studied complexes, the metal cations, Fe^{2+}, Co^{2+}, Ni^{2+}, and Pd^{2+} were found to have more positive charge than other atoms in the compound. Suggesting that they are more likely to be electrophilic centers during a chemical reaction. Variation in the NBO charge of the Fe1, Co1, Ni1, Pd1, Co2, and Ni2 metal complexes is as shown in Figure 4.14.

The NBO charge on the metal cation for Fe1, Co1, Ni1, Pd1, Co2, and Ni2 compounds are 2.3291 eV, 1.7797 eV, 1.1685 eV, 0.3361 eV, 1.7686 eV, and 1.1575 eV, respectively. In this series of compounds, the Fe1 has the highest NBO charge on the metal cation while Pd1 has the least. Comparison between the octahedral complexes, Fe1, Co1, and Ni1 indicate that the charge on the metal cation decreases from Fe^{2+} (2.3291 eV) to Co^{2+} (1.7797 eV) to Ni^{2+} (1.1685 eV) in line with the decrease in ionic radii from Fe^{2+} (0.76 Å) to Co^{2+} (0.74 Å) to Ni^{2+} (0.72 Å). Comparison between the two tetrahedral complexes, Co2 and Ni2 also show a similar pattern where the charge decreases from Co^{2+} (1.7686 eV) to Ni^{2+} (1.1575 eV).

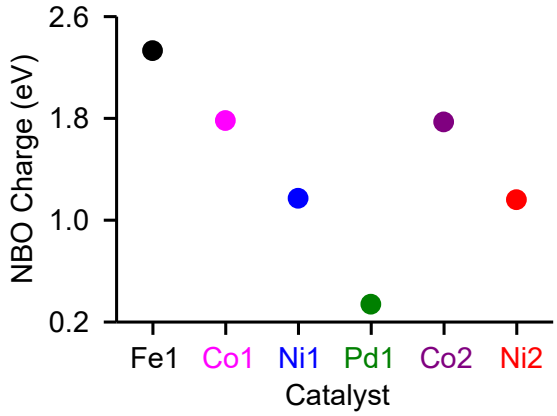

Figure 4.14. Variation in the NBO charge of the Fe1, Co1, Ni1, Pd1, Co2, and Ni2 metal complexes. Values determined at B3LYP level of theory.
Source: Researcher (2024)

4.4.10 Molecular Electrostatic Potential

Investigating the molecular electrostatic potential (MEP) generated in the space around a molecule by the charge distribution is very helpful in understanding the sites for electrophilic and nucleophilic attacks in reactions (Kosar & Albayrak, 2011). The electrostatic potential, $v(\vec{r})$ at any point, $\vec{r}$ is given by *Equation* 4.9, where $\rho(\vec{r})$ is the electron density of the molecule, Z_A is the charge on the nucleus A located at $\vec{R}_A$ and r' is the dummy integration variable.

$$v(\vec{r}) = \sum_A \frac{Z_A}{|\vec{R}_A - \vec{r}|} - \int \frac{\rho(\vec{r}')d\vec{r}'}{|\vec{r}' - \vec{r}|} \ldots\ldots\ldots (4.9)$$

MEP is an observable that can be measured experimentally by diffraction as well as can be evaluated computationally (Okulik & Jubert, 2004). To predict the molecular reactive sites, the MEP maps of the Fe1, Co1, Ni1, Pd1, Co2, and Ni2 metal complexes have been calculated at the B3LYP/6-311+G (2d, p) optimized geometry. Figure 4.15 shows the electrostatic potential contour map with the negative regions (assigned to red) of MEP related to electrophilic attacks and positive regions (assigned to blue) related to nucleophilic reactivity. The molecular electrostatic potential maps of the Fe1, Co1, Ni1, Pd1, Co2, and Ni2 complexes are generated using B3LYP level of theory.

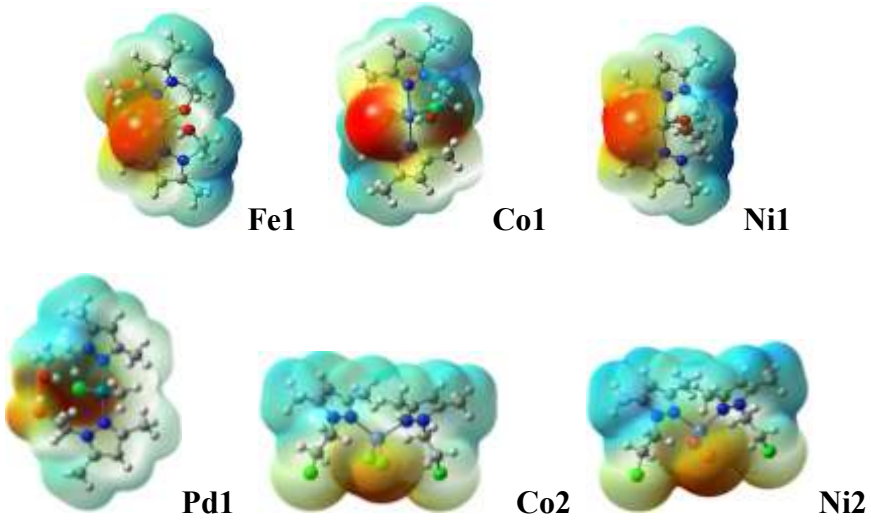

Figure 4.15: Molecular electrostatic potential maps of the Fe1, Co1, Ni1, Pd1, Co2, and Ni2 complexes generated from B3LYP geometry optimized structures.
Source: Researcher (2024)

As can be seen from the MEP map of the metal complexes, the positive regions are located around the Fe^{2+}, Co^{2+}, Ni^{2+}, Pd^{2+} metal cations indicating the possible sites for nucleophilic reactions. The regions having the negative potential are over the electronegative atoms such as the chlorine, bromine, and oxygen atoms, indicating possible sites for electrophilic attacks.

4.5 COMPARISONS OF B3LYP AND B3PW91 SIMULATED CHEMICAL REACTIVITY PARAMETERS

Two different DFT methods, B3LYP and B3PW91 functionals were used to calculate the chemical reactivity parameters of the Fe1, Co1, Ni1, Pd1, Co2, and Ni2 metal complexes.

The parameters obtained using B3LYP functional have been discussed in detail in previous section (section 4.4). Table 4.5 below provides the global reactivity parameters determined using B3PW91 functional including energies of frontier molecular orbitals (E_{HOMO} and E_{LUMO}), energy gap (E_{gap}) which explains the eventual charge transfer interaction within molecules, electronegativity, chemical potential, global hardness, global softness, and global electrophilicity index. Figures 4.16 and 4.17 illustrate a comparison between B3LYP and B3PW91 simulated chemical reactivity values for Fe1, Co1, Ni1, Pd1, Co2, and Ni2 metal complexes.

Table 4.5: Global reactivity descriptors using B3PW91 of the Fe1, Co1, Ni1, Pd1, Co2, and Ni2 metal complexes[a]

	Fe1	**Co1**	**Ni1**	**Pd1**	**Co2**	**Ni2**
E_{HOMO}	– 6.56	– 6.68	– 6.33	– 6.06	– 7.05	– 6.77
Ionization Energy	6.56	6.68	6.33	6.06	7.05	6.77
E_{LUMO}	– 0.11	– 0.15	– 0.06	– 1.01	– 0.45	– 0.52
Electron affinity	0.11	0.15	0.06	1.01	0.45	0.52
Energy gap	6.45	6.53	6.25	5.05	6.60	6.27
Electronegativity	3.335	3.415	3.195	3.535	3.750	3.645
Chemical potential	– 3.335	– 3.415	– 3.195	– 3.535	– 3.750	– 3.645
Chemical hardness	3.225	3.265	3.125	2.525	3.300	3.135
Global softness (eV^{-1})	0.155	0.153	0.160	0.198	0.152	0.159
Global electrophilicity index	1.724	1.786	1.628	2.475	2.131	2.126
NBO charge on M^{2+} metal cation	2.3117	1.7596	1.1418	0.2879	1.7528	1.1299

[a]Theoretically determined global reactivity descriptors using B3PW91 functional and LanL2DZ basis set for Pd1 metal atom and 6-311+G (2d, p) basis set for all the remaining atoms. All values are given in electron volts (eV) except for the global softness and are as indicated in parenthesis.

Source: Researcher (2024)

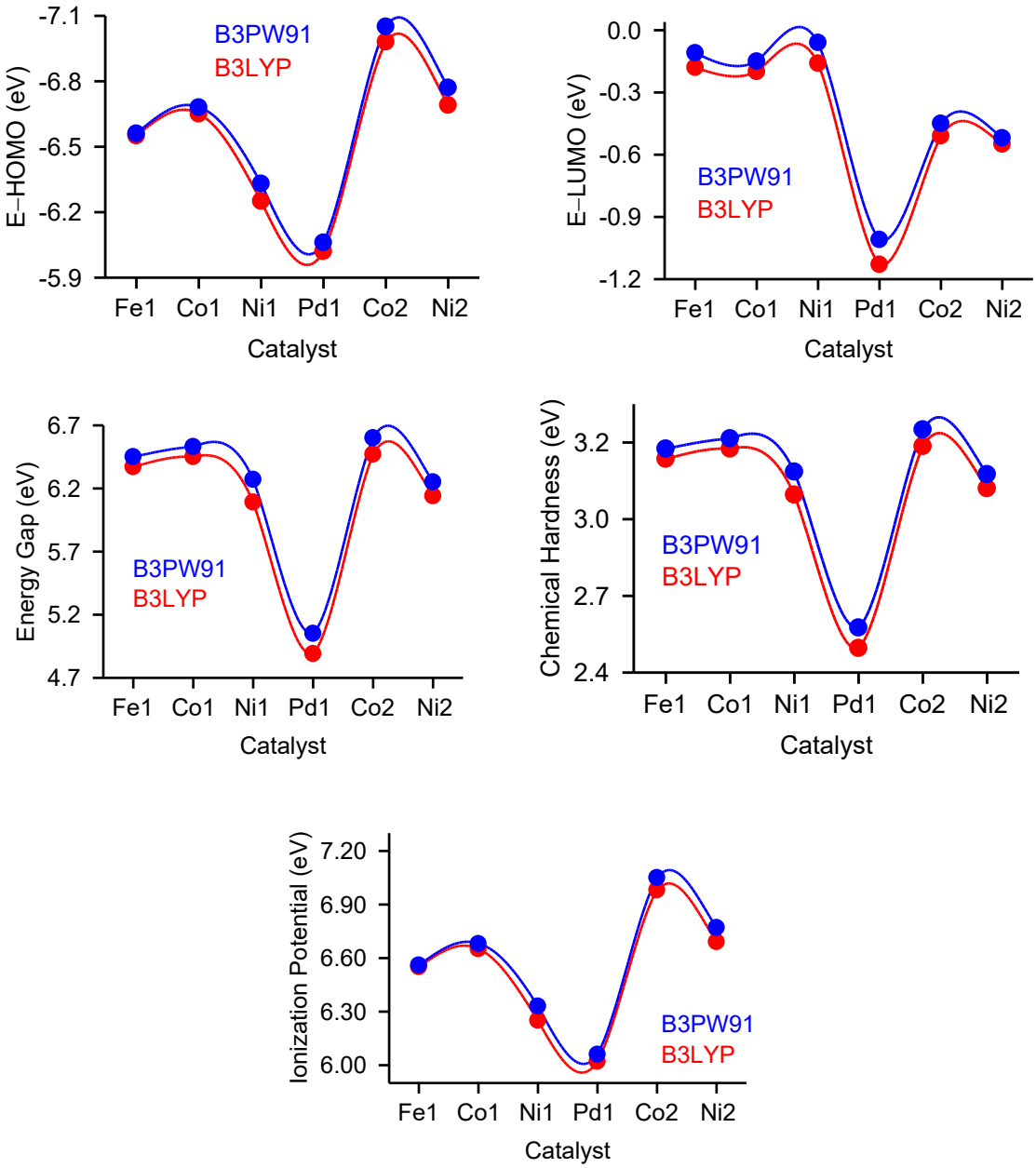

Figure 4.16: Comparison of select global chemical reactivity parameters of the Fe1, Co1, Ni1, Pd1, Co2, and Ni1 metal complexes as a function of B3PW91 and B3LYP DFT methods.

Source: Researcher (2024)

As can be seen in Figure 4.16 trends across the two levels of theory for E_{HOMO}, E_{LUMO}, E_{gap}, chemical hardness, and ionization potential are very similar with B3PW91 parameters generally being the largest and the B3LYP the smallest. The MAD between B3LYP and B3PW91 for all the six metal complexes is 0.05±0.03 eV, 0.07±0.03 eV, 0.12±0.04 eV, 0.06±0.02 eV, and 0.05±0.03 eV for E_{HOMO}, E_{LUMO}, E_{gap}, chemical hardness, and ionization

potential, respectively. As illustrated in Figure 4.17, trends across the two levels of theory, B3LYP and B3PW91 for *electron affinity, electronegativity, chemical potential, global softness, global electrophilicity index, and NBO charge* are generally systematic such that the B3LYP parameters are the largest and the B3PW91 the smallest. The MAD between B3LYP and B3PW91 for the six metal complexes are 0.07±0.03 eV, 0.02±0.01 eV, 0.02±0.01 eV, 0.01±0.01 eV, 0.05±0.04 eV, and 0.03±0.01 eV for electron affinity, electronegativity, chemical potential, global softness, global index, and NBO charge.

In general, the MAD values suggest that B3LYP functional exhibits a very good agreement with the B3PW91 functional in terms of predicting the chemical reactivity descriptors of the six metal complexes.

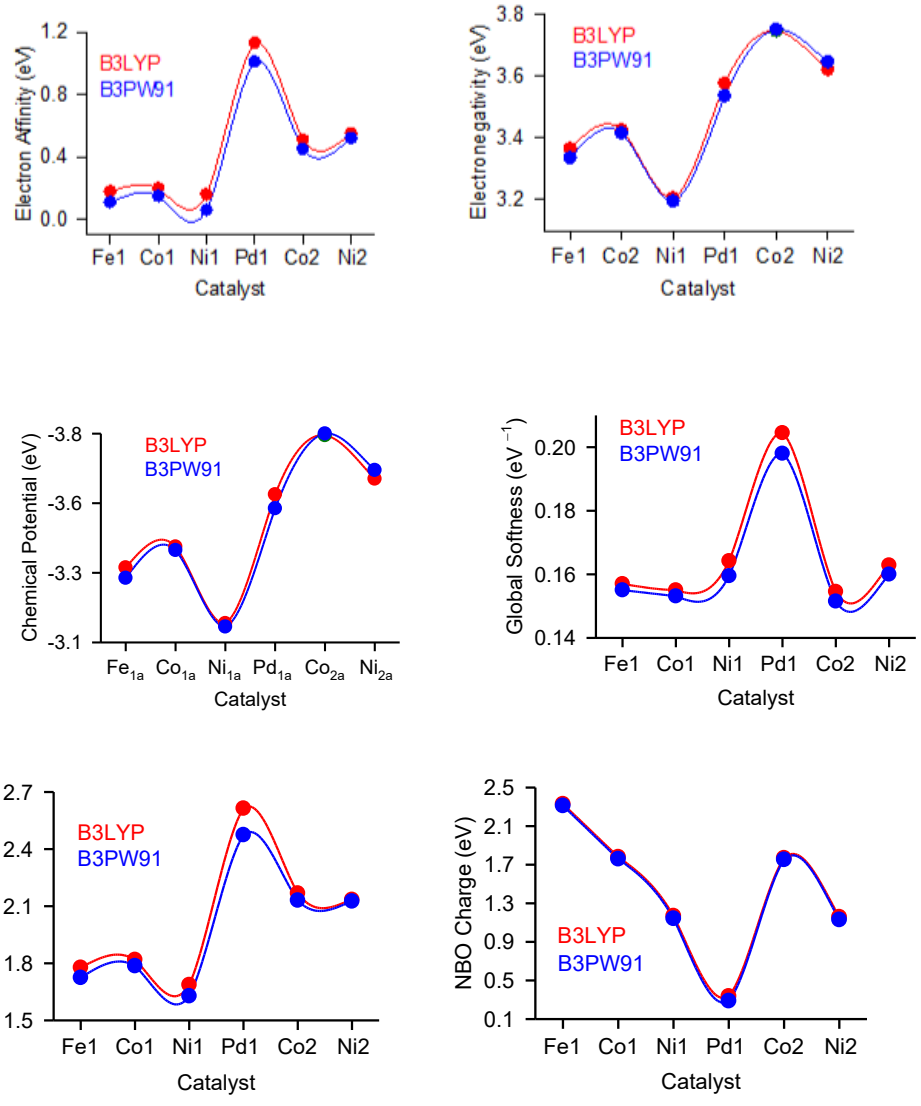

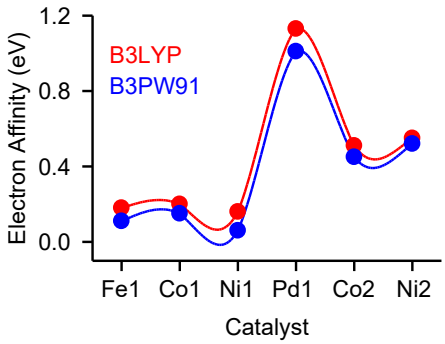

Figure 4.17: Comparison of select global chemical reactivity parameters of the Fe1, Co1, Ni1, Pd1, Co2, and Ni2 metal complexes as a function of B3LYP and B3PW91 DFT methods.

Source: Researcher (2024)

4.6 COMPARISON BETWEEN THEORETICAL AND EXPERIMENTAL VALUES

In this section, theoretically determined chemical reactivity values of different parameters are compared to the experimentally determined catalytic activities of Ni1 and Ni2 transition metal complexes. Theoretical values were obtained at two different functionals, that is, B3LYP and B3PW91 levels of theory. Parallel behavior is observed for the B3PW91 and B3LYP functionals such that the discussion will focus mainly on B3LYP values while the figures will show both theories. Only the two metal complexes, Ni1, and Ni2 are discussed in this section because they are the only two compounds that were found to be experimentally active catalysts for ethylene oligomerization reaction. The remaining Fe1, Co1, Pd1, and Co2 metal complexes were practically found inactive, experimentally (Ainooson, *et al*., 2011). Table 4.6 shows select descriptors for Ni1 and Ni2 metal complexes.

Table: 4.6. Comparison of Catalytic descriptors between Ni1 and Ni2.

Metal Complex	E gap (eV)	Chemical Hardness (eV)	Chemical Potential (eV)	Electrophilicity Index (eV)	Catalytic Activity (Kg/mol.Ni.h)
Ni1	6.09	3.045	-3.205	1.687	4197
Ni2	6.14	3.070	-3.620	2.134	78

Source: Researcher (2024)

Structures of the Fe1, Co1, and Ni1 are similar in several respects, particularly as they all exhibit a distorted octahedral geometry. Pd1 exhibits a distorted square planar geometry whereas Co2 and Ni2 exhibit a distorted tetrahedral geometry. The stability of the metal complexes is of possible significance to the mechanism of catalyst activation encountered during ethylene oligomerization reactions. 2-(3, 5-dimethyl-pyrazol-1-yl)-ethanol ligand binds to Pd^{2+} cation in a monodentate fashion via the pyrazolyl nitrogen atom leaving the OH group uncoordinated in a Pd1 complex. However, the same ligand, 2-(3, 5-dimethyl-pyrazol-1-yl)-ethanol binds to Fe^{2+}, Co^{2+}, and Ni^{2+} cation in a bidentate mode coordinating through a pyrazolyl nitrogen atom and the oxygen atom of the OH group in Fe1, Co1, and Ni1 complexes. When the OH group in 2-(3, 5-dimethyl-pyrazol-1-yl)-ethanol was replaced with a chlorine atom as in 1-(2-chloro-ethyl)-3, 5-dimethyl-1H-pyrazole ligand, the coordination chemistry of the ligand to the Fe^{2+}, Co^{2+}, and Ni^{2+} cations also changed. The Co2 and Ni2 showed no coordination of the chlorine atom to either the Co^{2+} or Ni^{2+} metal cation center. Instead, 1-(2-chloro-ethyl)-3, 5-dimethyl-1H-pyrazole ligand binds to Co^{2+} and Ni^{2+} in a monodentate fashion as shown in the Co2 and Ni2 complexes, respectively.

Despite Fe1, Co1, and Ni1 having the same ligand, Ni1 was found to be active catalyst experimentally, whereas Fe1 and Co1 were found to be inactive. This reactivity difference for the three complexes reflects theoretically determined chemical potential and chemical hardness of Ni1 compared to Fe1 and Co1. In a similar fashion, comparison between the square planar, Pd1 and tetrahedral complexes, Co2 and Ni2, show that Ni2 is active whereas Pd1 and Co2 are inactive. These results show that the bromide species are evidently better catalysts compared to the chloride species in the present series of complexes.

Comparison between the experimentally determined catalytic activities of Ni1 and Ni2 indicate that the catalytic activity of Ni1 is more than forty times greater than that of Ni2 (see Figure 4.18). The tendency of 2-(3, 5-dimethyl-pyrazol-1-yl)-ethanol ligand to form a

bidentate complex in Ni1 and 1-(2-chloro-ethyl)-3, 5-dimethyl-1H-pyrazole ligand to form a monodentate complex in Ni2 seems to play a role. The formation of the bidentate complex results into a stable Ni1 complex compared to its monodentate Ni2 counterpart due to chelate effect. Furthermore, the bidentate nature of Ni1 complex highlights how the two-oxygen donor ligand may substitute the metal-bound bromide ions during reaction to give stable and reactive species. Besides, Ni1 chelate has longer bond distances for the intrachelate interactions (Ni^{2+}–N = 2.1345 Å; Ni^{2+}–Br = 2.6482 Å) than the Ni2 complex (Ni^{2+}–N=2.0629 Å; Ni^{2+}–Br = 2.4522 Å). Qualitatively, steric hindrance about the metal ion due to the chelating ligand's structure is amply highlighted by these structures. The shorter Ni^{2+}–Br bonds for Ni2 reflects the increase in steric repulsion between the metal–bound bromide ions and the chloride ions of the —CH_2CH_2Cl pendant arm. As a result, the Ni^{2+} cation is evidently less accessible to nucleophilic attack by olefin during ethylene oligomerization reaction resulting into an immense loss of activity.

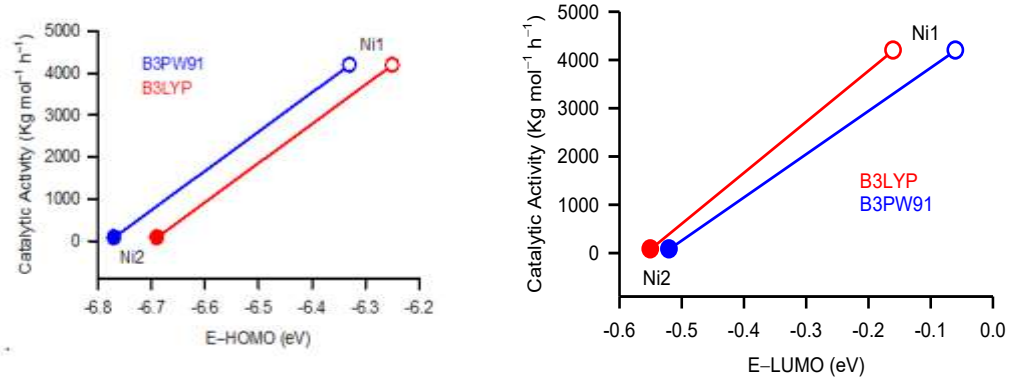

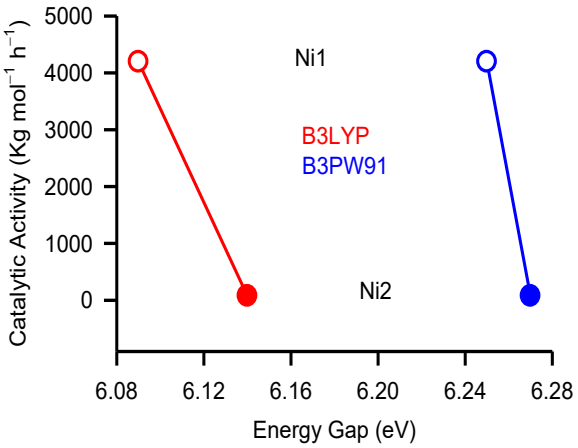

Figure 4.18. A comparison between catalytic activity with respect to E_{HOMO}, E_{LUMO} and $_{Egap}$ of the Fe1, Co1, Ni1, Pd1, Co2, and Ni2 metal complexes.
Source: Researcher (2024)

4.6.1 The Energy Gap

As can be seen in Figure 4.18 (previous page), Ni1 has a higher catalytic activity (4197 kg/mol.Ni.h) compared to Ni2 (78 kg/mol.Ni.h). The lower HOMO energy value of Ni2 (– 6.69 eV) shows that Ni2 donating ability is weaker. On the contrary, the higher HOMO energy of Ni1 (– 6.25 eV) implies that Ni1 is a good electron donor. Both compounds present the ability to receive electrons from low lying LUMO energies. The HOMO–LUMO energy gap of a metal complex shows the direction of flow of electrons. Since the HOMOs are predominantly occupied by d-orbital electrons, smaller HOMO–LUMO gap will facilitate π-back donation of electrons from the metal to the ligand system and hence the metal cation will be electrophilic. As can be seen from Figure 4.18, the E_{gap} for Ni2 (6.14 eV) is larger compared to that of Ni1 (6.09 eV). This suggests that the Ni^{2+} cation in Ni1 is more electrophilic compared to that of Ni2. The results correspond to the experimental results where Ni1 was found to be the most active compared to Ni2. It is therefore expected that Ni1 would be more active compared to Ni2 for olefin oligomerization reaction (Ainooson *et al.*, 2011).

4.6.2 Chemical Hardness

The chemical hardness of a complex is an electronic quantity which is used to characterize the relative stability and the resistance to changes in the number of electrons. The higher the value for chemical hardness, the more stable and less reactive is the compound (Abu El-Reash *et al*., 2014). A comparison between theoretical and experimental values with respect to chemical hardness are as shown in Figure 4.19a. As can be seen, Ni1 has a chemical hardness of 3.045 eV which makes it more reactive compared to Ni2 complex with a value of 3.070 eV. A linear correlation is observed between the calculated chemical hardness and the catalytic yield.

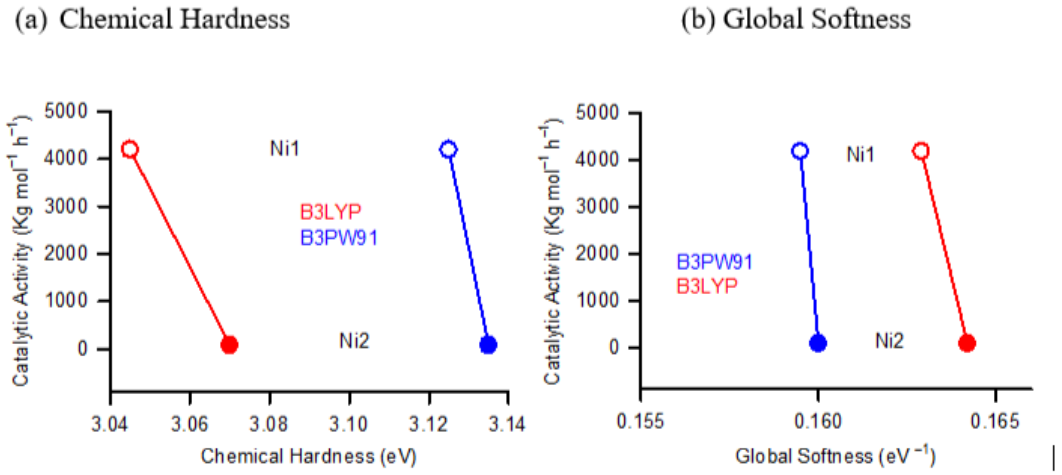

Figure 4.19: A comparison between theoretical and experimental catalytic activity values with respect to chemical hardness (a) and global softness (b) of the Fe1, Co1, Ni1, Pd1, Co2, and Ni2 metal complexes.

Source: Researcher (2024)

4.6.3 Global Softness

The global softness is the inverse of chemical hardness (Parthasarathi., *et al*., 2003). Both Ni1 and Ni2 complexes have comparable values for global softness of 0.164 and 0.163 eV, respectively, indicating that they are both stable compounds (see Figure 4.19b). The minor difference in global softness, however, brings about a huge difference in reactivity between the two complexes, with Ni1 exhibiting a very high catalytic activity compared to Ni2 with 4197 kg/mol.Ni.h and 78 kg/mol.Ni.h, respectively.

4.6.4 Chemical Potential

The chemical potential is the escaping tendency of electrons from a stable system (Abu El-Reash *et al*., 2014). Ni1 and Ni2 have a chemical potential of – 3.205 eV and – 3.620 eV, respectively. A comparison between theoretical and experimental values with respect to chemical potential is as shown below in figure 4.20a. The negative chemical potential values indicate that they are stable and do not decompose spontaneously into their elements. In addition, the chemical potential for Ni1 further indicates that it is a good electron acceptor compared to Ni2. The results correspond to the experimental catalytic activity where Ni1 was found to be more reactive than Ni2.

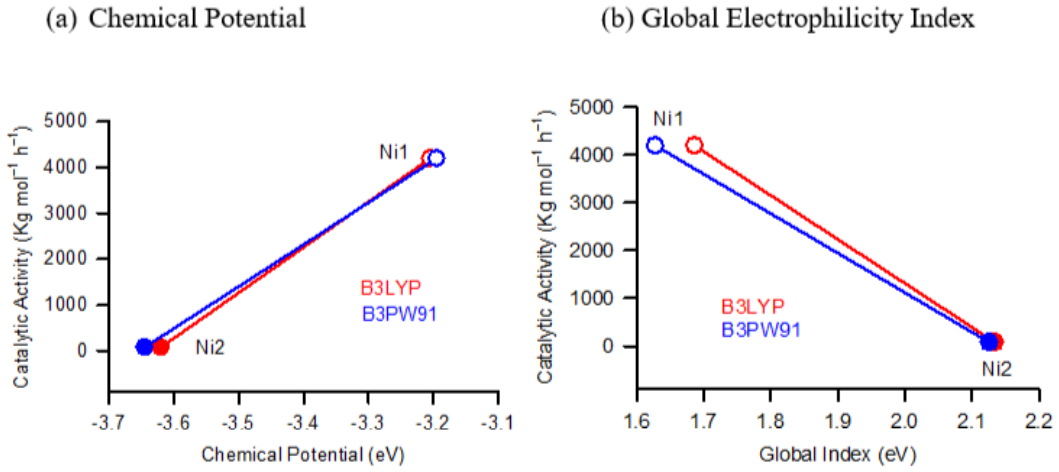

Figure 4.20. A comparison between theoretical and experimental catalytic activity values with respect to chemical potential (a) and global electrophilicity index (b) of Fe1, Co1, Ni1, Pd1, Co2, and Ni2 metal complexes.

Source: Researcher (2024)

4.6.5 Global Electrophilicity Index

The global electrophilicity index is a quantitative classification of the global electrophilic index nature of the complex (Pearson, 1989). A small value indicates a good electron acceptor. Figure 4.20b shows that Ni1 complex (1.687 eV) is more electrophilic compared to Ni2 complex (2.134 eV). This index agrees well with both the electron affinity and electronegativity values. Hence, Ni1 exhibits a higher catalytic activity for ethylene

oligomerization reaction compared to Ni2, with 4197 kg/mol.Ni.h. and 78 kg/mol.Ni.h reactivity's, respectively.

4.6.6 NBO Charge Density

The charge density of an atom or element shows the density of electrons located around it. The more positive the charge density, the more electrophilic the atom or element is. A comparison between theoretical and experimental values with respect to NBO charge of the Fe1, Co1, Ni1, Pd1, Co2, and Ni2 metal complexes is as shown in Figure 4.21. The NBO charge of Ni^{2+} cation in Ni1 and Ni2 complexes is 1.7797 eV and 1.7686 eV, respectively. The Ni^{2+} cation in Ni1 complex is more positive compared to that in Ni2 complex. This agrees well with the experimental catalytic activity where Ni1 is highly reactive compared to Ni2. The NBO charge for both Ni1 and Ni2 agrees with the prediction made with the HOMO–LUMO gap.

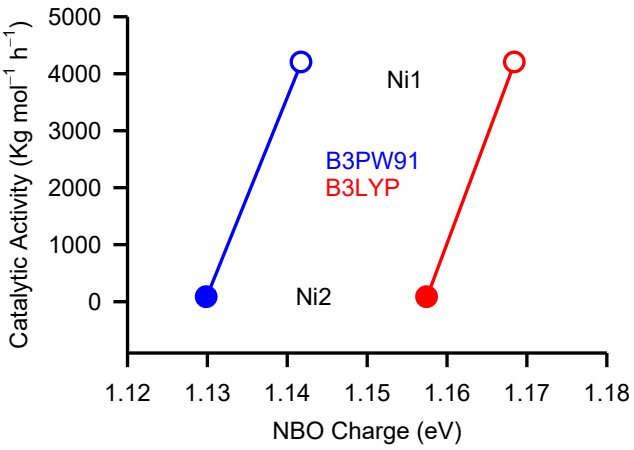

Figure 4.21. A comparison between theoretical and experimental values with respect to NBO charge of the Fe1, Co1, Ni1, Pd1, Co2, and Ni2 metal complexes.
Source: Researcher (2024)

4.7 ELECTRONIC EFFECTS ON THE CATALYTIC ACTIVITY OF THE METAL COMPLEXES

In order to delineate the dependence of the catalytic activity of the Fe1, Co1, Ni1, Pd1, Co2, and Ni2 metal complexes on the electronic nature of the metal cations, structures and

geometrical parameters of these complexes are discussed briefly. The Fe1, Co1, and Ni1 structures exhibit a distorted octahedral geometry whereas the Pd1 exhibits a square planar geometry and the Co2 and Ni2 exhibit a distorted tetrahedral geometry. A comparison between the octahedral complexes, Fe1, Co1, and Ni1 shows that the M^{2+}–N bond lengths decrease from 2.1753 Å (Fe1) to 2.1548 Å (Co1) to 2.1345 Å (Ni1). Similar observation is observed with the metal-oxygen bonds, where the metal-oxygen bond length decreases from 2.3528 Å (Fe1) to 2.2359 Å (Co1) to 2.2224 Å (Ni1). A decrease in the metal-nitrogen and metal-oxygen bond distances from Fe^{2+} to Co^{2+} to Ni^{2+} is expected on the basis of the sizes of these cations, and consequently, stronger electrostatic contributions to the binding.

The trend in the metal-nitrogen bond lengths being predominantly determined by the ionic radii of the bare metal cation: 0.76 Å (Fe^{2+}), 0.74 Å (Co^{2+}) and 0.72 Å (Ni^{2+}). The increase in effective nuclear charge across the period is reflected in the decrease in M^{2+}–N bond lengths of the Fe1, Co1, and Ni1, which further reflects the stability of these cations when they coordinate to the ligands to form the metal complexes. A similar observation is noted for the tetrahedral complexes, Co2 and Ni2 where the metal-nitrogen bond length decreases from 2.0969 Å (Co2) to 2.0629 Å (Ni2).

On the other hand, the metal-nitrogen bond length for the square planar Pd1, 2.0889 Å, is larger compared to that of tetrahedral complexes, Co2 and Ni2. This is consistent with the fact that the Pd^{2+} has a larger ionic radius (1.00 Å) compared to Co^{2+} (0.74 Å) and Ni^{2+} (0.72 Å). In addition, the metal-chloride bond lengths generally increase in the octahedral complexes, Fe1, Co1 and Ni1 complexes, with Ni1 having the longest bond length. Similar observations are made for the tetrahedral complexes, Co2 and Ni2, where the metal-bromide bond is longest for Ni2. Influence of the M^{2+}–Cl and M^{2+}–Br Bond Lengths on the Catalytic Activities of Fe1, Co1, Ni1, Pd1, Co2, and Ni2 complexes is as shown in Figure 4.22. As a way to create a vacant site for ethylene molecule to bind to the catalyst, a chloro ligand (Fe1,

Co1, Pd1, and Co2) must dissociate (a bromo ligand for Ni1 and Ni2. Thus, an increase in the bond length that affects the halogen leaving group is associated with easier loss of a leaving group thus facilitating the activation of a complex during catalytic reaction. In this case, the shorter Ni^{2+}–Br bond length of 2.4522 Å in Ni2 complex compared to the longer Ni^{2+}–Cl bond length of 2.6482 Å in Ni1 complex resulted in catalytic activities of 78 Kg/mol.Ni.h and 4197 Kg/mol.Ni.h for Ni2 and Ni1, respectively. Consequently, the reactivity difference for Ni1 and Ni2 complexes reflects the higher electropositivity of Ni^{2+} cation in Ni1 (1.7797 eV) compared to that of Ni^{2+} cation in Ni2 (1.7686 eV) complex.

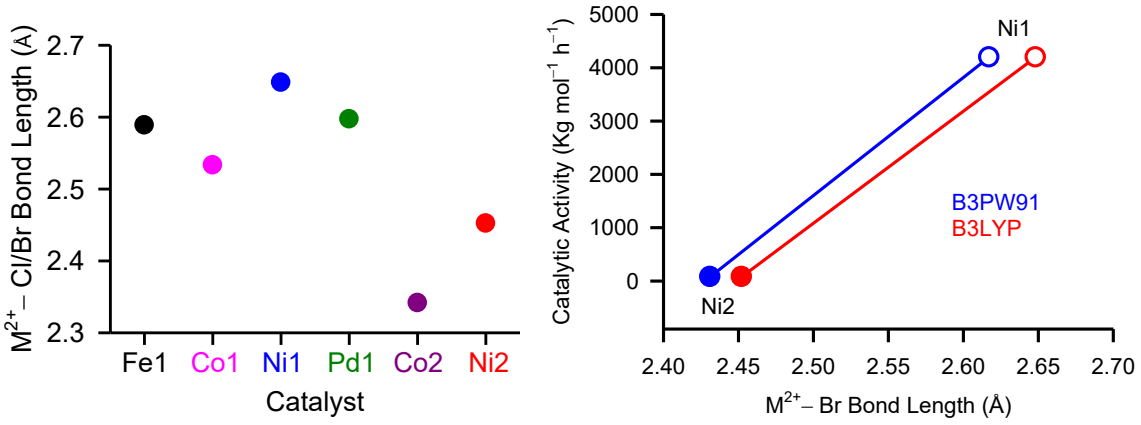

Figure 4.22: Influence of the M^{2+}–Cl and M^{2+}–Br Bond Lengths on the Catalytic Activities of Fe1, Co1, Ni1, Pd1, Co2, and Ni2 complexes.
Source: Researcher (2024)

CHAPTER FIVE

GENERAL CONCLUSIONS AND FUTURE DIRECTIONS

5.1 GENERAL CONCLUSIONS

Theoretical calculations that make use of B3LYP and B3PW91 Density Functional Theoretical Methods and LanL2DZ basis set for metals and 6-311+G (2d, p) basis set for non-metals have been used to simulate transition metal complexes as potential catalysts for ethylene oligomerization. The theoretical studies involve a series of modeling investigations that have been designed to probe the influence of the electronic structure of the metal cation, the nature of the ligand, as well as the effect of chelation and steric interactions on the activity of the catalysts for ethylene oligomerization reactions. Electronic structure theory calculations are employed to determine stable low-energy structures, energetics, and global reactivity descriptors of the transition metal complexes.

The four late transition metal cations in their +2 oxidation states, Fe^{2+}, Co^{2+}, Ni^{2+}, and $Pd1^{2+}$, are included in this work. The N^N hemilabile ligands investigated here include, 2-(3, 5-dimethyl-pyrazol-1-yl)-ethanol and 1-(2-chloro-ethyl)-3, 5-dimethyl-1H-pyrazole. By studying these complexes where the electron configuration of the metal cation is systematically varied from Fe^{2+} ($3d^6$), to Co^{2+} ($3d^7$), to Ni^{2+} ($3d^8$), and to $Pd1^{2+}$ ($4d^8$), periodic trends in the electronic effects and nature of the binding are elucidated. In addition, ligand field effects including chelate and steric effects are examined by comparing the behavior of the complexes among two related N^N donor ligands and by varying the extent of chelation. Theoretical studies of these complexes are compared with previous experimental studies of analogous complexes. Studies of this kind are relevant to the design and rapid development of effective catalysts for ethylene oligomerization reaction.

Relative energies of all possible spin states of the transition metal complexes were carefully evaluated to determine spin states of the ground-state species. Regarding the electronic

structure of the metal complexes, the data obtained theoretically confirms the high-spin states for the Fe^{2+}, Co^{2+}, and Ni^{2+} compounds. In all the five complexes with different spin states, the high spin structures were predicted to be lower in energy by about –75.6, –18.1, –36.1, –31.4, and –7.2 milliHartrees for Fe1, Co1, Ni1, Co2, and Ni2 complexes, respectively. Pd11 complex had only one spin state, singlet state at ground state. Energy differences of these sizes indicate that given the experimental conditions and equilibrium between the two spin states, only the high spin states will lead to the products, a result in agreement with related experimental results where Fe1, Co1, Ni1, Co2, and Ni2 complexes were found to be paramagnetic in nature.

The DFT-simulated structures show that the metal cation in Fe1, Co1, Ni1, Pd11, Co2, and Ni2 metal complexes binds to nitrogen, oxygen, chlorine, and bromine lone pair(s) regardless of the identity of the metal cation or level of theory employed. In all the six metal complexes, the geometry around the central metal cation closely approaches the ideal geometries predicted by the valence shell electron pair repulsion model where Fe1, Co1, and Ni1 metal complexes adopt a distorted octahedral coordination geometry. Both B3LYP and B3PW91 levels of theory show similar results. These DFT theories have been found to perform best for similar transition metals. In all the three metal complexes, the M^{2+}–N bond lengths predicted by B3LYP theory decreases from 2.1753 Å (Fe1) to 2.1548 Å (Co1), to 2.1345 Å (Ni1). Again, the M^{2+}–O bond lengths predicted by B3LYP theory decrease from 2.3528 Å (Fe1) to 2.2359 Å (Co1) to 2.2224 Å (Ni1). The Fe1 has longer bond distances than Co1 and Ni1 due to the large ionic radius of high-spin Fe^{2+} (0.76 Å), relative to that of Co^{2+}(0.74 Å) and to that of Ni^{2+}(0.72 Å). For all the three metal complexes, trends across the two levels of theory in terms of the bond lengths are very similar with B3PW91 bond lengths generally being the shortest and the B3LYP the longest. Structures for the Pd1, Co2, and Ni2 metal complexes indicate that the geometry around the palladium atom is a distorted square planar whereas

Co2 and Ni2 adopt a slightly distorted tetrahedral geometry. The M^{2+}–N bond lengths determined using B3LYP theory again decreases from 2.0969 Å for Co2 to 2.0629 Å for Ni2, in tandem with the ionic radii of the Co^{2+} and Ni^{2+} metal cations.

Theoretical chemical reactivity parameters are deduced from values of the highest occupied molecular orbital (HOMO) and the lowest unoccupied molecular orbital (LUMO). The parameters include: ionization energy, electron affinity, energy gap, electronegativity, chemical potential, chemical hardness, global softness, and global electrophilicity index. The E_{HOMO} and E_{LUMO} of all the six metal complexes are all negative which indicates that the compounds are stable. The E_{gap} increases in this order, Pd1 < Ni1 < Ni2 < Fe1 < Co1 < Co2. The trend shows that Pd1 has the smallest E_{gap} followed by Ni1 and that both compounds are more reactive compared to the remaining complexes.

The chemical hardness of the six metal complexes decreases in the order, Co2 > Co1 > Fe1 > Ni2 > Ni1 > Pd1. A small value for the chemical hardness implies that the compound can readily transfer electrons. As per this series, Pd1 is the most reactive followed by Ni1 and Co2 is the lease reactive metal complex. Thus, the values indicate that Pd1, Ni1, and Ni2 metal complexes are soft compounds and are easily polarized. The values of the global softness support this claim where Pd1, Ni1 and Ni2 were found to have larger values of the global softness compared to those of Fe1, Co1, and Ni2. A large global softness value means that a compound is unstable and easily react. The trend in global softness agrees well with E_{gap} and chemical hardness values. The chemical potential values of the six metal complexes were found to be –3.745, –3.620, –3.575, –3.425, –3.365, and –3.205 for Co2, Ni2, Pd1, Co1, Fe1, and Ni1, respectively. The trend shows that Ni1 is a good electron acceptor compared to the remaining compounds. In addition, the trend shows that the octahedral complexes, that is, Fe1, Co1, and Ni1 are good electron acceptors compared to both the square planar, Pd1 complex and the tetrahedral complexes, Co2 and Ni2. These results are seconded by the

electronegativity values of the same complexes that show Ni1 complex having the highest ability to attract electrons to itself and that makes Ni1 a good electrophile compared to the remaining complexes.

Lastly, the electrophilicity indices for the six metal complexes are 2.614 eV, 2.168 eV, 2.134 eV, 1.819 eV, 1.778 eV, and 1.687 eV for Pd1, Co2, Ni2, Co1, Fe1, and Ni1, respectively. This trend shows that Ni1 has the highest electrophilic power compared to the remaining compound. This also means that Ni1 has the highest capability to accept electrons and can make a good electrophile for ethylene oligomerization reaction. This trend also shows that the octahedral complexes, Fe1, Co1, and Ni1 make better electrophiles compared to the tetrahedral (Co2 and Ni2) and square planar (Pd1) complexes. The results also agree quite well with both trends observed for electron affinities and electronegativity.

Two different DFT methods, B3LYP and B3PW91 functionals were used to calculate the chemical reactivity parameters of the Fe1, Co1, Ni1, Pd1, Co2, and Ni2 metal complexes. Trends across the two levels of theory for E_{HOMO}, E_{LUMO}, E_{gap}, chemical hardness, and ionization potential are very similar with B3PW91 parameters generally being the largest and the B3LYP the smallest. Similarly, trends across the two levels of theory for electron affinity, electronegativity, chemical potential, global softness, electrophilicity index, and NBO charge are generally systematic such that the B3PW91 parameters are the largest and the B3LYP the smallest.

Comparison between theoretically determined chemical reactivity parameters and experimentally determined catalytic activities shows that the Egap for Ni2 (6.14 eV) is larger compared to that of Ni1 (6.09 eV). This suggests that Ni1 is more reactive compared to Ni2. It is therefore expected that Ni1 would be more active compared to Ni2 for olefin oligomerization reaction. Ni1 and Ni2 were found to exhibit catalytic activities of 4197 kg/mol.Ni.h and 78 kg/mol.Ni.h, respectively. These experimental results indicate that Ni1 is

the most active compound and are agree well with theoretical results. The remaining chemical reactivity parameters agree with this pattern. For example, Ni1 has a chemical hardness of 3.045 eV which makes it more reactive compared to Ni2 complex with a value of 3.070 eV. Both Ni1 and Ni2 have comparable values for global softness of 0.164 eV^{-1} and 0.163 eV^{-1}, respectively, indicating that they are both stable compounds. In addition, the negative chemical potential values for Ni1 (– 3.205 eV) and Ni2 (–3.620 eV) indicate that they are stable and do not decompose spontaneously into their elements. In addition, Ni1 is a good electron acceptor compared to Ni2. This is highly supported by the results of the charge density where the Ni^{2+} cation in Ni1 complex was found to be more positive compared to that in Ni2 complex with 1.7797 eV and 1.7686 eV, respectively.

The global electrophilic index for Ni1 (1.687 eV) and Ni2 (2.134 eV) also agrees well with the electron affinity and electronegativity values of the compounds and all point out that Ni1 is a good catalyst compared to Ni2, in agreement with experimental values that indicate the catalytic activity of Ni1 to be more than forty times greater than that of Ni2. The nature of the ligand also seems to control the catalytic reactivity's of the two complexes. The tendency of 2- (3, 5-dimethyl-pyrazol-1-yl)-ethanol ligand to form a bidentate complex in Ni1 and 1-(2-chloro-ethyl)-3, 5-dimethyl-1H-pyrazole ligand to form a monodentate complex in Ni2 seems to play a role. The formation of the bidentate complex results into a stable Ni1 complex compared to its monodentate Ni2 counterpart due to chelate effect. As a result, the Ni^{2+} cation in Ni2 is evidently less accessible to nucleophilic attack by olefin during ethylene oligomerization reaction resulting into its loss of activity.

5.2 FUTURE DIRECTIONS

The current study highlights Ni1 complex to be the best catalyst for ethylene oligomerization reaction. It has lower Homo–Lumo energy gap of 6.09 eV compared to Ni2 (6.09 eV) signifying that it is more reactive. The electrophilicity indices of 2.614 eV, 2.168 eV, 2.134

eV, 1.819 eV, 1.778 eV, and 1.687 eV for Pd1, Co2, Ni2, Co1, Fe1, and Ni1, respectively suggest that, Ni1 easily accepts a pair of electrons in covalent bond formation. In addition, the chemical potential values for Ni1 (– 3.205 eV) and Ni2 (–3.620 eV) indicate that stability i.e. Ni1 does not decompose spontaneously into their elements. In addition, Ni1 is a good electron acceptor compared to Ni2.

To be able to ascertain this truth, the following are recommended;

1. The mechanism of ethylene oligomerization using Ni1 compound as the catalyst should be modeled theoretically. Through such studies, the rate-determining steps involved in the reaction can be evaluated. Such studies can be challenging to investigate experimentally.
2. Based on the comparison between theoretical and experimental studies of Ni1 complex, suggestions on the modification of the substituents on the ligands of Ni1 compound arise. The modified compounds can also be studied theoretically so as to determine their effectiveness as ethylene oligomerization catalysts. Also, to determine ways to improve their catalytic activities before the final products are synthesized in the laboratories.
3. Use methylene linker pyrazolyl ligands have been found to be active and stable ethylene oligomerization catalysts (Ojwach *et al*., 2009). This will minimize costs and save on time in the long run.
4. Theoretical calculations at higher levels of theory such as B3LYP-D3 (Zhang *et al*., 2020) and/or using larger basis sets such as cc-pvTZ can be used to map the best catalysts as they provide highly reliable structures, energetics and global reactivity parameters.
5. Theoretical studies of the influence of other metal cations and higher oxidation states can be carried out. Such studies will allow assessment of new metals and different oxidation states in determining their influence on the catalytic activities of different catalysts for ethylene oligomerization reaction.

REFERENCES

Abu El-Reash, G. M., El-Gammal, O. A., Radwan, A. H. Spectrochimica Acta Part A: Molecular and Biomolecular Spectroscopy 121 (2014) 259–267

Adams, G. M., & Weller, A. S. (2018). POP-type ligands: Variable coordination and hemilabile behaviour. *Coordination Chemistry Reviews*, *355*, 150–172. https://doi.org/10.1016/j.ccr.2017.08.004

Ahmad, S., & Bühl, M. (2019). Design of a Highly Active Pd Catalyst with P,N Hemilabile Ligands for Alkoxycarbonylation of Alkynes and Allenes: A Density Functional Theory Study. *Chemistry - A European Journal*, *25*(50), 11625–11629. https://doi.org/10.1002/chem.201902402

Ahn, S., Hong, M., Sundararajan, M., Ess, D. H., & Baik, M. H. (2019). Design and Optimization of Catalysts Based on Mechanistic Insights Derived from Quantum Chemical Reaction Modeling [Review-article]. *Chemical Reviews*, *119*(11), 6509–6560. https://doi.org/10.1021/acs.chemrev.9b00073

Ainooson, M. K., Ojwach, S. O., Guzei, I. A., Spencer, L. C., & Darkwa, J. (2011). Pyrazolyl iron, cobalt, nickel, and palladium complexes: Synthesis, molecular structures, and evaluation as ethylene oligomerization catalysts. *Journal of Organometallic Chemistry*, *696*(8), 1528–1535. https://doi.org/10.1016/j.jorganchem.2010.12.029

Aragay, G., Pons, J., Branchadell, V., García-Antón, J., Solans, X., Font-Bardía, M., & Ros, J. (2010). Synthesis and characterization of new N-alkylamino-3,5-diphenylpyrazole ligands and reactivity toward PdII and PtII. Study of the cis-trans isomerization. *Australian Journal of Chemistry*, *63*(2), 257–269. https://doi.org/10.1071/CH09371

Austin, A., Petersson, G. A., Frisch, M. J., Dobek, F. J., Scalmani, G., & Throssell, K. (2012). A density functional with spherical atom dispersion terms. *Journal of Chemical Theory and Computation*, *8*(12), 4989–5007. https://doi.org/10.1021/ct300778e

Avcl, D., Bahçeli, S., Tamer, O., & Atalay, Y. (2015). Comparative study of DFT/B3LYP, B3PW91, and HSEH1PBE methods applied to molecular structures and spectroscopic and electronic properties of flufenpyr and amipizone. *Canadian Journal of Chemistry*, *93*(10), 1147–1156. https://doi.org/10.1139/cjc-2015-0176

Bai, T., Ma, S., & Jia, G. (2009). Insertion reactions of allenes with transition metal complexes. *Coordination Chemistry Reviews*, *253*(3–4), 423–448.

https://doi.org/10.1016/j.ccr.2008.04.003

Baseden, K. A., & Tye, J. W. (2014). Introduction to density functional theory: Calculations by hand on the helium atom. *Journal of Chemical Education*, *91*(12), 2116–2123. https://doi.org/10.1021/ed5004788

Bekmukhamedov, G. E., Sukhov, A. V., Kuchkaev, A. M., & Yakhvarov, D. G. (2020). Ni-based complexes in selective ethylene oligomerization processes. In *Catalysts* (Vol. 10, Issue 5). https://doi.org/10.3390/catal10050498

Bell, A. T. (2004). Challenges for the application of quantum chemical calculations to problems in catalysis. *Molecular Physics*, *102*(3 PART II), 319–329. https://doi.org/10.1080/00268970410001668480

Belov, G. P. (2008). Selective dimerization, oligomerization, homopolymerization and copolymerization of olefins with complex organometallic catalysts. *Russian Journal of Applied Chemistry*, *81*(9), 1655–1666. https://doi.org/10.1134/S107042720809036X

Belov, G. P., & Matkovsky, P. E. (2010). Processes for the production of higher linear α-olefins. *Petroleum Chemistry*, *50*(4), 283–289. https://doi.org/10.1134/S0965544110040055

Bhattacharjee, A. (2022). *Exploring Structure-Function Relationship in Small- Molecular Catalysts Using Computational and Experimental Methodologies*.

Bogdos, M. K., Stepanović, O., Bismuto, A., Luraschi, M. G., & Morandi, B. (2022). Mechanistically informed selection rules for competing β-hydride and β-heteroatom eliminations. *Nature Synthesis*, *1*(10), 787–793. https://doi.org/10.1038/s44160-022-00145-x

Bogojeski, M., Vogt-Maranto, L., Tuckerman, M. E., Müller, K. R., & Burke, K. (2020). Quantum chemical accuracy from density functional approximations via machine learning. *Nature Communications*, *11*(1). https://doi.org/10.1038/s41467-020-19093-1

Brambilla, N., Krein, G., Tarrús Castellà, J., & Vairo, A. (2018). Born-Oppenheimer approximation in an effective field theory language. *Physical Review D*, *97*(1), 1–16. https://doi.org/10.1103/PhysRevD.97.016016

Bursch, M., Mewes, J. M., Hansen, A., & Grimme, S. (2022). Best-Practice DFT Protocols for Basic Molecular Computational Chemistry**. *Angewandte Chemie - International*

Edition, *61*(42). https://doi.org/10.1002/anie.202205735

Camacho, D. H., & Guan, Z. (2010). Designing late-transition metal catalysts for olefin insertion polymerization and copolymerization. *Chemical Communications*, *46*(42), 7879–7893. https://doi.org/10.1039/c0cc01535k

Cao, W., Ren, C., & Liu, S. (2023). Developments in Binuclear Late Transition Metal Catalysts for Ethylene Homo- and Copolymerization. *E3S Web of Conferences*, *406*, 0–4. https://doi.org/10.1051/e3sconf/202340602022

Cetto, A. M., la Peña, L. de, & Valdés-Hernández, A. (2015). Specificity of the Schrödinger equation. *Quantum Studies: Mathematics and Foundations*, *2*(3), 275–287. https://doi.org/10.1007/s40509-015-0047-5

Chacko, R., Keller, K., Tischer, S., Shirsath, A. B., Lott, P., Angeli, S., & Deutschmann, O. (2023). Automating the Optimization of Catalytic Reaction Mechanism Parameters Using Basin-Hopping: A Proof of Concept. *Journal of Physical Chemistry C*, *127*(16), 7628–7639. https://doi.org/10.1021/acs.jpcc.2c08179

Chen, B. W. J., Xu, L., & Mavrikakis, M. (2021). Computational Methods in Heterogeneous Catalysis. *Chemical Reviews*, *121*(2), 1007–1048. https://doi.org/10.1021/acs.chemrev.0c01060

Chen, J., Gao, Y., & Marks, T. J. (2020). Early Transition Metal Catalysis for Olefin–Polar Monomer Copolymerization. *Angewandte Chemie - International Edition*, *59*(35), 14726–14735. https://doi.org/10.1002/anie.202000060

Chen, L., Ding, X., Wang, Z., Xu, S., Jiang, Q., Dun, C., & Urban, J. J. (2024). Advances in in situ/operando techniques for catalysis research: enhancing insights and discoveries. *Surface Science and Technology*, *2*(1). https://doi.org/10.1007/s44251-024-00038-5

Choudhury, N. (2024). *Importance of Theoretical and Computational Chemistry in State-of-the-art Chemistry Research*. *February*, 15–19.

Comas-Vilà, G., & Salvador, P. (2024). Quantification of the Donor-Acceptor Character of Ligands by the Effective Fragment Orbitals. *ChemPhysChem*, *25*(18). https://doi.org/10.1002/cphc.202400582

Comp Theo, T., & Karakaş, D. (2017). Turkish Computational and Theoretical Chemistry Theoretical investigation on electrophilicity indexes and proton affinities of some boron-

nitrogen open-chain species. *Chem (TC&TC)*, *1*(1), 1.

de Oliveira, L. L., Batista, F. I., Oliboni, R. S., Casagrande, A. C. A., Stieler, R., & Casagrande, O. L. (2021). Chromium(III) complexes based on phenoxy-imine ligands with pendant N- and O-donor groups as precatalysts for ethylene oligomerization: synthesis, characterization, and DFT studies. *Journal of Organometallic Chemistry*, *936*, 121710. https://doi.org/10.1016/j.jorganchem.2021.121710

Donchev, A. G., Taube, A. G., Decolvenaere, E., Hargus, C., McGibbon, R. T., Law, K. H., Gregersen, B. A., Li, J. L., Palmo, K., Siva, K., Bergdorf, M., Klepeis, J. L., & Shaw, D. E. (2021). Quantum chemical benchmark databases of gold-standard dimer interaction energies. *Scientific Data*, *8*(1), 1–9. https://doi.org/10.1038/s41597-021-00833-x

Dong, F., & Deng, R. (2019). *Olefin Polymerization with Ziegler-Natta Catalyst - Chemistry LibreTexts*. *Figure 1*, 4–9. https://chem.libretexts.org/Bookshelves/Inorganic_Chemistry/Supplemental_Modules_and_Websites_(Inorganic_Chemistry)/Catalysis/Catalyst_Examples/Olefin_Polymerization_with_Ziegler-Natta_Catalyst%0Ahttps://chem.libretexts.org/Bookshelves/Inorganic_Chemistry

Durand, D. J., & Fey, N. (2019). Computational Ligand Descriptors for Catalyst Design [Review-article]. *Chemical Reviews*, *119*(11), 6561–6594. https://doi.org/10.1021/acs.chemrev.8b00588

Durand, D. J., & Fey, N. (2021). Building a Toolbox for the Analysis and Prediction of Ligand and Catalyst Effects in Organometallic Catalysis. *Accounts of Chemical Research*, *54*(4), 837–848. https://doi.org/10.1021/acs.accounts.0c00807

Echanisms, M. (2014). *Chapter 12: Coordination Chemistry IV: Reactions and Mechanisms A: Problem 12.19-12.21 relevant*. 172–180. https://www.chem.uci.edu/~lawm/Ch 12 Solutions.pdf

El-Gammal, O. A., Abu El-Reash, G. M., Ghazy, S. E., & Radwan, A. H. (2012). Synthesis, characterization, molecular modeling and antioxidant activity of (1E,5E)-1,5-bis(1-(pyridin-2-yl)ethylidene)carbonohydrazide (H2APC) and its zinc(II), cadmium(II) and mercury(II) complexes. *Journal of Molecular Structure*, *1020*, 6–15. https://doi.org/10.1016/j.molstruc.2012.04.029

El-Gammal, O. A., Rakha, T. H., Metwally, H. M., & Abu El-Reash, G. M. (2014). Synthesis, characterization, DFT and biological studies of isatinpicolinohydrazone and its Zn(II), Cd(II) and Hg(II) complexes. *Spectrochimica Acta - Part A: Molecular and Biomolecular Spectroscopy*, *127*, 144–156. https://doi.org/10.1016/j.saa.2014.02.008

Enders, M. (2020). Hemilabile Ligands. *Catalysis from A to Z*. https://doi.org/10.1002/9783527809080.cataz07876

Fernandes, P. A., Joao Ramos, M., & Sousa, S. (2007). General Performance of Density Functionals. *Journal of Physical Chemistry A*, *111*, 10439–10452.

Foresman, J. B. (2015). *Exploring Chemistry with Electronic Structure Methods Third Edition*.

Forget, S., Olivier-Bourbigou, H., & Delcroix, D. (2017). Homogeneous and Heterogeneous Nickel-Catalyzed Olefin Oligomerization: Experimental Investigation for a Common Mechanistic Proposition and Catalyst Optimization. *ChemCatChem*, *9*(12), 2408–2417. https://doi.org/10.1002/cctc.201700348

Freeman, E. E., Neeway, J. J., Motkuri, R. K., Rimer, J. D., & Mpourmpakis, G. (2020). Understanding initial zeolite oligomerization steps with first principles calculations. *AIChE Journal*, *66*(12). https://doi.org/10.1002/aic.17107

Funes-Ardoiz, I., & Maseras, F. (2018). Oxidative Coupling Mechanisms: Current State of Understanding. *ACS Catalysis*, *8*(2), 1161–1172. https://doi.org/10.1021/acscatal.7b02974

Funes-Ardoiz, I., & Schoenebeck, F. (2020). Established and Emerging Computational Tools to Study Homogeneous Catalysis—From Quantum Mechanics to Machine Learning. *Chem*, *6*(8), 1904–1913. https://doi.org/10.1016/j.chempr.2020.07.008

Gansukh, B., Zhang, R., Guo, J., Zhang, W., Sun, W.-H., Gansukh, B., Zhang, R., Guo, J., Zhang, W., & Sun, W.-H. (2020). Paradox of Late Transition-Metal Catalysts in Ethylene Polymerization. *General Chemistry*, *6*(1), 190031–190031. https://doi.org/10.21127/yaoyigc20190031

Gogoi, R., Pathak, C., & Borah, G. (2019). Synthesis and characterization of cobalt(II) complexes with hemilabile p^N donor ligands. *Asian Journal of Chemistry*, *31*(3), 566–568. https://doi.org/10.14233/ajchem.2019.21685

Goonesinghe, C., Roshandel, H., Diaz, C., Jung, H. J., Nyamayaro, K., Ezhova, M., & Mehrkhodavandi, P. (2020). Cationic indium catalysts for ring opening polymerization: Tuning reactivity with hemilabile ligands. *Chemical Science*, *11*(25), 6485–6491. https://doi.org/10.1039/d0sc01291b

Götz, A. W. (2016). Overview of Electronic Structure Methods. *Electronic Structure Calculations on Graphics Processing Units: From Quantum Chemistry to Condensed Matter Physics*, 39–65. https://doi.org/10.1002/9781118670712.ch3

Grambow, C. A., Jamal, A., Li, Y. P., Green, W. H., Zádor, J., & Suleimanov, Y. V. (2018). Unimolecular Reaction Pathways of a γ-Ketohydroperoxide from Combined Application of Automated Reaction Discovery Methods. *Journal of the American Chemical Society*, *140*(3), 1035–1048. https://doi.org/10.1021/jacs.7b11009

Guo, L., Dai, S., Sui, X., & Chen, C. (2016). Palladium and Nickel Catalyzed Chain Walking Olefin Polymerization and Copolymerization. *ACS Catalysis*, *6*(1), 428–441. https://doi.org/10.1021/acscatal.5b02426

Guo, S. tai, Liu, J., Qian, W., Zhu, W. hua, & Zhang, C. yang. (2021). A review of quantum chemical methods for treating energetic molecules. *Energetic Materials Frontiers*, *2*(4), 292–305. https://doi.org/10.1016/j.enmf.2021.10.004

Gupta, S., Fernandes, R., Patel, R., Spreitzer, M., & Patel, N. (2023). A review of cobalt-based catalysts for sustainable energy and environmental applications. *Applied Catalysis A: General*, *661*(January). https://doi.org/10.1016/j.apcata.2023.119254

Hargittai, I., & Chamberland, B. (1986). The VSEPR model of molecular geometry. *Computers and Mathematics with Applications*, *12*(3-4 PART 2), 1021–1038. https://doi.org/10.1016/0898-1221(86)90438-4

Hayashi, H., Maeda, S., & Mita, T. (2023). Quantum chemical calculations for reaction prediction in the development of synthetic methodologies. *Chemical Science*, *14*(42), 11601–11616. https://doi.org/10.1039/d3sc03319h

Herron, J. A., Mavrikakis, M., & Maravelias, C. T. (2016). Optimization Methods for Catalyst Design. In *Computer Aided Chemical Engineering* (Vol. 38). Elsevier Masson SAS. https://doi.org/10.1016/B978-0-444-63428-3.50054-0

Hill, J. G. (2013). Gaussian basis sets for molecular applications. *International Journal of*

Quantum Chemistry, *113*(1), 21–34. https://doi.org/10.1002/qua.24355

Hu, W., Ye, S., Zhang, Y., Li, T., Zhang, G., Luo, Y., Mukamel, S., & Jiang, J. (2019). Machine Learning Protocol for Surface-Enhanced Raman Spectroscopy. *Journal of Physical Chemistry Letters*, *10*(20), 6026–6031. https://doi.org/10.1021/acs.jpclett.9b02517

Jensen, S. R., Durdek, A., Bjørgve, M., Wind, P., Flå, T., & Frediani, L. (2023). Kinetic energy-free Hartree–Fock equations: an integral formulation. *Journal of Mathematical Chemistry*, *61*(2), 343–361. https://doi.org/10.1007/s10910-022-01374-3

Kandel, R. (2018). *Phosphaamidines and Phosphaguanidines as Ligands : Coordination Chemistry and Catalysis*.

Kaya, S., & Kaya, C. (2015). A new method for calculation of molecular hardness: A theoretical study. *Computational and Theoretical Chemistry*, *1060*, 66–70. https://doi.org/10.1016/j.comptc.2015.03.004

Kinoshita, S., Kawamura, K., & Fujita, T. (2011). Early-transition-metal catalysts with phenoxy-imine-type ligands for the oligomerization of ethylene. *Chemistry - An Asian Journal*, *6*(2), 284–290. https://doi.org/10.1002/asia.201000563

Kocharekar, A. R. (2021). *A Study on Coordination Chemistry in Catalysis : Investigating the role of coordination complexes in catalytic processes , including homogeneous and heterogeneous catalysis , and their applications in industrial and environmental chemistry*. *11*(08), 268–278.

Kohn, W., Becke, A. D., & Parr, R. G. (1996). Density functional theory of electronic structure. *Journal of Physical Chemistry*, *100*(31), 12974–12980. https://doi.org/10.1021/jp9606691

Kosar, B., & Albayrak, C. (2011). Spectroscopic investigations and quantum chemical computational study of (E)-4-methoxy-2-[(p-tolylimino)methyl]phenol. *Spectrochimica Acta - Part A: Molecular and Biomolecular Spectroscopy*, *78*(1), 160–167. https://doi.org/10.1016/j.saa.2010.09.016

Lee, D. H., Lee, J. H., Park, B. K., Kim, E. Y., Kim, Y., Kim, C., & Lee, I. M. (2009). High catalytic activities in the norbornene polymerization with neutral palladium complexes containing N4-type tetradentate chelating ligands. *Inorganica Chimica Acta*, *362*(14),

5097–5102. https://doi.org/10.1016/j.ica.2009.08.026

Lee, Y. K. (2021). Density functional theory (Dft) calculations and catalysis. *Catalysts*, *11*(4), 10–12. https://doi.org/10.3390/catal11040454

Lewars, E. G. (2016). Computational chemistry: Introduction to the theory and applications of molecular and quantum mechanics: Third Edition 2016. In *Computational Chemistry: Introduction to the Theory and Applications of Molecular and Quantum Mechanics: Third Edition 2016*. https://doi.org/10.1007/978-3-319-30916-3

LiBretto, N. J., Xu, Y., Quigley, A., Edwards, E., Nargund, R., Vega-Vila, J. C., Caulkins, R., Saxena, A., Gounder, R., Greeley, J., Zhang, G., & Miller, J. T. (2021). Olefin oligomerization by main group Ga3+ and Zn2+ single site catalysts on SiO2. *Nature Communications*, *12*(1), 1–9. https://doi.org/10.1038/s41467-021-22512-6

Liu, R. (2024). Ideal Site Geometry for Heterogeneous Catalytic Reactions: A DFT Study. *Catalysts*, *14*(1). https://doi.org/10.3390/catal14010034

Louis, H., Egemonye, T. G. C., Edet, H. O., Agwamba, E. C., Unimuke, T. O., & Adeyinka, A. S. (2022). Synthesis, characterization, DFT studies, and molecular modeling of hydrazinelidene-3-oxo-3-(p-olyl) propanal derivatives as potential candidate for Hepatitis B and C treatment. *Vietnam Journal of Chemistry*, *60*(6), 817–835. https://doi.org/10.1002/vjch.202200086

Lu, W., Wei, Z., Gu, Z. Y., Liu, T. F., Park, J., Park, J., Tian, J., Zhang, M., Zhang, Q., Gentle, T., Bosch, M., & Zhou, H. C. (2014). Tuning the structure and function of metal-organic frameworks via linker design. *Chemical Society Reviews*, *43*(16), 5561–5593. https://doi.org/10.1039/c4cs00003j

Ma, X. (2022). Development of Computational Chemistry and Application of Computational Methods. *Journal of Physics: Conference Series*, *2386*(1). https://doi.org/10.1088/1742-6596/2386/1/012005

Mahmood, Q., & Sun, W. H. (2018). N,N-chelated nickel catalysts for highly branched polyolefin elastomers: A survey. *Royal Society Open Science*, *5*(7). https://doi.org/10.1098/rsos.180367

Mao, Y., Wang, H. F., & Hu, P. (2017). Theory and applications of surface micro-kinetics in the rational design of catalysts using density functional theory calculations. *Wiley*

Interdisciplinary Reviews: Computational Molecular Science, *7*(6), 1–15. https://doi.org/10.1002/wcms.1321

Marzari, N., Ferretti, A., & Wolverton, C. (2021). Electronic-structure methods for materials design. *Nature Materials*, *20*(6), 736–749. https://doi.org/10.1038/s41563-021-01013-3

Matsugi, T., & Fujita, T. (2008). High-performance olefin polymerization catalysts discovered on the basis of a new catalyst design concept. *Chemical Society Reviews*, *37*(6), 1264–1277. https://doi.org/10.1039/b708843b

Mazurek, A. H., Szeleszczuk, Ł., & Pisklak, D. M. (2020). Periodic DFT calculations—Review of applications in the pharmaceutical sciences. *Pharmaceutics*, *12*(5). https://doi.org/10.3390/pharmaceutics12050415

Mecking, S. (2001). Olefin polymerization by late transition metal complexes - A root of ziegler catalysts gains new ground. *Angewandte Chemie - International Edition*, *40*(3), 534–540. https://doi.org/10.1002/1521-3773(20010202)40:3<534::AID-ANIE534>3.0.CO;2-C

Medford, A. J., Vojvodic, A., Hummelshøj, J. S., Voss, J., Abild-Pedersen, F., Studt, F., Bligaard, T., Nilsson, A., & Nørskov, J. K. (2015). From the Sabatier principle to a predictive theory of transition-metal heterogeneous catalysis. *Journal of Catalysis*, *328*, 36–42. https://doi.org/10.1016/j.jcat.2014.12.033

Miessler G.L., Fischer P.J, Tarr D.A (2014)., *Inorganic chemistry* (5th Edition): Organometallic reactions and catalysis, Pearsons PP 541 to 543.

Moments, M., & Molecules, O. F. (2018). *24 . 6 : Magnetic Properties of Coordination Compounds Bulk Magnetism : Ferromagnetism*. 9–11.

Mou, L. H., Han, T. T., Smith, P. E. S., Sharman, E., & Jiang, J. (2023). Machine Learning Descriptors for Data-Driven Catalysis Study. *Advanced Science*, *10*(22), 1–20. https://doi.org/10.1002/advs.202301020

Mukherjee, R. (2000). Coordination chemistry with pyrazole-based chelating ligands: Molecular structural aspects. *Coordination Chemistry Reviews*, *203*(1), 151–218. https://doi.org/10.1016/S0010-8545(99)00144-7

Narendrapurapu, B. S., Richardson, N. A., Copan, A. V., Estep, M. L., Yang, Z., & Schaefer, H. F. (2013). Investigating the effects of basis set on metal-metal and metal-ligand bond

distances in stable transition metal carbonyls: Performance of correlation consistent basis sets with 35 density functionals. *Journal of Chemical Theory and Computation*, *9*(7), 2930–2938. https://doi.org/10.1021/ct4002398

Ngcobo, M., Nose, H., Jayamani, A., & Ojwach, S. O. (2022). Structural and ethylene oligomerization studies of chelating (imino)phenol Fe(ii), Co(ii) and Ni(ii) complexes: an experimental and theoretical approach. *New Journal of Chemistry*, *46*(13), 6219–6229. https://doi.org/10.1039/d1nj06065a

Nochebuena, J., Naseem-Khan, S., & Cisneros, G. A. (2021). Development and application of quantum mechanics/molecular mechanics methods with advanced polarizable potentials. *Wiley Interdisciplinary Reviews: Computational Molecular Science*, *11*(4), 1–27. https://doi.org/10.1002/wcms.1515

Nyamato, G. S., Ojwach, S. O., & Akerman, M. P. (2015). *Potential Hemilabile (Imino) pyridine Palladium (II) Complexes as Selective Ethylene Dimerization Catalysts : An Experimental and Theoretical Approach*. *Ii*. https://doi.org/10.1021/acs.organomet.5b00860

Nzuzo, Y., Oseghale, C. O., Chike-Ekwughe, A., Maumela, M., & Bingwa, N. (2024). Electronic distribution and dynamics as catalytic descriptors in heterogeneous catalysis: A mini review. *Catalysis Communications*, *187*(January), 106901. https://doi.org/10.1016/j.catcom.2024.106901

Ojwach, S. O., & Darkwa, J. (2010). Pyrazole and (pyrazol-1-yl)metal complexes as carbon-carbon coupling catalysts. *Inorganica Chimica Acta*, *363*(9), 1947–1964. https://doi.org/10.1016/j.ica.2010.02.014

Ojwach, S. O., Guzei, I. A., Benade, L. L., Mapolie, S. F., & Darkwa, J. (2009). (Pyrazol-l-ylmethyl)pyridine nickel complexes: Ethylene oligomerization and unusual friedel - crafts alkylation catalysts. *Organometallics*, *28*(7), 2127–2133. https://doi.org/10.1021/om8006322

Okulik, N., & Jubert, A. H. (2004). Theoretical study on the structure and reactive sites of non-steroidal anti-inflammatory drugs. *Journal of Molecular Structure: THEOCHEM*, *682*(1–3), 55–62. https://doi.org/10.1016/j.theochem.2004.04.069

Pal, R., & Chattaraj, P. K. (2023). Electrophilicity index revisited. *Journal of Computational*

Chemistry, *44*(3), 278–297. https://doi.org/10.1002/jcc.26886

Parr, R. G., & Pearson, R. G. (1983). Absolute Hardness: Companion Parameter to Absolute Electronegativity. *Journal of the American Chemical Society*, *105*(26), 7512–7516. https://doi.org/10.1021/ja00364a005

Pearson, R. G. (1989). Absolute electronegativity and hardness: applications to organic chemistry. *The Journal of Organic Chemistry*, *54*(6), 1423–1430. https://doi.org/10.1021/jo00267a034

Pelletier, J. D. A., & Basset, J. M. (2016). Catalysis by Design: Well-Defined Single-Site Heterogeneous Catalysts. *Accounts of Chemical Research*, *49*(4), 664–677. https://doi.org/10.1021/acs.accounts.5b00518

Pfenning B.W (2015)., *Principles of Inorganic Chemistry:* Reactions of organometallic compounds., John Wiley & Sons., PP 656- 659

Pratihar, S., Ma, X., Homayoon, Z., Barnes, G. L., & Hase, W. L. (2017). Direct Chemical Dynamics Simulations. *Journal of the American Chemical Society*, *139*(10), 3570–3590. https://doi.org/10.1021/jacs.6b12017

Qi, S. C., Hayashi, J. I., & Zhang, L. (2016). Recent application of calculations of metal complexes based on density functional theory. *RSC Advances*, *6*(81), 77375–77395. https://doi.org/10.1039/c6ra16168e

Qiu, Z., Wang, W., Zheng, H., Wang, D., Zhao, X., Tu, G., Yang, J., & Gao, H. (2024). Late Transition Metal Olefin Polymerization Catalysts Derived from 8-Arylnaphthylamines. *Inorganics*, *12*(11), 1–15. https://doi.org/10.3390/inorganics12110277

Raugei, S., Dubois, D. L., Rousseau, R., Chen, S., Ho, M., Bullock, R. M., & Dupuis, M. (2015). *Toward Molecular Catalysts by Computer*. https://doi.org/10.1021/ar500342g

Recchia, P., Basu, D., Gattobigio, M., Miniatura, C., & Bressan, S. (2024). The Steepest Slope toward a Quantum Few-Body Solution: Gradient Variational Methods for the Quantum Few-Body Problem. *Few-Body Systems*, *65*(4), 0–36. https://doi.org/10.1007/s00601-024-01965-7

Reed, A. E., Weinstock, R. B., & Weinhold, F. (1985). Natural population analysis. *The Journal of Chemical Physics*, *83*(2), 735–746. https://doi.org/10.1063/1.449486

Reek, J. N. H., de Bruin, B., Pullen, S., Mooibroek, T. J., Kluwer, A. M., & Caumes, X. (2022). Transition Metal Catalysis Controlled by Hydrogen Bonding in the Second Coordination Sphere. *Chemical Reviews*, *122*(14), 12308–12369. https://doi.org/10.1021/acs.chemrev.1c00862

Sancho-García, J. C., & Adamo, C. (2013). Double-hybrid density functionals: Merging wavefunction and density approaches to get the best of both worlds. *Physical Chemistry Chemical Physics*, *15*(35), 14581–14594. https://doi.org/10.1039/c3cp50907a

Sandhu, G. S. (2018). Wrong Potential Energy Term in Schrödinger's Equation for Hydrogen Atom. *Journal of Modern Physics*, *09*(04), 607–619. https://doi.org/10.4236/jmp.2018.94042

Sanjeeva Kumar, V., Narayana, Tvvs., Babu, Vr., Pavani, G., Naga Subrahmanyeswara Swami, K., & VGVAPrasad, D. (2024). *Advances in Computational Quantum Chemistry: Methods, Applications, and Future Directions*. *34*(5), 204–212.

Sarkari, M., Fazlollahi, F., Atashi, H., Mirzaei, A. A., & Hosseinpour, V. (2012). Fischer-Tropsch synthesis: Development of kinetic expression for a sol-gel Fe-Ni/Al 2O 3 catalyst. *Fuel Processing Technology*, *97*, 130–139. https://doi.org/10.1016/j.fuproc.2012.01.008

Sauer, J., & Freund, H. J. (2015). Models in Catalysis. *Catalysis Letters*, *145*(1), 109–125. https://doi.org/10.1007/s10562-014-1387-1

Scerri, E. (2025). The Born-Oppenheimer Approximation and its role in the reduction of chemistry. *Foundations of Chemistry*, *0123456789*. https://doi.org/10.1007/s10698-025-09543-3

Simm, G. N., Vaucher, A. C., & Reiher, M. (2019). Exploration of Reaction Pathways and Chemical Transformation Networks. *Journal of Physical Chemistry A*, *123*(2), 385–399. https://doi.org/10.1021/acs.jpca.8b10007

Smith, J. S., Nebgen, B. T., Zubatyuk, R., Lubbers, N., Devereux, C., Barros, K., Tretiak, S., Isayev, O., & Roitberg, A. E. (2019). Approaching coupled cluster accuracy with a general-purpose neural network potential through transfer learning. *Nature Communications*, *10*(1), 1–8. https://doi.org/10.1038/s41467-019-10827-4

Soleimani, M., Khan, S., Mendenhall, D., Lau, W., & Winnik, M. A. (2012). Effect of

molecular weight distribution on polymer diffusion during film formation of two-component high-/low-molecular weight latex particles. *Polymer*, *53*(13), 2652–2663. https://doi.org/10.1016/j.polymer.2011.12.012

Soyemi, A., & Szilvási, T. (2021). Trends in computational molecular catalyst design. *Dalton Transactions*, *50*(30), 10325–10339. https://doi.org/10.1039/d1dt01754c

Spackman, P. R., Jayatilaka, D., & Karton, A. (2016). Basis set convergence of CCSD(T) equilibrium geometries using a large and diverse set of molecular structures. *Journal of Chemical Physics*, *145*(10). https://doi.org/10.1063/1.4962168

Stamatakis, M. (2015). Kinetic modelling of heterogeneous catalytic systems. *Journal of Physics Condensed Matter*, *27*(1). https://doi.org/10.1088/0953-8984/27/1/013001

Sumiya, Y., Harabuchi, Y., Nagata, Y., & Maeda, S. (2022). Quantum Chemical Calculations to Trace Back Reaction Paths for the Prediction of Reactants. *JACS Au*, *2*(5), 1181–1188. https://doi.org/10.1021/jacsau.2c00157

Sydora, O. L. (2018). *Selective Ethylene Oligomerization*. https://doi.org/10.1021/acs.organomet.8b00799

Sydora, O. L. (2019). Selective Ethylene Oligomerization. *Organometallics*, *38*(5), 997–1010. https://doi.org/10.1021/acs.organomet.8b00799

Talari, S., Ibrahim, S. M., Bhavani, P., Prasanna, C. L., Thomas, R., & Rao, G. S. (2025). *Advancements in Coordination Chemistry : Design and Applications of Metal Complexes*.

Tekarli, S. M., Drummond, M. L., Williams, T. G., Cundari, T. R., & Wilson, A. K. (2009). Performance of density functional theory for 3d transition metal-containing complexes: Utilization of the correlation consistent basis sets. *Journal of Physical Chemistry A*, *113*(30), 8607–8614. https://doi.org/10.1021/jp811503v

Tognetti, V., & Joubert, L. (2024). Exchange-correlation effects in interatomic energies for pure density functionals and their application to the molecular energy prediction. *Journal of Computational Chemistry*, *45*(27), 2270–2283. https://doi.org/10.1002/jcc.27431

Tolasa, D. (2025). The Role of Electron Correlation in Determining Molecular Properties: A Theoretical Approach. *Engineering Physics*, *8*(1), 1–8.

https://doi.org/10.11648/j.ep.20250801.11

Tsuneda, T., & Hirao, K. (2014). Long-range correction for density functional theory. *Wiley Interdisciplinary Reviews: Computational Molecular Science*, *4*(4), 375–390. https://doi.org/10.1002/wcms.1178

Vogiatzis, K. D., Polynski, M. V., Kirkland, J. K., Townsend, J., Hashemi, A., Liu, C., & Pidko, E. A. (2019). Computational Approach to Molecular Catalysis by 3d Transition Metals: Challenges and Opportunities [Review-article]. *Chemical Reviews*, *119*(4), 2453–2523. https://doi.org/10.1021/acs.chemrev.8b00361

Wang, F., & Chen, C. (2019). A continuing legend: The Brookhart-type α-diimine nickel and palladium catalysts. *Polymer Chemistry*, *10*(19), 2354–2369. https://doi.org/10.1039/c9py00226j

Wang, S., & Jiang, J. (2023). Interpretable Catalysis Models Using Machine Learning with Spectroscopic Descriptors. *ACS Catalysis*, *13*(11), 7428–7436. https://doi.org/10.1021/acscatal.3c00611

Wang, Z., Liu, Q., Solan, G. A., & Sun, W. H. (2017). Recent advances in Ni-mediated ethylene chain growth: Nimine-donor ligand effects on catalytic activity, thermal stability and oligo-/polymer structure. *Coordination Chemistry Reviews*, *350*, 68–83. https://doi.org/10.1016/j.ccr.2017.06.003

Weijing, D., Weihong, Z., Xiaodong, Z., Baofeng, Z., Lei, C., Laizhi, S., Shuangxia, Y., Haibin, G., Guanyi, C., Liang, Z., & Ge, S. (2018). The application of DFT in catalysis and adsorption reaction system. *Energy Procedia*, *152*, 997–1002. https://doi.org/10.1016/j.egypro.2018.09.106

Winther, K. T., Hoffmann, M. J., Boes, J. R., Mamun, O., Bajdich, M., & Bligaard, T. (2019). Catalysis-Hub.org, an open electronic structure database for surface reactions. *Scientific Data*, *6*(1), 1–10. https://doi.org/10.1038/s41597-019-0081-y

Yousef, T. A., Abu El-Reash, G. M., & El Morshedy, R. M. (2012). Quantum chemical calculations, experimental investigations and DNA studies on (E)-2-((3-hydroxynaphthalen-2-yl)methylene)-N-(pyridin-2-yl) hydrazinecarbothioamide and its Mn(II), Ni(II), Cu(II), Zn(II) and Cd(II) complexes. *Polyhedron*, *45*(1), 71–85. https://doi.org/10.1016/j.poly.2012.07.041

Zhang, H. X., Zhang, H., Zhang, C. Y., Bai, C. X., & Zhang, X. Q. (2012). A simple modification makes a big improvement to ziegler-natta catalyst. *Journal of Polymer Science, Part A: Polymer Chemistry*, *50*(23), 4805–4808. https://doi.org/10.1002/pola.26307

Zhang, K., Chen, L., Geng, D., Lu, J., & Wu, J. (2020). Thermal stability mechanism: Via energy absorption by chemical bonds bending and stretching in free space and the interlayer reaction of layered molecular structure explosives. *Physical Chemistry Chemical Physics*, *22*(23), 13248–13260. https://doi.org/10.1039/d0cp01470b

APPENDICES

Appendix A.1. Cartesian Coordinates of the B3LYP Optimized Structures of the Fe1, Co1, Ni1, Pd1, Co2, and Ni2 Metal Complexes using LanL2DZ basis set for metal cations and 6-311+G (2d, p) basis set for all the remaining atoms.

Fe1				**Co1**			
	x	**y**	**z**		**x**	**y**	**z**
O	-0.19188900	-0.13635800	1.07890800	O	-0.25801400	-0.61706900	0.29055100
N	1.99164400	2.09147500	-0.28087100	N	1.42451500	1.94884100	-0.79404400
N	1.79742900	-2.22288200	0.23326500	N	2.32042000	-1.91686800	0.88713500
N	1.15838100	-2.82984500	1.28068500	N	1.49868500	-2.51170400	1.80369800
C	2.47324900	4.17295600	-0.96833800	C	0.67485800	4.00838400	-1.27334100
C	2.11233300	4.24074400	0.36658900	C	1.81907600	3.79030900	-2.02039200
C	2.16095300	-3.20878600	-0.59777700	C	3.28076500	-2.81017800	0.61631100
C	1.76357500	-4.44669100	-0.07281500	C	3.07007800	-3.97641000	1.36643500
C	1.12391300	-4.17404800	1.12388000	C	1.92586100	-3.75833300	2.11348800
C	-0.58809500	-1.20100300	1.96537000	C	-0.72921300	-1.56224600	1.27286300
C	0.60618900	-2.04545300	2.37466500	C	0.33287100	-1.81379500	2.32502600
C	2.68630200	2.21877000	-2.66422700	C	-0.63677900	2.58592300	0.45268300
H	-1.01922100	-0.75198300	2.86375000	H	-1.01838000	-2.49032900	0.77708100
H	1.35087700	-1.81535700	1.48388700	H	-1.60896500	-1.13364500	1.75852800
H	0.29387200	-2.73910300	3.15330100	H	0.66083100	-0.86748800	2.75644400
H	1.92358700	-5.42027600	-0.50732600	H	3.67632300	-4.86785400	1.36540600
C	2.84701200	-2.94987200	-1.89700200	C	4.38171200	-2.55395300	-0.35959400
H	2.11709000	-2.74629700	-2.68539200	H	3.98106000	-2.29380900	-1.34115900
H	3.51535100	-2.09218600	-1.82472200	H	5.01940900	-1.73032900	-0.03522200
H	3.42869700	-3.82368800	-2.19541200	H	4.99609000	-3.44920700	-0.46160900
C	0.50900900	-5.10757100	2.11132600	C	1.23815100	-4.65083600	3.09084600
H	-0.55711900	-4.90966000	2.24886400	H	0.21104800	-4.87074800	2.78869600
H	0.61885600	-6.13173200	1.75589000	H	1.77875100	-5.59448200	3.15923000
H	0.99145100	-5.03534200	3.08976500	H	1.20498800	-4.20704900	4.08942000
H	1.39273500	-1.40874500	2.77818600	H	-0.09188100	-2.42500600	3.11920800
H	3.22776300	2.93572400	-3.28294300	H	-1.27447600	1.76230100	0.12830700
H	3.29671000	1.32017500	-2.56125100	H	-1.25115600	3.48117700	0.55469900
H	1.76769600	1.93810800	-3.18366400	H	-0.23612800	2.32577600	1.43424700
H	3.59551200	0.34529100	1.71264500	H	4.00678400	1.05855800	0.68744900
O	2.68583300	0.40603200	2.06994100	O	4.00294900	0.64903900	-0.19745800
N	1.82679400	2.97450600	0.75050700	N	2.24625200	2.54367900	-1.71060500
C	2.38984100	2.82136000	-1.33137600	C	0.46417000	2.84215000	-0.52322100
C	2.02352900	5.42220700	1.27290100	C	2.50678800	4.68281400	-2.99774700
H	2.70837600	5.33634900	2.12060800	H	3.53389100	4.90272600	-2.69559400
H	1.01348100	5.55135600	1.67075200	H	2.53995400	4.23902900	-3.99632200

H	2.28565100	6.32270600	0.71807700	H	1.96618800	5.62646000	-3.06613100
H	2.76202100	4.99933100	-1.59762800	H	0.06861300	4.89982800	-1.27231100
C	1.43461900	2.50499100	2.07016500	C	3.41206800	1.84577200	-2.23193100
C	2.50369900	1.66390100	2.74674100	C	4.47414900	1.59422000	-1.17976600
H	1.23186600	3.37922100	2.68629400	H	3.08411000	0.89946700	-2.66335300
H	0.51343500	1.93062800	1.97593400	H	3.83682200	2.45698600	-3.02611000
H	2.18331300	1.45416900	3.77031600	H	4.76331400	2.52230100	-0.68398000
H	3.45333600	2.20060500	2.78378800	H	5.35390200	1.16562100	-1.66543000
H	-0.66141000	-0.22001600	0.22913900	H	-0.26186400	-1.02658700	-0.59435600
Fe	1.87047100	-0.07283100	-0.07319400	Cl	2.36915700	1.09811300	2.28247200
Cl	4.53235900	-0.12461500	-0.18581300	Cl	1.37578200	-1.06613300	-2.18938600
Cl	0.14728000	-0.22956700	-1.89548900	Co	1.87246700	0.01598500	0.04654200

Ni1				**Pd1**			
	x	**y**	**z**		**x**	**y**	**z**
O	0.03180100	-0.19009500	1.20457900	N	-0.22454700	0.45133200	-0.21740500
N	1.53841400	2.16101100	0.02418500	N	2.85250200	-1.81502800	1.46376100
N	2.02075500	-2.06757900	0.05528800	N	2.84521800	-2.44915600	2.67474900
N	0.88184300	-2.82509000	-0.03539700	C	-1.53163900	1.46497800	-1.72265600
C	1.57295900	4.40594400	0.04139500	C	-2.05981500	1.70805800	-0.46788100
C	0.41821300	4.01025800	-0.60491000	C	4.07430300	-1.98847500	0.94739300
C	3.03097200	-2.93750400	0.18169800	C	4.85538700	-2.74167400	1.83641600
C	2.53442900	-4.25052400	0.16075900	C	4.04761700	-3.02167300	2.92405700
C	1.16359000	-4.14922800	0.02737500	C	0.55119500	0.14098000	-2.55281900
C	-0.74764200	-1.40320500	1.17562900	H	5.87754700	-3.05458600	1.69768100
C	-0.43742200	-2.21339300	-0.06859100	C	4.47317200	-1.42820300	-0.37693700
C	3.55973300	3.15066200	1.11288400	H	4.85957400	-0.41003200	-0.27768100
H	-1.80469700	-1.12641500	1.16079100	H	3.62534900	-1.40054100	-1.06204000
H	-0.55327300	-1.98886700	2.07563000	H	5.26025900	-2.04031200	-0.82015200
H	-1.16640600	-3.01729800	-0.15116900	C	4.33844300	-3.81203000	4.15435400
H	3.10734500	-5.16048500	0.23822000	H	3.71215900	-4.70647400	4.21320500
C	4.46007400	-2.53785000	0.33537400	H	4.17113800	-3.22823100	5.06260300
H	4.55460500	-1.65745900	0.96924500	H	5.38063600	-4.13005700	4.14171900
H	4.91181400	-2.29922400	-0.62889100	H	0.57949000	-0.95056500	-2.52952700
H	5.01869100	-3.36100900	0.78511300	H	1.56884200	0.50348900	-2.39102100
C	0.13011500	-5.22292400	-0.04283900	H	0.23129400	0.45439900	-3.54717500
H	-0.44352700	-5.17381900	-0.97201200	N	-1.25060600	1.08372900	0.42429600
H	0.62002500	-6.19536700	-0.00003700	C	-0.38763000	0.67837200	-1.52466300
H	-0.57598900	-5.16499900	0.78977600	C	-3.26155100	2.49684400	-0.07074400
H	-0.51998400	-1.59110900	-0.95835000	H	-3.72791000	2.91732900	-0.96124600
H	3.43212800	2.90887900	2.16906200	H	-2.99760900	3.32201800	0.59672600
H	4.07005800	4.11245000	1.03483800	H	-4.00328000	1.87972200	0.44225000
Ni	1.93684800	0.06449400	0.08972600	H	-1.92148500	1.81731100	-2.66377300
Br	2.76987900	0.05048600	2.60345300	C	-1.41885700	1.04679300	1.87288200

Br	3.99454200	0.41456300	-1.53992500	C	-2.35090100	-0.05429000	2.39137900
H	4.19066600	2.37818100	0.67471300	H	-0.43190700	0.94274400	2.32063200
H	1.84611600	0.08064300	-2.32509000	H	-1.82124700	2.01600500	2.16833500
O	0.96574600	-0.02392100	-1.90775500	H	-3.17915600	-0.20726800	1.69283600
N	0.42169900	2.65519000	-0.59861000	H	-2.77077900	0.28349100	3.34039800
C	2.24602300	3.23057800	0.41058100	C	1.63076900	-2.53707900	3.47423300
C	-0.66513800	4.83527100	-1.21499700	C	1.34913100	-1.27493700	4.29482400
H	-0.75679500	4.65746300	-2.28972400	H	0.80618200	-2.72670500	2.78814100
H	-0.43864300	5.89094900	-1.06739300	H	1.72797200	-3.40011200	4.13093300
H	-1.63684400	4.63097100	-0.75767500	H	2.07415200	-1.17381800	5.10513200
H	1.89458800	5.41919300	0.22072600	H	1.43700300	-0.39238100	3.65202800
C	-0.53617400	1.77594100	-1.24957700	Cl	-0.23138700	-2.80207900	0.30106900
C	0.06587000	0.99032100	-2.39887700	C	2.32576600	1.00839900	0.97551500
H	-0.96075500	1.10036600	-0.50859700	H	1.66576900	1.75745400	1.41598800
H	-1.34040100	2.39877600	-1.63595900	H	3.16957100	0.81716000	1.63740900
H	-0.73887300	0.49320200	-2.94603400	H	2.68095900	1.36354700	0.00562600
H	0.59578400	1.65383300	-3.08451700	O	-1.70662200	-1.29270400	2.67763500
H	0.53163600	-0.13506100	2.04548900	O	0.06213500	-1.35059900	4.89106700
				H	-1.36215200	-1.71075900	1.85966300
				H	-0.59618100	-1.34347600	4.16724500
				Pd	11.25922500	-0.70770900	0.67104000

Co2			**Ni2**			
	x	**y**	**z**		**x**	**y**	**z**
N	-0.60118400	1.00170200	0.17148100	N	-0.27664300	0.79529800	-0.61639100
N	2.23030900	1.90812500	1.91499200	N	2.80662900	0.69939700	-1.24763700
N	2.88987700	1.55102400	3.05807000	N	3.67776700	0.25691600	-2.20861600
C	-2.79806000	1.14079400	0.59760800	C	-1.80802700	2.08941200	-1.62056100
C	-2.62968700	1.16165100	-0.77527700	C	-2.07749400	2.09071900	-0.26563600
C	2.10492000	3.24110700	1.95200900	C	3.02284900	2.01576900	-1.12185800
C	2.68820100	3.73854900	3.12585500	C	4.03378100	2.41512600	-2.00729600
C	3.18434200	2.64258000	3.80710800	C	4.43792900	1.27751500	-2.67836100
C	-1.15175100	0.92693700	2.59474800	C	0.00418700	0.96616400	-3.09012700
H	2.73804700	4.76760000	3.44289400	H	4.42294700	3.41172500	-2.13834100
C	1.42969800	4.01083500	0.86554900	C	2.26172600	2.88515300	-0.17704700
H	0.90827100	3.35171800	0.17156200	H	2.03193400	2.35810400	0.74861800
H	0.70643100	4.71255500	1.28660200	H	2.85709500	3.76623700	0.06631400
H	2.16040700	4.58982500	0.29475200	H	1.32319800	3.22931700	-0.61817300
C	3.90392600	2.56573500	5.10972100	C	5.48976900	1.10058700	-3.71939500
H	3.35623600	1.95570800	5.83317400	H	5.94792200	2.06439200	-3.93847500
H	4.90037600	2.13164400	4.99578600	H	5.07101200	0.70194500	-4.64704000
H	4.01407700	3.56758900	5.52309500	H	6.27574400	0.41710600	-3.38875100
H	-1.93259500	1.37317600	3.21157300	H	-0.68620600	1.12834100	-3.91887400
H	-0.20901500	1.42936900	2.81049800	H	0.34617300	-0.06800600	-3.12205000

H -1.04931300 -0.12092100 2.89112100	H 0.86794500 1.61769900 -3.24379000
N -1.29681300 1.08056600 -1.00413400	N -1.13575200 1.31006500 0.31941200
C -1.51556000 1.03314800 1.15096200	C -0.68475700 1.27104800 -1.80147500
C -3.64203600 1.25491200 -1.86508800	C -3.16119400 2.77360500 0.49654500
H -3.47127900 2.12929000 -2.49854200	H -3.80163900 2.05809300 1.01838200
H -4.63698000 1.33916600 -1.42948000	H -3.78153400 3.34636600 -0.19185100
H -3.62512400 0.37082000 -2.50729900	H -2.75410700 3.46146100 1.24234700
H -3.73286500 1.19849600 1.13101200	H -2.35648900 2.61371600 -2.38613400
Cl 1.49914600 -1.63132600 0.66628600	C -1.10562600 0.89868900 1.71635300
Cl 2.90089900 1.24970200 -1.37264400	C -1.98941000 -0.32446100 1.93849900
Co .46086600 0.69088600 0.39054900	H -1.45619600 1.73669500 2.31670900
C -0.63327200 0.99132000 -2.29769200	H -0.07555100 0.68563800 1.99504700
C -0.50643300 -0.46195600 -2.74076600	H -3.01421400 -0.14688200 1.62410600
H 0.34843500 1.45378600 -2.21646300	H -1.59765600 -1.20924200 1.44371200
H -1.22428200 1.55920400 -3.01396600	C 3.87998300 -1.16137500 -2.47365800
H 0.18066400 -1.02124000 -2.11143800	C 4.90078900 -1.74879900 -1.50428800
H -1.47038700 -0.96208100 -2.77741800	H 4.22776300 -1.25947500 -3.50053800
C 3.29834500 0.17646500 3.31225300	H 2.92388000 -1.67372600 -2.38582900
C 4.68592300 -0.08774600 2.73776400	H 4.53728600 -1.75587400 -0.47985700
H 2.56476000 -0.49043400 2.86373400	H 5.85488600 -1.23089900 -1.55542400
H 3.29508600 0.02142600 4.39005000	Cl -2.06040000 -0.71669000 3.71584300
H 5.42710400 0.60172000 3.13296600	Ni 1.36355500 -0.40955200 -0.27704800
H 4.69021700 -0.05832200 1.65159900	Cl 5.23666500 -3.48444700 -1.94363600
Cl 5.24065700 -1.75752300 3.21234500	Br 0.57649400 -2.46337300 -1.36534400
Cl 0.16771700 -0.53008100 -4.43241200	Br 2.36978900 -0.45899900 1.95671500

Source: Researcher (2024)

Appendix A.2 Vibrational Frequencies, IR activities, and Raman activities of the B3LYP Optimized Structures of the Fe1, Co1, Ni1, Pd1, Co2, and Ni2 Metal Complexes using LanL2DZ basis set for metal cations and 6-311+G(2d,p) basis set for all the remaining atoms at 298 K.

	Fe1				Co1			
Mode	**Unscaled Frequency (cm^{-1})**	**Scaled Frequency (cm^{-1})**	**IR Activity**	**Raman Activity**	**Unscaled Frequency (cm^{-1})**	**Scaled Frequency (cm^{-1})**	**IR Activity**	**Raman Activity**
1	26	25	3.0	0.6	18	18	7.7	0.0
2	31	30	1.2	0.9	28	27	0.0	3.2
3	38	37	1.3	1.7	28	27	2.5	0.0
4	41	39	1.2	2.4	41	39	0.8	0.0
5	50	48	1.6	1.3	42	41	0.0	6.7
6	64	62	4.8	3.5	52	50	5.2	0.0
7	71	68	10.2	2.6	79	76	0.0	5.8
8	89	86	23.0	0.8	90	87	0.0	2.8
9	93	89	5.8	1.5	95	92	15.0	0.0
10	101	97	14.4	0.7	104	100	12.5	0.0
11	105	101	9.5	0.8	112	108	0.0	1.6
12	115	111	2.6	1.6	117	113	41.5	0.0
13	126	121	8.4	0.5	121	116	0.0	1.8
14	137	131	6.7	0.4	135	129	0.0	2.3
15	137	132	12.0	0.5	137	132	5.5	0.0
16	142	136	49.3	0.7	140	135	14.2	0.0
17	144	138	5.1	0.5	140	135	0.0	1.7
18	153	147	8.0	0.1	155	149	0.0	2.2
19	156	150	31.6	0.6	159	152	106.4	0.0
20	161	155	9.8	1.5	167	161	0.0	0.6
21	171	165	79.4	0.5	175	168	18.8	0.0
22	183	176	17.5	2.1	198	190	0.0	6.8
23	195	187	3.4	2.9	198	190	12.3	0.0
24	197	190	0.3	4.3	204	196	63.0	0.0
25	215	207	71.5	1.1	220	212	0.0	14.2
26	232	223	46.1	7.3	224	215	77.7	0.0
27	237	228	63.7	0.4	243	233	51.0	0.0
28	260	249	10.8	0.9	268	257	0.0	4.3
29	266	256	14.1	1.7	274	263	28.9	0.0
30	292	280	42.2	0.2	296	284	61.9	0.0
31	297	285	1.3	2.8	300	288	0.0	5.5
32	318	306	3.0	3.1	321	309	0.0	4.5
33	322	309	5.4	2.9	325	312	8.1	0.0
34	365	351	10.9	3.9	367	353	0.0	10.6
35	374	359	7.9	3.3	370	355	14.3	0.0
36	458	440	72.9	1.6	458	440	0.0	1.9

37	467	448	38.7	1.3	464	446	114.1	0.0
38	509	489	43.0	3.6	512	492	0.0	8.1
39	518	497	27.6	2.9	516	496	64.9	0.0
40	553	532	103.5	7.3	567	545	0.0	23.1
41	591	568	1.5	27.7	577	555	225.5	0.0
42	592	569	0.4	25.9	592	569	0.0	47.4
43	624	599	125.7	3.6	592	569	18.4	0.0
44	632	608	16.1	3.9	632	607	0.0	9.3
45	636	611	73.7	6.7	633	609	34.0	0.0
46	658	632	4.6	1.7	659	634	0.0	2.8
47	659	634	5.5	1.3	661	636	6.3	0.0
48	681	654	2.1	0.9	680	654	0.0	2.2
49	683	656	1.3	0.6	681	655	4.2	0.0
50	785	754	7.3	2.0	784	753	0.0	10.8
51	786	755	1.1	9.4	786	756	7.4	0.0
52	797	766	40.9	4.0	798	767	0.0	8.7
53	798	767	51.4	4.0	798	767	93.7	0.0
54	876	842	45.9	16.2	879	845	92.4	0.0
55	878	844	49.3	10.9	881	846	0.0	24.1
56	971	933	2.4	6.0	973	936	0.0	17.9
57	972	934	2.7	12.9	974	936	3.2	0.0
58	1002	963	19.6	1.4	1002	963	0.0	3.5
59	1003	964	20.8	1.5	1002	963	40.4	0.0
60	1009	970	3.7	5.4	1012	972	0.0	13.2
61	1011	972	1.8	4.1	1012	972	14.9	0.0
62	1041	1001	79.8	6.7	1042	1001	0.0	18.2
63	1044	1003	83.8	8.9	1044	1004	146.2	0.0
64	1057	1016	41.8	6.4	1062	1021	0.0	12.9
65	1062	1020	18.5	2.9	1063	1021	98.8	0.0
66	1062	1021	26.3	21.8	1064	1023	0.0	13.7
67	1064	1022	35.5	3.4	1064	1023	19.0	0.0
68	1066	1024	22.9	7.8	1066	1025	0.0	39.0
69	1067	1025	25.4	8.4	1068	1026	0.0	21.8
70	1068	1026	4.6	15.2	1068	1026	60.8	0.0
71	1069	1027	31.5	23.3	1068	1026	45.1	0.0
72	1142	1097	25.8	8.0	1143	1098	0.0	22.7
73	1145	1100	9.4	16.7	1144	1099	29.3	0.0
74	1175	1129	2.2	7.3	1177	1131	0.0	22.0
75	1176	1130	2.8	11.6	1177	1131	3.1	0.0
76	1237	1189	5.1	15.2	1236	1188	0.0	26.3
77	1241	1192	7.8	21.9	1237	1189	26.8	0.0
78	1259	1210	84.4	6.4	1259	1210	0.0	84.3
79	1261	1211	29.1	54.2	1259	1210	98.3	0.0
80	1328	1277	60.0	22.0	1327	1275	0.0	45.1
81	1329	1277	79.5	22.4	1327	1276	134.8	0.0
82	1346	1293	109.9	14.1	1341	1288	0.0	46.1

83	1354	1301	139.4	16.5	1343	1291	234.2	0.0
84	1398	1343	27.9	33.1	1400	1345	66.0	0.0
85	1400	1345	36.4	37.6	1400	1346	0.0	89.1
86	1405	1350	44.3	70.4	1405	1350	0.0	127.8
87	1405	1350	40.3	47.7	1407	1352	64.3	0.0
88	1408	1353	6.0	5.5	1410	1355	0.0	6.2
89	1409	1354	5.9	9.8	1410	1355	12.3	0.0
90	1417	1362	38.1	27.8	1417	1362	0.0	88.9
91	1418	1362	12.9	75.2	1419	1364	93.1	0.0
92	1425	1369	16.5	15.2	1426	1370	7.5	0.0
93	1430	1374	1.1	3.5	1427	1371	0.0	25.5
94	1444	1388	102.5	31.4	1444	1387	145.5	0.0
95	1445	1389	47.0	52.6	1444	1388	0.0	97.6
96	1466	1409	11.8	29.7	1467	1409	0.0	37.9
97	1469	1412	12.7	40.8	1467	1410	21.3	0.0
98	1471	1414	17.7	31.6	1470	1413	47.8	0.0
99	1471	1414	13.9	17.2	1470	1413	0.0	48.6
100	1473	1416	26.3	25.5	1473	1416	20.4	0.0
101	1476	1418	7.7	49.8	1474	1416	0.0	75.5
102	1482	1424	32.1	29.6	1482	1424	0.0	133.7
103	1484	1426	12.7	63.0	1482	1424	37.0	0.0
104	1494	1435	4.4	13.5	1493	1435	13.9	0.0
105	1495	1437	22.1	36.6	1493	1435	0.0	16.5
106	1495	1437	37.4	51.9	1495	1437	0.0	152.9
107	1496	1438	48.5	61.4	1496	1437	112.2	0.0
108	1521	1462	41.2	16.6	1520	1460	0.0	61.2
109	1521	1462	7.4	45.4	1520	1461	32.7	0.0
110	1577	1515	46.2	37.7	1578	1517	170.2	0.0
111	1578	1516	128.0	61.5	1578	1517	0.0	90.0
112	3032	2914	21.1	460.0	3033	2915	45.8	0.0
113	3032	2914	25.7	396.2	3033	2915	0.0	921.7
114	3034	2915	22.0	566.0	3043	2924	59.4	0.0
115	3041	2922	26.5	473.9	3043	2924	0.0	933.2
116	3042	2924	35.1	116.5	3047	2928	120.3	0.0
117	3043	2924	98.9	739.3	3047	2928	0.0	820.5
118	3080	2960	8.6	262.1	3072	2952	31.3	0.0
119	3081	2961	4.0	117.7	3072	2952	0.0	736.1
120	3082	2961	21.6	212.6	3082	2962	0.0	339.8
121	3083	2963	13.9	439.2	3082	2962	25.2	0.0
122	3090	2970	16.6	187.7	3099	2978	0.0	372.2
123	3097	2977	32.6	199.3	3099	2978	57.0	0.0
124	3098	2977	34.7	218.8	3102	2981	0.0	284.4
125	3099	2978	6.4	147.3	3102	2981	12.0	0.0
126	3112	2991	20.0	146.2	3114	2993	38.6	0.0
127	3119	2997	3.6	152.5	3114	2993	0.0	278.5
128	3119	2998	13.5	149.8	3120	2998	28.3	0.8

129	3120	2999	13.9	147.1	3120	2998	0.1	293.0
130	3139	3016	1.7	142.2	3135	3013	0.0	300.2
131	3140	3017	1.2	124.5	3135	3013	2.5	0.1
132	3247	3120	0.7	180.4	3248	3121	0.9	0.0
133	3247	3120	0.2	303.9	3248	3121	0.0	482.9
134	3512	3375	634.6	178.9	3607	3466	0.0	306.8
135	3614	3473	421.7	165.5	3608	3468	843.5	0.0

Source: Researcher (2024)

Appendix A.2 (continued) Vibrational Frequencies, IR activities, and Raman activities of the B3LYP Optimized Structures of the Fe1, Co1, Ni1, Pd1, Co2, and Ni2 Metal Complexes using LanL2DZ basis set for metal cations and 6-311+G(2d,p) basis set for all the remaining atoms at 298 K.

	Ni1				**Pd1**			
Mode	**Unscaled Frequency (cm^{-1})**	**Scaled Frequency (cm^{-1})**	**IR Activity**	**Raman Activity**	**Unscaled Frequency (cm^{-1})**	**Scaled Frequency (cm^{-1})**	**IR Activity**	**Raman Activity**
1	29	28	2.6	0.3	25	24	3.4	1.5
2	36	35	0.3	3.6	33	32	0.8	1.6
3	39	37	0.9	1.3	42	40	1.5	1.9
4	64	62	1.9	3.7	47	46	4.4	4.3
5	71	68	1.9	3.3	49	47	0.5	4.3
6	74	71	2.1	1.7	65	62	6.8	8.6
7	76	73	2.5	3.4	70	67	0.3	0.5
8	88	84	1.9	4.2	74	71	0.1	1.1
9	93	90	8.2	0.8	80	77	6.0	3.4
10	99	95	1.7	0.2	100	96	11.3	0.9
11	109	105	9.6	0.9	110	106	3.2	0.9
12	114	109	5.9	4.4	114	110	2.9	0.3
13	122	117	1.0	0.1	123	118	0.2	0.4
14	128	123	0.6	4.1	126	121	1.5	1.7
15	140	135	18.1	4.8	128	123	2.8	0.3
16	143	137	2.0	0.8	130	125	3.6	1.3
17	149	143	2.2	0.8	134	129	2.7	1.7
18	153	147	0.2	0.2	145	139	2.2	0.4
19	162	156	5.8	0.8	150	144	12.2	2.0
20	169	162	13.1	0.7	167	160	10.0	0.5
21	186	179	77.6	0.1	181	174	5.4	1.2
22	197	189	4.5	5.6	190	182	15.1	3.5
23	199	191	0.9	1.0	193	185	29.4	2.6
24	202	194	17.7	1.7	197	189	8.2	4.4
25	215	207	33.3	0.9	207	199	2.3	5.6
26	227	218	1.8	12.4	216	208	6.6	0.6
27	235	226	37.8	0.1	238	228	0.5	3.6
28	275	264	19.8	0.4	267	257	1.9	0.8
29	276	265	12.6	2.1	274	263	4.1	1.6

30	301	289	34.5	0.4	303	291	13.7	2.0
31	306	294	6.3	4.2	317	304	14.7	2.9
32	322	309	0.1	2.9	327	314	10.8	1.3
33	326	314	17.6	5.1	334	321	5.7	6.1
34	374	360	7.7	2.3	353	339	4.1	2.9
35	378	363	6.9	3.3	373	358	0.8	3.4
36	464	446	58.5	0.6	391	376	0.7	6.0
37	468	450	22.5	4.7	475	456	12.2	2.1
38	522	501	23.0	1.9	499	480	1.5	0.5
39	525	505	18.4	2.6	511	491	4.1	4.1
40	591	568	0.8	17.3	524	504	17.2	154.2
41	591	568	1.1	38.6	589	566	1.2	34.6
42	627	603	44.2	6.7	595	572	0.0	29.3
43	630	605	62.0	6.1	626	602	45.4	2.9
44	635	610	52.8	11.7	642	617	130.5	3.2
45	638	613	218.8	21.9	649	624	1.4	3.1
46	653	628	8.4	1.7	663	637	16.7	1.8
47	654	629	14.0	1.3	677	651	0.8	1.6
48	677	651	2.7	1.1	679	652	6.6	10.2
49	678	652	3.3	0.8	704	676	4.3	2.4
50	787	756	11.2	4.1	733	705	87.4	0.7
51	788	757	3.9	5.9	759	729	15.4	0.4
52	793	762	38.7	3.7	788	757	17.0	1.3
53	793	762	44.5	3.5	792	761	43.2	4.2
54	879	845	53.3	9.8	795	764	5.3	4.7
55	882	847	55.2	12.9	797	766	44.6	4.5
56	976	938	3.2	3.8	811	779	1.3	7.7
57	977	939	3.5	6.5	836	803	3.6	8.5
58	1002	963	19.9	2.1	863	829	27.1	6.4
59	1004	965	22.2	2.1	972	934	1.0	5.8
60	1013	973	8.3	3.9	1000	961	1.8	3.5
61	1014	974	7.5	12.1	1004	965	5.1	5.7
62	1041	1001	74.1	4.4	1005	965	8.5	0.1
63	1043	1002	78.3	5.4	1005	966	0.9	5.0
64	1063	1021	6.4	9.9	1038	997	1.9	14.8
65	1064	1022	2.7	14.4	1051	1010	165.0	5.2
66	1064	1022	27.6	0.6	1056	1015	7.6	2.6
67	1065	1024	15.7	2.0	1061	1020	4.6	0.4
68	1068	1026	28.2	2.9	1063	1022	45.7	3.1
69	1068	1027	24.0	11.6	1064	1023	30.1	2.8
70	1069	1027	37.6	7.1	1066	1024	4.1	1.1
71	1070	1028	32.2	1.7	1069	1027	53.4	3.2
72	1139	1095	32.1	5.2	1073	1031	5.1	23.3
73	1141	1097	3.9	14.7	1076	1034	2.6	43.4
74	1177	1131	2.9	8.3	1079	1036	13.5	2.6
75	1178	1132	3.6	9.2	1151	1106	17.5	2.6

76	1241	1192	5.1	8.8	1156	1111	11.5	11.0
77	1244	1196	3.4	8.5	1174	1128	1.8	8.7
78	1261	1212	60.0	4.1	1177	1131	6.2	10.6
79	1263	1214	12.9	51.4	1204	1157	36.6	133.9
80	1325	1274	63.4	27.1	1227	1179	14.9	19.4
81	1329	1277	63.3	27.8	1235	1187	25.7	36.0
82	1344	1292	84.3	0.2	1251	1202	43.7	7.4
83	1348	1295	163.5	24.6	1288	1238	12.5	44.0
84	1396	1342	41.7	8.3	1337	1285	7.1	28.7
85	1401	1347	23.4	30.9	1339	1286	63.7	33.7
86	1408	1353	45.2	32.3	1357	1304	14.9	2.3
87	1410	1355	19.5	12.9	1383	1329	12.5	15.7
88	1412	1357	12.4	1.9	1400	1345	16.7	13.6
89	1413	1358	0.4	7.7	1405	1351	36.8	22.7
90	1417	1362	27.8	36.6	1407	1352	14.9	36.4
91	1419	1363	53.5	37.0	1410	1355	12.6	9.5
92	1431	1375	11.9	8.1	1412	1357	20.7	39.7
93	1432	1376	0.7	4.4	1417	1362	26.8	42.0
94	1445	1388	100.3	26.8	1420	1364	23.9	23.7
95	1445	1388	49.6	48.5	1422	1367	36.4	86.1
96	1469	1411	15.6	19.3	1430	1375	40.7	7.6
97	1469	1412	7.3	31.0	1442	1386	99.9	24.5
98	1470	1413	30.6	26.0	1445	1389	99.6	33.1
99	1470	1413	20.6	43.4	1449	1393	5.7	13.0
100	1478	1420	2.4	22.6	1454	1398	3.1	11.2
101	1479	1421	13.3	95.7	1464	1407	26.6	44.7
102	1485	1427	30.8	15.9	1465	1408	1.3	13.1
103	1487	1429	3.1	22.4	1466	1409	8.7	11.3
104	1494	1436	32.7	40.3	1468	1411	55.5	10.4
105	1495	1436	15.9	47.6	1469	1412	29.0	12.1
106	1496	1437	58.7	68.6	1472	1414	22.6	16.8
107	1498	1440	17.0	13.6	1480	1422	12.3	44.9
108	1518	1459	21.3	26.6	1482	1424	10.3	121.2
109	1519	1459	13.1	27.4	1488	1430	11.7	48.3
110	1582	1521	28.3	35.3	1489	1431	36.7	74.2
111	1583	1522	134.9	42.0	1490	1431	10.7	42.4
112	3031	2913	22.1	434.9	1491	1433	39.5	148.7
113	3032	2913	25.7	522.9	1503	1445	9.5	8.3
114	3043	2924	40.7	348.4	1517	1458	13.3	31.8
115	3044	2925	54.2	457.9	1520	1460	15.2	45.8
116	3045	2926	40.7	170.1	1580	1518	38.3	26.7
117	3045	2926	78.7	888.4	1582	1520	117.4	40.8
118	3080	2960	9.1	149.1	3014	2896	41.3	252.3
119	3080	2960	15.1	203.7	3021	2903	70.7	432.6
120	3089	2968	7.1	120.1	3031	2913	5.0	148.2
121	3090	2970	4.3	459.8	3033	2915	87.3	593.6

122	3100	2980	17.1	158.8	3033	2915	26.2	416.8
123	3102	2981	40.1	230.4	3035	2916	16.2	645.9
124	3103	2982	29.1	289.9	3038	2919	20.6	554.3
125	3103	2982	29.2	142.1	3074	2954	70.3	326.8
126	3119	2997	15.6	142.3	3076	2956	5.0	214.8
127	3119	2997	14.5	164.3	3081	2961	17.5	216.7
128	3120	2998	6.6	114.7	3081	2961	7.6	174.6
129	3124	3002	5.6	112.8	3083	2963	10.8	181.6
130	3143	3020	4.4	192.9	3090	2969	15.6	183.3
131	3144	3021	0.1	73.1	3092	2971	10.1	124.3
132	3247	3120	0.6	237.1	3092	2972	53.3	373.1
133	3247	3120	0.5	259.8	3103	2982	42.9	236.8
134	3502	3365	244.7	77.8	3112	2991	26.6	187.2
135	3505	3368	968.5	284.9	3115	2993	14.5	117.0
					3120	2999	15.1	151.8
					3121	2999	14.5	157.2
					3124	3002	68.8	208.6
					3130	3008	0.6	49.0
					3133	3011	5.6	123.3
					3249	3122	0.3	273.0
					3251	3124	0.3	267.2
					3473	3338	843.6	354.3
					3540	3402	794.0	195.4

Source: Researcher (2024)

Appendix A.2 (continued) Vibrational Frequencies, IR activities, and Raman activities of the B3LYP Optimized Structures of the Fe1, Co1, Ni1, Pd1, Co2, and Ni2 Metal Complexes using LanL2DZ basis set for metal cations and 6-311+G(2d,p) basis set for all the remaining atoms at 298 K.

	Co2				**Ni2**			
Mode	**Unscaled Frequency (cm^{-1})**	**Scaled Frequency (cm^{-1})**	**IR Activity**	**Raman Activity**	**Unscaled Frequency (cm^{-1})**	**Scaled Frequency (cm^{-1})**	**IR Activity**	**Raman Activity**
1	26	25	0.2	2.4	14	14	0.2	1.6
2	28	27	1.6	3.0	20	19	1.2	1.6
3	32	31	3.0	1.6	26	25	0.9	2.4
4	45	43	0.7	1.3	32	31	1.9	2.4
5	51	49	0.9	2.2	37	36	2.0	1.9
6	54	52	1.8	0.9	42	41	1.0	1.0
7	72	69	4.9	1.0	49	47	1.0	3.6
8	80	77	2.4	2.7	59	57	4.8	5.3
9	92	88	1.6	1.1	66	64	3.4	2.3
10	95	91	3.6	3.4	73	70	1.7	1.7
11	104	100	0.7	1.0	76	73	9.5	0.7
12	112	108	2.6	0.8	82	79	3.2	0.9
13	115	111	3.4	0.3	93	89	0.0	1.3

14	117	112	24.0	0.9	97	94	0.9	1.1
15	123	118	2.3	0.7	110	106	0.5	1.9
16	131	126	4.9	0.9	116	111	0.8	0.8
17	132	127	2.9	1.0	119	115	1.8	0.4
18	136	131	2.8	0.4	121	117	1.3	0.7
19	139	134	1.0	3.0	128	123	0.7	1.0
20	151	145	1.6	0.8	140	135	0.2	0.8
21	159	153	4.9	1.0	151	145	1.8	5.8
22	189	182	8.1	2.5	161	155	2.6	7.3
23	198	190	12.4	2.1	193	185	6.1	3.0
24	198	190	21.6	2.7	200	192	8.7	0.7
25	208	200	4.5	1.3	203	195	20.0	0.7
26	233	224	4.3	2.7	222	214	33.3	13.1
27	234	225	3.2	4.8	232	223	5.8	1.6
28	265	255	84.1	10.5	237	227	2.2	2.1
29	283	272	10.0	5.0	245	236	72.2	1.3
30	292	280	2.8	0.2	286	275	3.6	2.6
31	297	285	109.7	4.6	295	283	38.3	0.4
32	310	298	8.0	3.3	310	298	3.6	5.3
33	313	301	25.2	0.9	317	305	14.3	1.2
34	321	308	17.9	3.4	329	316	20.8	2.6
35	331	319	27.1	1.3	333	320	13.8	2.9
36	371	356	2.1	9.3	374	359	1.8	7.5
37	373	359	3.0	0.9	377	363	3.1	4.2
38	495	476	8.8	1.3	495	476	11.3	1.4
39	504	484	4.8	0.8	499	480	2.5	0.9
40	591	568	0.9	27.9	592	569	0.6	29.6
41	594	571	0.5	21.7	593	570	0.7	20.2
42	650	625	13.0	10.9	650	624	33.7	19.8
43	652	627	19.0	15.3	650	625	13.4	15.1
44	664	638	51.9	7.9	664	638	44.6	8.1
45	664	639	78.9	15.4	666	640	61.9	8.5
46	682	655	0.7	1.6	679	652	1.7	0.3
47	684	657	1.6	1.3	680	654	1.7	1.8
48	747	718	35.2	32.2	744	715	32.5	39.8
49	749	719	23.6	52.7	749	720	32.6	41.9
50	772	742	10.4	1.5	775	745	6.6	2.7
51	772	742	8.0	2.0	781	750	7.5	2.3
52	800	769	45.9	3.6	807	775	45.4	3.3
53	805	774	43.8	3.6	812	780	43.4	3.5
54	828	795	0.3	13.2	829	796	0.6	9.1
55	833	801	0.8	32.2	831	799	0.6	29.5
56	996	958	4.9	6.9	1002	963	4.9	4.3
57	1002	963	0.3	7.9	1003	963	0.9	5.4
58	1003	964	9.2	0.4	1004	964	4.0	1.9
59	1005	966	8.9	0.5	1004	965	7.2	2.7

60	1035	995	5.2	4.6	1037	996	2.7	5.0
61	1039	998	7.1	13.5	1038	997	4.5	11.3
62	1042	1001	3.2	9.3	1040	1000	3.6	7.9
63	1043	1002	2.3	9.0	1041	1000	3.4	9.0
64	1062	1021	8.7	1.8	1059	1018	15.1	4.3
65	1064	1022	5.6	21.9	1061	1020	5.9	8.2
66	1065	1024	13.7	5.8	1063	1021	2.7	4.0
67	1066	1024	24.1	27.8	1065	1024	5.4	1.0
68	1067	1025	5.9	1.8	1066	1025	8.9	6.9
69	1070	1028	22.2	29.2	1067	1026	34.8	28.4
70	1132	1088	19.3	2.6	1128	1084	10.4	1.8
71	1135	1091	14.7	14.5	1130	1086	10.5	8.6
72	1169	1124	4.9	14.3	1173	1127	5.9	12.8
73	1174	1129	5.9	11.3	1174	1128	5.6	12.3
74	1218	1171	9.3	10.0	1219	1172	9.0	8.4
75	1219	1172	5.0	8.9	1221	1173	3.7	6.1
76	1273	1224	37.7	17.2	1273	1223	34.8	19.5
77	1275	1226	44.5	45.9	1276	1227	30.0	31.0
78	1290	1240	22.8	4.7	1290	1240	17.2	5.1
79	1292	1242	19.8	3.8	1293	1242	30.1	4.2
80	1348	1295	48.8	17.3	1344	1292	45.6	12.1
81	1349	1297	44.9	26.0	1345	1292	46.2	33.7
82	1393	1339	140.4	113.6	1395	1341	167.6	67.4
83	1396	1342	55.1	68.9	1398	1343	4.6	36.1
84	1398	1344	10.7	20.6	1399	1344	8.2	8.2
85	1400	1345	5.9	7.6	1403	1348	8.9	10.7
86	1411	1356	1.7	6.4	1408	1353	6.6	10.2
87	1412	1357	6.1	13.2	1411	1356	4.6	9.0
88	1415	1359	23.3	34.4	1414	1359	30.9	26.0
89	1418	1362	24.8	44.1	1416	1361	12.2	28.9
90	1444	1388	97.1	25.2	1443	1387	42.9	0.6
91	1447	1391	99.6	14.1	1444	1387	122.2	44.1
92	1466	1408	13.1	13.3	1465	1407	13.0	12.6
93	1466	1409	8.8	19.9	1469	1411	6.1	20.0
94	1469	1412	34.4	45.9	1470	1413	22.1	48.3
95	1470	1412	13.3	45.3	1472	1415	32.6	89.7
96	1472	1415	3.3	28.4	1477	1419	9.6	54.5
97	1473	1416	7.1	26.1	1480	1422	3.1	39.8
98	1480	1422	11.6	41.3	1482	1425	18.4	44.5
99	1480	1423	22.6	124.7	1483	1425	4.5	25.4
100	1487	1429	40.8	53.5	1488	1430	37.1	40.7
101	1490	1432	20.6	88.5	1489	1431	39.8	115.1
102	1498	1439	46.7	37.8	1502	1443	42.0	13.5
103	1503	1444	36.6	15.1	1505	1446	27.6	9.0
104	1522	1463	20.8	34.6	1521	1462	22.2	49.2
105	1523	1464	30.4	32.9	1522	1462	22.0	5.2

106	1579	1517	98.0	50.4	1582	1521	104.8	39.2
107	1582	1521	99.1	45.0	1583	1521	90.2	38.4
108	3035	2917	16.4	477.6	3035	2917	18.0	447.2
109	3036	2917	15.9	476.0	3036	2917	15.2	477.8
110	3039	2920	17.0	568.2	3039	2921	22.2	629.9
111	3041	2922	15.7	489.8	3040	2922	22.7	450.1
112	3085	2964	9.7	182.0	3082	2962	29.4	373.1
113	3085	2965	10.6	219.1	3083	2963	18.4	517.7
114	3087	2967	11.8	386.2	3085	2965	16.3	253.3
115	3088	2968	16.9	467.6	3086	2965	9.6	200.4
116	3093	2972	10.7	187.4	3096	2976	15.7	184.3
117	3097	2976	8.1	174.3	3097	2976	10.0	172.9
118	3106	2984	10.2	71.6	3103	2982	8.9	72.7
119	3107	2986	11.1	67.0	3106	2985	9.9	96.3
120	3119	2998	14.9	153.7	3120	2999	8.1	115.0
121	3124	3002	11.8	148.0	3121	2999	5.4	103.7
122	3124	3002	11.5	144.0	3124	3002	10.0	144.5
123	3128	3006	13.8	128.6	3124	3003	10.8	137.1
124	3138	3015	4.8	169.7	3132	3010	11.4	197.3
125	3139	3017	7.4	181.0	3134	3012	10.3	189.6
126	3171	3047	0.0	42.3	3167	3044	0.5	38.8
127	3173	3049	0.0	37.4	3170	3047	0.0	41.9
128	3251	3125	0.1	238.1	3251	3124	0.1	246.8
129	3252	3125	0.1	242.9	3252	3125	0.0	251.0

Source: Researcher (2024)

Appendix A.3. HOMO and LUMO Maps of Fe1, Co1, Ni1, Pd11, Co2, and Ni2 Metal Complexes generated using B3LYP functional and LanL2DZ basis set for metal atoms and6-311+G(2d, p) basis set for all the remaining atoms.

Compound[a]	HOMO	LUMO
Fe1 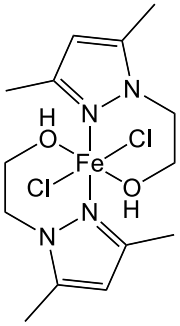	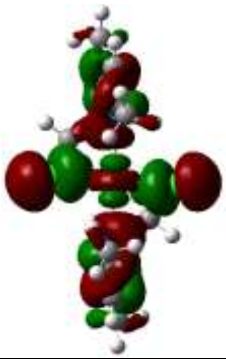	
Co1 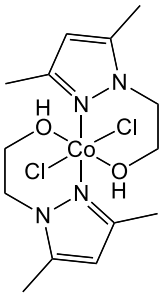	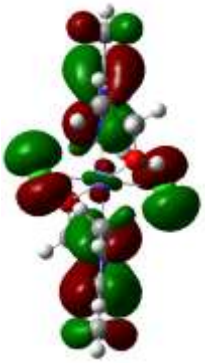	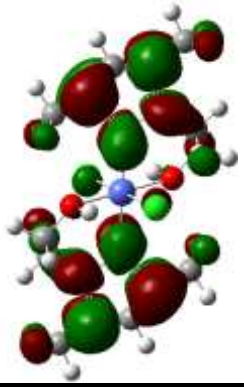
Ni1 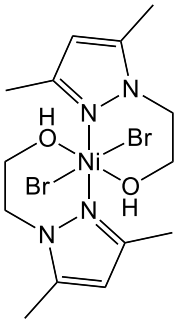	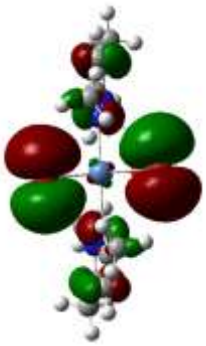	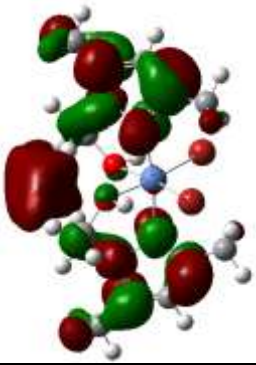

[a]ChemDraw structures of Fe1, Co1, and Ni1 metal complexes.
Source: Researcher (2024)

Appendix A.3. (continued) HOMO and LUMO Maps of Fe1, Co1, Ni1, Pd11, Co2, and Ni2 Metal Complexes generated using B3LYP functional and LanL2DZ basis set for metal atoms and6-311+G(2d,p) basis set for all the remaining atoms.

Compound[a]	HOMO	LUMO
Pd1	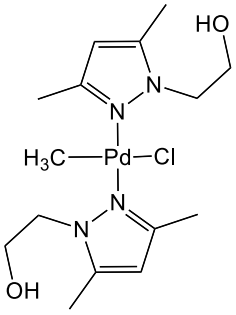	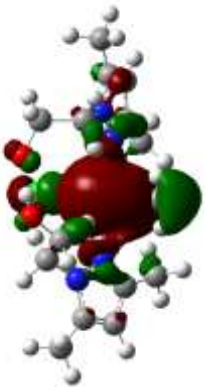	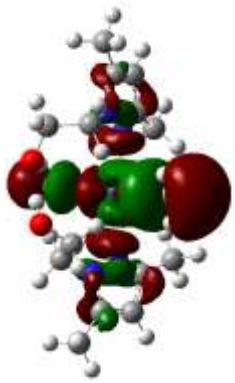
Co2	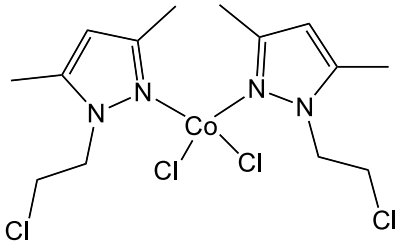	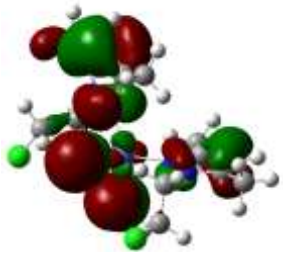	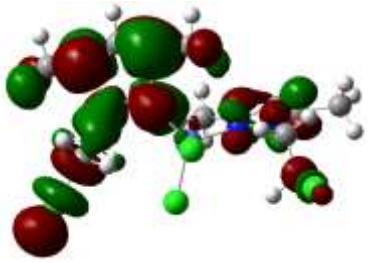
Ni2	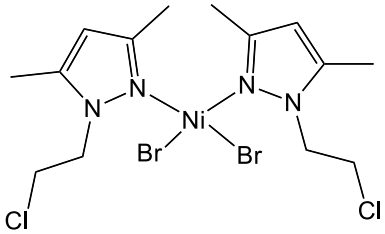	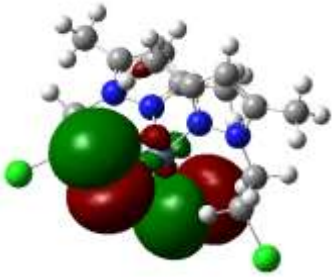	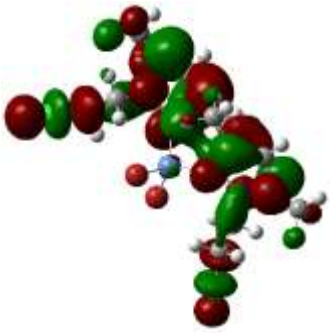

[a]ChemDraw structures of Pd1, Co2, and Ni2 metal complexes.
Source: Researcher (2024)

Appendix A.4. HOMO and LUMO Maps of Fe1, Co1, Ni1, Pd1, Co2, and Ni2 Metal Complexes generated using B3PW91 functional and LanL2DZ basis set for metal atoms and6-311+G (2d, p) basis set for all the remaining atoms.

Compound	HOMO	LUMO
Fe1 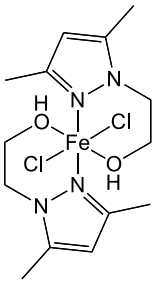	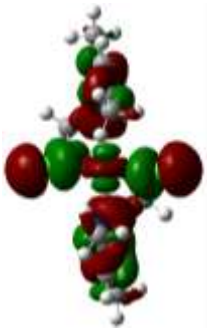	
Co1 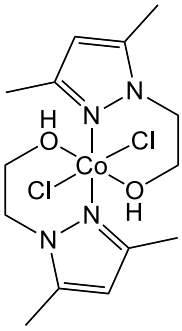		
Ni1 	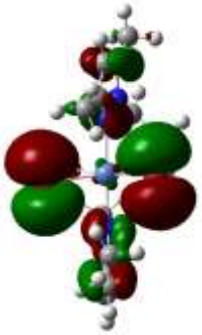	

[a]ChemDraw structures of Fe1, Co1, and Ni1 metal complexes.

Source: Researcher (2024)

Appendix A.4. (continued) HOMO and LUMO Maps of Fe1, Co1, Ni1, Pd1, Co2, and Ni2 Metal Complexes generated using B3PW91 functional and LanL2DZ basis set for metal atoms and6-311+G(2d,p) basis set for all the remaining atoms

Compound	HOMO	LUMO
Pd1	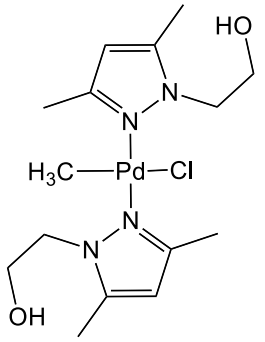		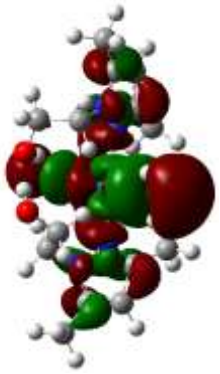
Co2	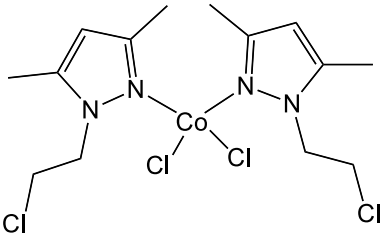	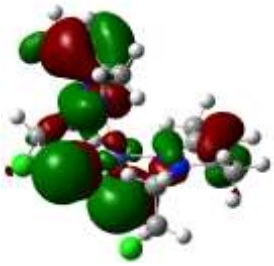	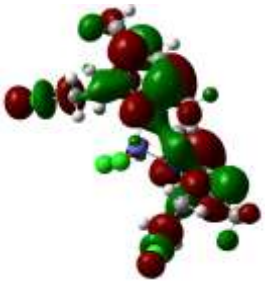
Ni2	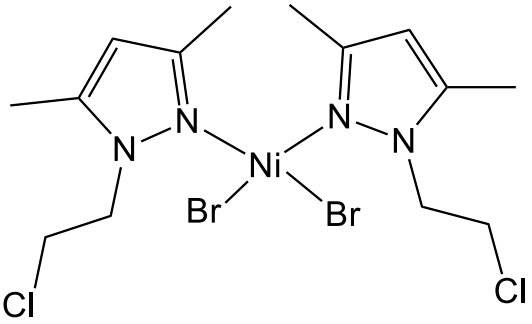	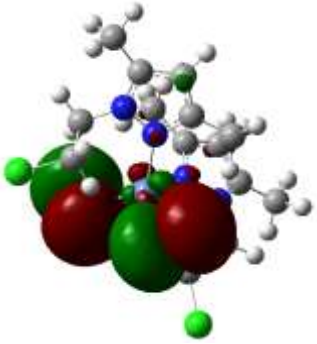	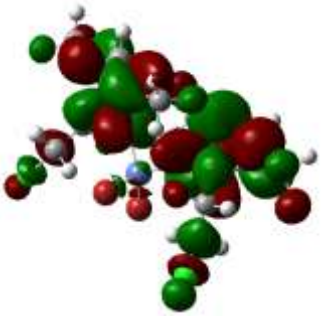

[a]ChemDraw structures of Pd1, Co2, and Ni2 metal complexes.

Source: Researcher (2024)

Appendix A.5. Similarity Report

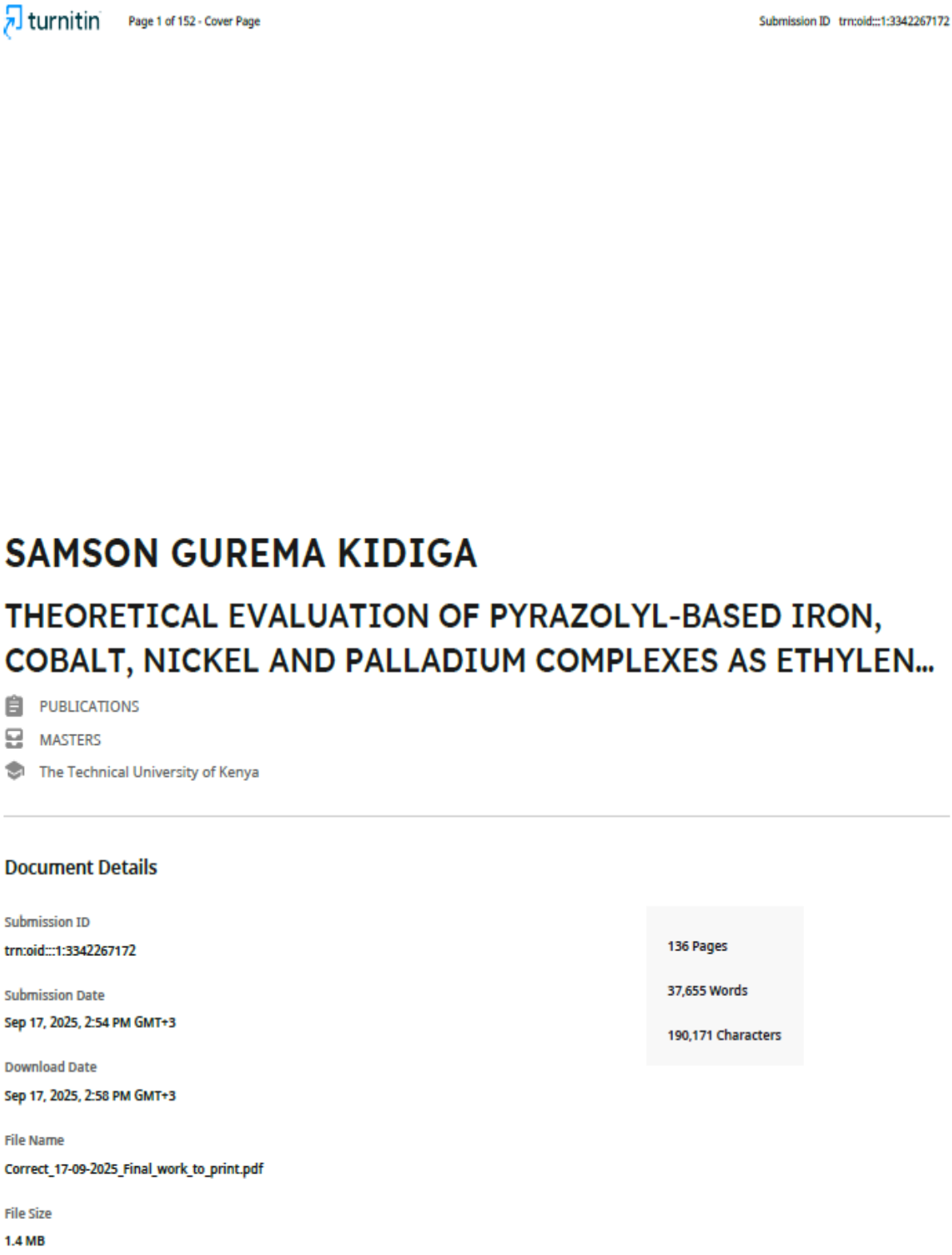

turnitin Page 1 of 152 - Cover Page Submission ID trn:oid:::1:3342267172

SAMSON GUREMA KIDIGA

THEORETICAL EVALUATION OF PYRAZOLYL-BASED IRON, COBALT, NICKEL AND PALLADIUM COMPLEXES AS ETHYLEN...

PUBLICATIONS

MASTERS

The Technical University of Kenya

Document Details

Submission ID
trn:oid:::1:3342267172

Submission Date
Sep 17, 2025, 2:54 PM GMT+3

Download Date
Sep 17, 2025, 2:58 PM GMT+3

File Name
Correct_17-09-2025_Final_work_to_print.pdf

File Size
1.4 MB

136 Pages

37,655 Words

190,171 Characters

17% Overall Similarity

The combined total of all matches, including overlapping sources, for each database.

Filtered from the Report

- Bibliography
- Quoted Text

Match Groups

412 Not Cited or Quoted 15%
Matches with neither in-text citation nor quotation marks

55 Missing Quotations 2%
Matches that are still very similar to source material

0 Missing Citation 0%
Matches that have quotation marks, but no in-text citation

0 Cited and Quoted 0%
Matches with in-text citation present, but no quotation marks

Top Sources

14% Internet sources

12% Publications

3% Submitted works (Student Papers)

Integrity Flags

1 Integrity Flag for Review

Replaced Characters
866 suspect characters on 64 pages
Letters are swapped with similar characters from another alphabet.

Our system's algorithms look deeply at a document for any inconsistencies that would set it apart from a normal submission. If we notice something strange, we flag it for you to review.

A Flag is not necessarily an indicator of a problem. However, we'd recommend you focus your attention there for further review.

Match Groups

412 Not Cited or Quoted 15%
Matches with neither in-text citation nor quotation marks

55 Missing Quotations 2%
Matches that are still very similar to source material

0 Missing Citation 0%
Matches that have quotation marks, but no in-text citation

0 Cited and Quoted 0%
Matches with in-text citation present, but no quotation marks

Top Sources

14% Internet sources
12% Publications
3% Submitted works (Student Papers)

Top Sources

The sources with the highest number of matches within the submission. Overlapping sources will not be displayed.

1	Internet	
digitalcommons.wayne.edu		4%
2	Internet	
www2.mdpi.com		<1%
3	Internet	
pubs.rsc.org		<1%
4	Publication	
Michael K. Ainooson, Stephen O. Ojwach, Ilia A. Guzei, Lara C. Spencer, James Dar...		<1%
5	Internet	
researchspace.ukzn.ac.za		<1%
6	Internet	
hdl.handle.net		<1%
7	Publication	
Ralph G. Pearson. "Recent advances in the concept of hard and soft acids and bas...		<1%
8	Internet	
ir-library.ku.ac.ke		<1%
9	Internet	
www.researchgate.net		<1%
10	Internet	
pubs.acs.org		<1%